Tawarah, Khalid Moh'd

KINETICS AND MECHANISM OF METHANOL DECOMPOSITION OVER ZINC OXIDE

Iowa State University PH.D. 1982

Kinetics and mechanism of methanol decomposition over zinc oxide

by

Khalid Moh'd Tawarah

A Dissertation Submitted to the
Graduate Faculty in Partial Fulfillment of the
Requirements for the Degree of
DOCTOR OF PHILOSOPHY

Department: Chemistry
Major: Physical Chemistry

Approved:

Signature was redacted for privacy.

In Charge of Major Work

Signature was redacted for privacy.

For the Major Department

Signature was redacted for privacy.

For the Graduate College

Iowa State University
Ames, Iowa

1982

TABLE OF CONTENTS

INTRODUCTION

Methanol is a valuable chemical produced from several feedstocks and is consumed in a variety of end uses. Prior to the development of a synthetic route to methanol, commercial quantities were obtained from the destructive distillation of wood [1, 2]. About half of the methanol currently consumed in the world goes into formaldehyde production [3]. Newer uses for methanol include a new technology for acetic acid [4], single cell protein [5], and water denitrification [6]. Methanol may potentially be used as a carrier for coal in pipelines, as a source of hydrogen or synthesis gas for direct reduction of iron ores, and as a direct additive to or a feedstock for gasoline [6]. The decomposition of methanol into hydrogen and carbon monoxide has been proposed as a means for the storage of solar energy [7]. Catalytic steam reformation of methanol for onboard hydrogen generation (hydrogen engine) seems to be a potential fuel-related use of methanol [8, 9].

The synthesis of methanol from hydrogen and carbon monoxide predates World War I, when Badische Anilin-und Soda-Fabric AG in Germany succeeded in this synthesis by the reaction:

$$CO_{(g)} + 2H_{2(g)} = CH_3OH_{(g)} \quad (1)$$

But CO and H_2 also react in other ways [10] such as:

$$CO_{(g)} + H_{2(g)} = HCHO_{(g)} \quad (2)$$

$$CO_{(g)} + 3\ H_{2(g)} = CH_{4(g)} + H_2O_{(g)} \quad (3)$$

$$2CO_{(g)} + 2H_{2(g)} = CH_{4(g)} + CO_{2(g)} \quad (4)$$

$$nCO_{(g)} + (2n+1)H_{2(g)} = C_nH_{(2n+2)(g)} + nH_2O_{(g)} \quad (5)$$

$$2CO_{(g)} = CO_{2(g)} + C_{(s)} \quad (6)$$

If these reactions should occur, then the secondary reactions may also proceed:

$$CO_{(g)} + H_2O_{(g)} = CO_{2(g)} + H_{2(g)} \quad (7)$$

$$2CH_3OH_{(g)} = CH_3OCH_{3(g)} + H_2O_{(g)} \quad (8)$$

$$CH_3OH_{(g)} + nCO + 2nH_{2(g)} = C_nH_{(2n+1)}CH_2OH_{(g)} + nH_2O_{(g)} \quad (9)$$

$$CH_3OH_{(g)} + nCO + 2(n-1)H_{2(g)} = C_nH_{(2n+1)}COOH_{(g)} + (n-1)H_2O \quad (10)$$

All these reactions are undesirable when the aim of the synthesis is methanol. So, by using a selective catalyst, the formation of methanol may be made predominant, and by choosing a set of appropriate operating conditions, all of the undesirable reactions may be minimized. Values of the free energies of some of these reactions have been reported by Paul [11] and Natta [12].

Until around 1966, the only commercial catalyst available for methanol synthesis was the old historic ZnO/Cr_2O_3 catalyst. A temperature of about 623 K and a pressure of about 3.5×10^7 Pa are required for producing CH_3OH over this catalyst. The old literature (up to 1955) concerning synthesis of methanol over pure zinc oxide and promoted ZnO has been discussed by Natta [12]. Around 1966, Imperial Chemical

Industries (ICI) reported discovery of a new low-pressure methanol catalyst [13, 14], consisting of $CuO/ZnO/Cr_2O_3$ or $CuO/ZnO/Al_2O_3$. However, the activity and selectivity of copper based catalysts for methanol synthesis had been known prior to commercial utilization [15]. The stumbling block, preventing earlier use of the catalysts, is the sensitivity of the catalysts to sulfur. This has been solved by the development of methods to remove sulfur from natural gas before it is reformed [16].

There are three principal routes to synthesis gas, $CO+H_2$ [6]: steam reforming of lighter hydrocarbon feedstocks, primarily methane and naphtha, partial oxidation of lighter hydrocarbon and residual oil feedstocks, and coal gasification.

The following catalytic liquid-phase process [17] has been disclosed:

$$3CO_{(g)} + 2H_2O_{(\ell)} = CH_3OH_{(\ell)} + 2CO_{2(g)} \qquad (11)$$

The process is carried out over CuO/ZnO catalyst at a pressure of 4.3×10^7 Pa and a temperature of 568 K. A 20% CO conversion into CH_3OH in 30 min. has been claimed [17]. The process obviates the need for synthesis gas produced by steam reforming of naphtha or natural gas, and could lead to a reduction in methanol production cost.

A noncatalytic process for methanol synthesis has also been disclosed by Brockhaus [18]. In this process, a mixture of methanol and formaldehyde can be obtained in good yield by a noncatalytic partial oxidation of methane, viz.,

$$3CH_{4(g)} + \frac{7}{2} O_{2(g)} = CH_3OH_{(g)} + HCHO_{(g)} + CO_{2(g)} + 3H_2O_{(g)} \quad (12)$$

The methanol and formaldehyde yields were claimed to be 71% and 14%, respectively. The process operates at a pressure of 6.1×10^6 Pa and a temperature of 713 K.

Poutsma et al. [19] have recently reported that palladium (as well as Pt and Ir) deposited on silica had, at 533 K to 623 K and 1.2×10^6 Pa to 1.0×10^8 Pa, excellent catalytic activity for methanol synthesis with only very small amounts of hydrocarbon by-product. This result contrasts with other reports [20] that under moderate synthesis gas pressures these metals catalyze largely methane formation.

Many metal carbonyl complexes have recently been reported as homogeneous catalysts for hydrogenating CO to methanol at pressures substantially above 1.0×10^8 Pa [21, 22]. A ruthenium carbonyl catalyst has been found quite active for hydrogenating CO to methanol and ethylene glycol under moderate pressures (below 3.4×10^7 Pa) [23].

A process for the manufacture of gasoline from methanol and/or dimethyl ether was announced by Mobil Corporation [24]. The catalyst is a shape-selective zeolite catalyst (ZSM-5). The importance of this process lies in the possibility of converting either coal or natural gas via methanol (a well-established old technology) to gasoline. Conversion of coal into gasoline (Fischer-Tropsch reaction) had been practiced in Germany during World War II, and the process is still in practice in South Africa [25]. However, the Mobil process (methanol to gasoline) adds a new dimension to the importance of methanol as a potential source

of fuel. Gigantic methanol plants can be operated near Middle East gas sources. Moreover, the use of renewable resources (biomass) for producing methanol might assume an important role in solving future energy shortages.

The simplest possible compounds that can result from the hydrogenation of carbon monoxide are: formaldehyde, methane, and methanol. Because of its potential simplicity, the direct synthesis of formaldehyde from CO and H_2 had been the subject of considerable study in the old literature [26]. The failure of most investigators to obtain more than a trace of formaldehyde may be due either to an unfavorable equilibrium or to lack of the proper catalyst. The equilibrium constant for the reduction of CO over ZnO/CuO catalysts was determined by Newton and Dodge [26] for the reaction:

$$CO_{(g)} + H_{2(g)} \rightleftarrows CH_2O_{(g)}$$

The total pressure was about 3.0×10^5 Pa. According to their findings, as based on experiments at 523 K, the equilibrium constant of the CH_2O synthesis is given as follows:

$$K_p = \frac{P(CH_2O)}{P(CO) \cdot P(H_2)} \tag{13}$$

$$\log\left(\frac{K_p}{\text{atm.}}\right) = \frac{374}{T} - 5.431 \tag{14}$$

where T is the reaction temperature in degrees Kelvin and 1 atm. = 1.013×10^5 Pa. Yield calculations based on this formula [27] had indicated that impractically high pressures would be required to obtain

useful yields. For example, at a temperature of 400 K, a yield of 6.9 (mole percent of CH_2O) requires a pressure of $1x10^4$ atm. In addition to this problem, an extremely active and selective catalyst would be needed to obtain equilibrium at a reasonable rate and at the same time avoid hydrogenation of the formaldehyde produced to methanol. The equilibrium constant for the hydrogenation of formaldehyde to methanol was also determined by Newton and Dodge [26] over several catalysts including ZnO/CuO mixed catalysts. The equilibrium constant for the reaction:

$$CH_2O_{(g)} + H_{2(g)} \rightleftarrows CH_3OH_{(g)} \tag{15}$$

is given as follows:

$$K_p = \frac{P(CH_3OH)}{P(CH_2O) \cdot P(H_2)} \tag{16}$$

The temperature dependence of K_p, as given by Newton and Dodge [26], is given by the equation:

$$\log\left(\frac{K_p}{atm.}\right) = \frac{4.6x10^3}{T} - 6.470 \tag{17}$$

where T is the reaction temperature in degrees Kelvin. From this equation it is possible to calculate, for equilibrium at atmospheric pressure, that dehydrogenation of CH_3OH vapor into CH_2O and H_2 would be 46% at T=673 K, and 98% at 973 K. These yields are not readily obtained by dehydrogenation alone, since in the absence of oxygen (or air) the dehydrogenation reaction is relatively slow compared to the rate of CH_2O decomposition to CO and H_2 [28]. At present, no process is

available for the direct synthesis of CH_2O from synthesis gas ($H_2 + CO$). Indirect synthesis is accomplished via the catalytic dehydrogenation of CH_3OH over Ag, Cu, or Fe_2O_3-MoO_3 catalysts [28].

The equilibrium between CO, H_2, and CH_3OH (reaction 1) is highly dependent on the temperature and on the partial pressures of the gases. For the reaction:

$$CO_{(g)} + 2H_{2(g)} \rightleftarrows CH_3OH_{(g)}$$

the equilibrium constant is

$$K_f = \frac{f(CH_3OH)}{f(CO) \cdot f^2(H_2)} = e^{-\frac{\Delta G}{RT}} \tag{18}$$

where K_f = reaction equilibrium constant based on the fugacity of reactants, f(i) = fugacity of component "i", and ΔG is the free energy change of the reaction. At standard conditions, the pressures approximate the fugacities, thus:

$$\begin{aligned} K_f &\simeq K_p^\circ \\ &= \left[\frac{P(CH_3OH)}{P(CO) \cdot P^2(H_2)}\right]\left[\frac{\gamma(CH_3OH)}{\gamma(CO) \cdot \gamma^2(H_2)}\right] \\ &= \left[\frac{N(CH_3OH)}{N(CO) \cdot N^2(H_2)}\right] K_\gamma P^{-2} \end{aligned} \tag{19}$$

where N(i) is the mole fraction of component "i", P is the total pressure, $\gamma(i)$ is the activity coefficient of component "i", and K_p° is the reaction equilibrium constant based on partial pressures of reactants when the total pressure is 1 atm. The values of K_p° as calculated by

various investigators have been reviewed by Strelzoff [10], who concluded that the values obtained by Cherednichenko [29] were good representatives, namely:

$$\log K_p^\circ = \frac{3.971 \times 10^3}{T} - 7.492 \log T + 1.77 \times 10^{-3} T - 3.11 \times 10^{-8} T^2 + 9.218 \quad (20)$$

where T is the reaction temperature in degrees Kelvin, and K_p° is in atm.$^{-2}$. The activity coefficient ratio, K_γ, for methanol synthesis was calculated by Ewell [30] at different pressures and temperatures. Rearrangement of Equation 19 gives the equilibrium mole fraction of methanol as follows:

$$N_{CH_3OH} = \frac{K_p^\circ N_{CO} N_{H_2}^2 P^2}{K_\gamma} \quad (21)$$

Since K_p° decreases with increasing temperature (see Equations 18 and 19), and K_γ increases with temperature [30], Equation 21 shows that N_{CH_3OH} should decrease with increasing temperature. The equation also shows that N_{CH_3OH} increases with pressure to the second power. The predictions of Equation 21 are in accordance with Le Chatelier's principle. The methanol synthesis reaction is a highly exothermic reaction (ΔH_{298}° = -90.64 kJ mol^{-1}) and three moles of the reacting gases result in one mol of product. Thus, high pressure and low temperature would drive the reaction toward completion. Because of these thermodynamic predictions regarding the methanol synthesis, together with the inherent economic advantages of the low pressure technology, the high pressure, high temperature units (ZnO/Cr_2O_3 catalyst) are in the

process of being phased out or converted to low pressure units ($ZnO/CuO/Cr_2O_3$ or $ZnO/CuO/Al_2O_3$ catalysts).

To investigate the feasibility of methanol synthesis at T=573 K and a total pressure of 1 atm. in a static reactor with an initial mixture of $CO:H_2$ = 1:2, the following was done:

(1) $CO_{(g)} + 2H_{2(g)} \rightleftarrows CH_3OH_{(g)}$

(2) Let the amounts of CO and H_2 at zero time reaction = 1 and 2 mol, respectively.

(3) Let the fraction of CO converted to CH_3OH at equilibrium = x.

(4) The total relative number of moles at equilibrium = 3-2x.

(5) Using Equation 20, $K_P^\circ = 3.08 \times 10^{-4}$ atm.$^{-2}$ at 573 K.

(6) Using Equation 21, with $K_\gamma \approx 1$, and $P^2 = 1$:

$$N_{CH_3OH} = (3.08 \times 10^{-4}) \frac{(1-x)(2-2x)^2}{(3-2x)^3} = \frac{x}{3-2x} .$$

(7) Assuming that 1-x≈1, 2-2x≈2, and 3-2x≈3, and solving for x gives $x = 1.369 \times 10^{-4}$. This conversion (about 1.4×10^{-2}%) corresponds to P_{CH_3OH} = 4.6 Pa. This pressure is too small to be detected in a total pressure of 1 atm. = 1.013×10^5 Pa.

The above example demonstrates that if one is seeking a kinetic and/or mechanistic study of the methanol synthesis in a static reactor, the best approach is to study the reaction in the reverse direction, i.e., the decomposition of methanol to carbon monoxide and hydrogen. The principle of microscopic reversibility assures that all the information obtained by studying the decomposition reaction is applicable to the

synthesis reaction.

Two main approaches have been adopted in studying the kinetics of the methanol synthesis. The first approach is based on fitting the synthesis data, obtained under conditions close to those encountered industrially, to a certain rate law [12, 31]. For example, Natta [12] found that his data could be fitted by the following rate equation:

$$r_m = \frac{f(CO)f^2(H_2) - f(CH_3OH)/K_p^\circ}{[A + Bf(CO) + Cf(H_2) + Df(CH_3OH)]^3} \qquad (22)$$

where r_m = rate of methanol formation, A, B, C, and D are constants that vary with temperature. The data were obtained over ZnO/Cr_2O_3 and $ZnO/CuO/Cr_2O_3$ catalysts in the temperature range 573 K to 663 K and at total pressure of 2×10^7 - 3×10^7 Pa. The rate-determining step proposed in deriving Equation 22 was a trimolecular surface reaction, viz.,

$$CO_* + 2H_2* \rightleftarrows CH_3OH_* + 2* \qquad (23)$$

where the star, *, represents an unoccupied site on the catalyst surface. On the other hand, Uchida and Ogino [32], who carried out the methanol synthesis over ZnO/Cr_2O_3 catalyst in the temperature range 573 K to 633 K and at total pressure of 9×10^6 - 1.5×10^7 Pa, reported the following rate equation:

$$r_m = k\{[P(CO)\cdot P^2(H_2)]^{0.7} - P(CH_3OH)[P(CO)\cdot P^2(H_2)]^{-0.3}(K_p^\circ)^{-1}\} \qquad (24)$$

where k is a constant at a definite temperature. The rate-determining step assumed in deriving Equation 24 is the desorption of methanol. A logarithmic adsorption isotherm was also assumed. However, Leonov

et al. [33] have proposed that hydrogen adsorption is a rate-determining step in the methanol synthesis over $ZnO/CuO/Al_2O_3$ catalyst.

The second approach used in studying the kinetics of the methanol synthesis reaction is based on carrying out the synthesis reaction at a constant pressure (usually less than $1x10^5$ Pa) in a closed flowing system. The methanol formed during the experiment is condensed in a cold trap and the rate of the reaction is followed by the pressure decrease [34, 35]. As was pointed out earlier, when the total pressure is $1x10^5$ Pa (1 atm.), the equilibrium pressure of the produced methanol is about 4.6 Pa. This means that the per-pass conversion of CO into CH_3OH in a closed circulating system is extremely small. Consequently, longer times are required in order to obtain a measurable quantity of methanol. Temkin [35] studied the kinetics of methanol synthesis over ZnO/Cr_2O_3 catalyst in the temperature range 457 K to 575 K at a total pressure of $1.5x10^4$ - $8.6x10^4$ Pa and concluded that hydrogen adsorption is a rate-determining step. On the other hand, Saida and Ozaki [34], who attempted to study the hydrogen isotope effect on methanol synthesis, reported the following rate law:

$$r_m = \frac{kP(CO)P^2(H_2)}{[1 + a_1P(H_2) + a_2P(CO)]^2} \qquad (25)$$

where k, a_1, and a_2 are constants at a definite temperature. Their study was carried out on a $ZnO/CuO/Cr_2O_3$ catalyst at 453 K with total pressure of $2x10^4$ - $4x10^4$ Pa. Although their rate law shows that the rate of methanol production, r_m, depends on $P(H_2)$, no hydrogen isotope effect was detected.

The copper-based catalysts ($ZnO/CuO/M_2O_3$, M=Al or Cr) are receiving much attention in the recent literature with emphasis being placed on their structure [36-38]. Herman et al. [38] discovered that the copper-based catalysts contain a new compound identified as a Cu(I) solution in ZnO. The dissolution of Cu(I) in ZnO is probably favored by the fact that Cu(I) is isoelectronic with Zn(II) and it assumes, like Zn in ZnO, a tetrahedral coordination [39]. According to Herman et al. [38], the Cu(I) centers nondissociatively chemisorb and activate CO, while the ZnO surface activates H_2. The hydrogenation of CO occurs by a series of steps, one of which causes the hydrogenation of the oxygen end of CO and another causes the hydrogenolysis of the Cu-C bond. Herman et al. [38] also remarked that catalyst deactivation in CO/H_2 mixtures is explained as the reduction of Cu(I) to inactive Cu metal, while the rate enhancing effect of O_2, H_2O, and CO_2 is due to the maintenance of an oxidation potential high enough to keep the copper in the active Cu(I) state.

Infrared (IR) spectroscopic evidence of formyl species (HCO) formed by CO and H_2 co-adsorption on ZnO and CuO/ZnO has been recently reported by Saussey et al. [40]. The IR spectrum of a mixture of CO and H_2 adsorbed on ZnO or ZnO/CuO showed a pair of weak bands at 2770 and 2661 cm^{-1}, while a mixture of CO and D_2 gave rise to a corresponding single band at 2020 cm^{-1}. Saussey et al. [40] assigned these bands to vibrations of a surface formyl species.

The kinetics of methanol decomposition (reverse reaction of methanol synthesis) has been studied over pure ZnO and doped ZnO by several

investigators [41-46]. These studies can be classified into three categories. The first category involved establishing the kinetic order of the methanol catalytic decomposition reaction [41, 42]. According to Dohse [41], the catalytic decomposition of methanol over ZnO proceeds via a scheme of two first-order reactions. The first step is the dehydrogenation of methanol into hydrogen and formaldehyde and the second step is the decomposition of formaldehyde into hydrogen and carbon monoxide. The same scheme was also adopted by Tamura [42]. The second type of study aimed at establishing a relationship between the apparent activation energy of the methanol decomposition reaction and the nature of the doping ion used to induce a change in the semiconductivity of ZnO [43-45]. The doping ions used were Li(I), Al(III), and Ga(III). Contradicting results were reported in this regard. For example, Dandy [43] found the same apparent activation energy for doped and undoped ZnO, while Menold [44] reported that doping affects the ZnO activity towards methanol decomposition. In the third category, followed by Ueno et al. [46], infrared spectroscopy was applied to identify and study the dynamic behavior of the surface species occurring during the decomposition of methanol over ZnO catalysts. Formate and methoxide species have been detected by using this approach.

The adsorptive behavior as well as the decomposition of both methanol and formaldehyde over some methanation metal catalysts have been the subject of several ultrahigh vacuum investigations [47-52]. A major goal of these investigations was to elucidate the mechanism of the methanation reaction which has long been suspected to involve surface intermediates

such as HCO (ads.) or HCOH (ads.) [53].

In conclusion, the kinetics as well as the mechanistic aspects of both the methanol synthesis and its decomposition are far from being completely understood. Since ZnO is a major component of any recipe used for methanol synthesis, pure ZnO was used as catalyst in the present study of the kinetics of methanol decomposition. An ultrahigh vacuum technique was chosen in order to study the decomposition reaction under well-defined conditions. As previously explained, the equilibrium position precluded study of the synthesis reaction at low reactant pressures. The effect of the methanol pressure on the kinetics of methanol decomposition was established over two orders of magnitude (3 Pa to 130 Pa) pressure variation. Such wide range of reactant pressure was not achieved in previous studies of methanol decomposition. The kinetic hydrogen isotope effect on methanol decomposition was investigated (for the first time) by comparing the initial rate of CH_3OH decomposition with those of CH_3OD and CD_3OD. Most aspects of the present kinetic study were not attempted before. Following the experimental section, the findings of this study are discussed in detail and a mechanism accounting for all the observations reported in this dissertation is proposed.

EXPERIMENTAL

Apparatus

The need for studying the kinetics of the ZnO-catalyzed decomposition of methanol at low methanol pressures ($P_m \leq 1.3 \times 10^2$ Pa) required the design of a vacuum system. Figure 1 shows a schematic of the vacuum system used in this study. The vacuum system consisted of two major parts: the reaction enclosure part and the mass spectrometer part. These two parts were connected by a variable leak valve, which allowed continuous sampling from the reaction enclosure to the mass spectrometer part during the course of an experiment.

The reaction enclosure was pumped by a two-stage mercury diffusion pump backed by a roughing pump. A base pressure of about 5×10^{-5} Pa was attained in this part of the vacuum system. The residual gas pressure over the catalyst was measured by means of a conventional Bayard-Alpert ionization gauge. Several glass storage bulbs, including one for CH_3OH storage, were connected to the reaction enclosure via a glass manifold. This manifold was used for admitting the required amount of reactant or any other mixture of gases before expanding to the catalyst vessel. The pressure in the manifold was measured by means of a capacitance manometer (Granville Phillips Co., series 212). Pressures up to 1.3×10^3 Pa were measured using this manometer. The reference side of the capacitance manometer was continually pumped to about 5×10^{-5} Pa in order to obtain a stable baseline. The sensor head of the manometer was water thermostated at 306.5 K to prevent drift due to changes in the ambient temperature. The manometer was calibrated against a McLeod

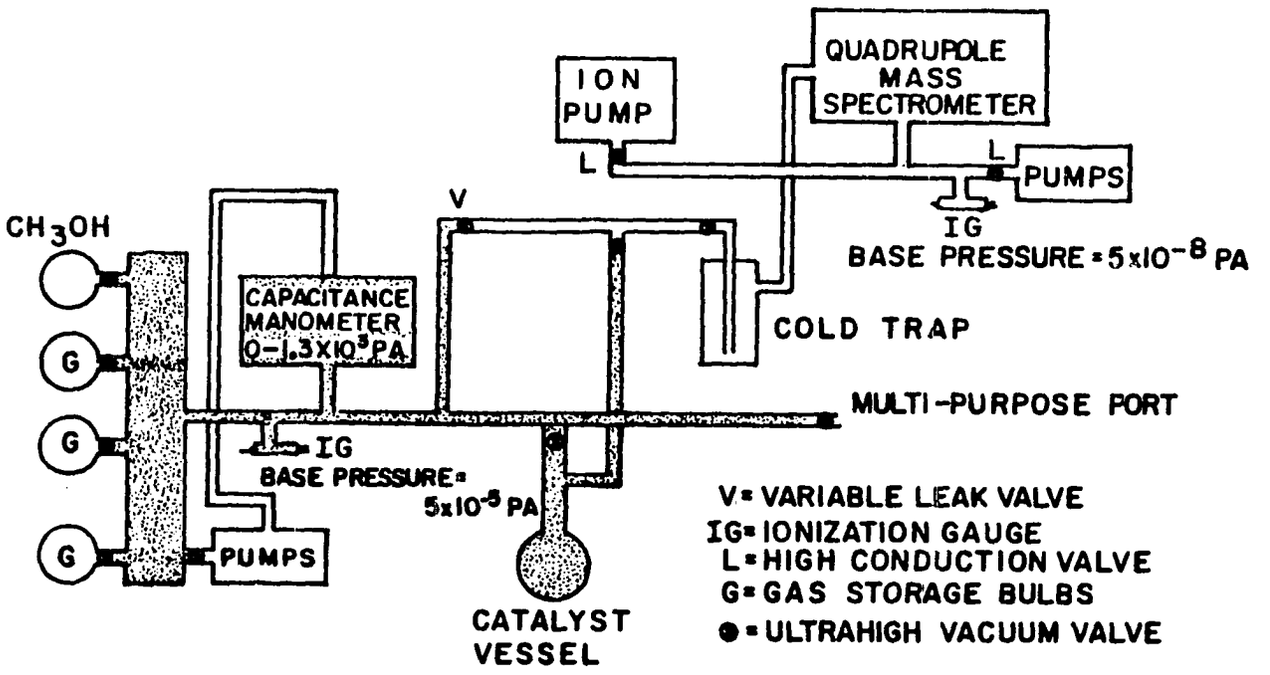

Figure 1. Schematic of the vacuum system used in the kinetic study (shaded area = reaction volume = 2.04×10^{-3} m^3)

gauge (Consolidated Vacuum Corp.) using argon gas.

The pressure changes were read directly as a meter deflection on the manometer control unit, or recorded by means of an x-y recorder (Hewlett-Packard, series 7044A). The control unit of the capacitance manometer has five ranges with maximum pressures of approximately 13, 40, 1.3×10^2, 4.0×10^2, and 1.3×10^3 Pa. Each range yielded a linear calibration of the form:

$$\text{Pressure (Pa)} = aX \text{ (scale deflection)} + b$$

The constant b was close to the sensitivity of the corresponding range. The original calibration was checked after several months and was found to agree with the recheck calibration within ±10%. The pressures reported in the present study were calculated by using the average of these two calibrations. The volume of the manifold (shaded area in Figure 1 excluding the catalyst vessel) was measured by argon expansion from a standard volume (1.142×10^{-3} m^3 round bottom pyrex flask) attached to the manifold via an ultrahigh vacuum valve. The volume of the manifold was found to be 1.06×10^{-3} m^3. The catalyst vessel consisted of a 500 ml round bottom pyrex flask. The volume of the vessel and its connections was measured by expanding argon from the manifold to the empty vessel at room temperature. Its volume was found to be 9.75×10^{-4} m^3 of which 6.0×10^{-4} m^3 was estimated to be at the reaction temperature and the remainder was assumed to be at the ambient temperature.

The catalyst vessel was heated by means of a tube furnace (S. B. Lindberg, type SP). The bottom of the furnace was sealed and the top

was covered to prevent air conduction through the furnace. In this manner, the catalyst vessel could be conveniently heated to any temperature between room temperature and 775 K (the approximate softening point of pyrex). The temperature was monitored by a chromel-alumel thermocouple which was inside the tube furnace and in direct thermal contact with the catalyst vessel. The temperature of the reference junction of the thermocouple was maintained at 273 K by means of a slush of ice and distilled water. The potential difference between the high temperature and the cold temperature junctions was displayed on a digital multimeter (Hewlett-Packard, series 3465A) which has a sensitivity of 1 μV. The thermoelectric voltage was converted into actual temperature readings by means of the chromel-alumel thermocouple table supplied by Omega Engineering, Inc. During the actual time of an experiment, the temperature fluctuation was within ±0.5 K.

The mass spectrometer part consisted mainly of a cold trap, quadrupole mass spectrometer, and an ion pump. The cold trap was maintained at 195 K by means of a dry ice-acetone slush. The function of the cold trap was to condense methanol and/or formaldehyde before reaching the mass spectrometer. This trapping was necessary in order to eliminate the contribution of methanol and/or formaldehyde to peak $\frac{m}{e}=28$, which was used to monitor the production of CO during the high temperature decomposition experiments. The residual gas analyzer used was a Finnigan Spectrascan 400 quadrupole mass spectrometer (Finnigan Corp.). The output of the mass spectrometer was directed onto a two-channel strip chart oscillographic recorder (Hewlett-Packard, model

7402A). An oscilloscope (Tektronix, Inc., type RM503) was occasionally used for the purpose of instrument adjustment and/or troubleshooting. The mass spectrometer output (signal in mV) was calibrated against the actual gas pressure in the manifold. The gas under consideration was leaked to the mass spectrometer via the variable leak valve shown in Figure 1. The calibration resulted in establishing a sensitivity factor $S_i = \frac{\text{gas pressure in Pa}}{\text{signal in mV}}$ for each gas used in this study. No reliable sensitivity factors were obtained for methanol or formaldehyde due to the slow attainment of a steady flow through the leak valve.

The ion pump used is a 20 $\ell\ s^{-1}$ differential ion pump (Ultek, model 203-2000). The pump was used in conjunction with two two-stage mercury diffusion pumps backed by a roughing pump. This arrangement of pumps resulted in the attainment of a base pressure of 5×10^{-8} Pa in the mass spectrometer part of the vacuum system. The purpose of having the ion pump was to attain ultrahigh vacuum pressures required for depositing a thin film of zinc metal, which could then be oxidized into a film of ZnO. However, the ZnO films obtained were found to be both thermally instable and catalytically inactive. Consequently, no kinetic study was performed on such ZnO films and a powder sample of ZnO was used instead. The ion pump was found helpful in protecting the mass spectrometer during periods of system malfunction or shutdown.

The multi-purpose port shown in Figure 1 was used for attaching to the vacuum system the McLeod gauge, standard volume, apparatus for handling CH_3OH, apparatus for handling the deuterated compounds, or the apparatus used for formaldehyde preparation. The CH_3OH handling

apparatus consisted of two round bottom pyrex flasks in which CH_3OH was purified by bulb-to-bulb vacuum distillation before use. One of the flasks had a breakable glass seal and was used as a storage bulb for liquid CH_3OH as indicated in Figure 1. A similar apparatus was used for handling D_2O, CH_3OD, and CD_3OD. The two deuterated methanols, CH_3OD and CD_3OD, were injected into the handling apparatus by means of a 10 μℓ syringe (Hamilton Co.). The injection was carried out through a rubber-capped glass tube extension attached to the handling apparatus via a vacuum stop cock. The vapor pressure of both CH_3OD and CD_3OD inside the handling apparatus was maintained below the room temperature saturation pressure of methanol, which is about 1.3×10^4 Pa.

The apparatus used for the preparation of formaldehyde was similar to that described by Spence and Wild [54]. The flow reactor apparatus used for testing the production of formaldehyde during the ZnO-catalyzed decomposition of methanol consisted of three major parts. The first part was a pyrex glass tube (reactor) held in a vertical position and heated by a tube furnace. About two grams of ZnO powder was placed in the bottom of the reactor. The second part of the flow apparatus consisted of a 500 mℓ round bottom pyrex flask through which a helium stream was passed in order to carry methanol vapor to the reactor. Methanol in the flask was kept at its boiling point by means of a heating mantle. The third part was a 500 mℓ pyrex conical flask, containing about 250 mℓ distilled water. The effluent gas, after leaving the reactor, was directed through the conical flask in order to get an aqueous solution of formaldehyde.

The instrument used for the surface area measurements was Orr surface-area pore-volume analyzer (Micromeritics Instrument Corp., model 2100D, serial number 348). Computation of the BET surface area of the ZnO catalyst sample was accomplished by a computer program, which is included in the instrument manual. About 0.3 to 0.6 g of ZnO powder sample was outgassed at 393 K for 17 hours. Nitrogen was used as the adsorbate and a molecular area of 1.62×10^{-1} nm^2 was assumed for N_2. The adsorption temperature was 77.2 K at which the saturation vapor pressure of nitrogen is 9.962×10^4 Pa. Values of $\frac{P_e}{P_o}$ ranged from 0.04 to 0.15, where P_o is the saturation vapor pressure of nitrogen at 77.2 K and P_e is the equilibrium pressure of nitrogen over the adsorbent (ZnO) at the adsorption temperature. The purity of a ZnO catalyst sample was examined by high dispersion emission spectographic analysis. In addition, the sample was analyzed by energy dispersion x-ray fluorescence spectroscopy (Tracor x-ray, model 440). All the metal vacuum valves shown in Figure 1 were purchased from Granville Phillips Co.

Kinetics Procedure

The kinetics of methanol decomposition on ZnO was studied over two temperature ranges 453 K to 513 K and 563 K to 613 K. Dehydrogenation of methanol into hydrogen and formaldehyde was studied in the low temperature range, while the total decomposition of methanol into hydrogen and carbon oxides was studied in the high temperature range. The effect of CH_3OH pressure on the initial rate of H_2 production in

the low temperature range was examined at 500 K. CH_3OH pressures of about 3 Pa to 31 Pa were used at this temperature. The high temperature CH_3OH decomposition, where CO, CO_2, and H_2 were produced, was studied at 593 K. CH_3OH pressures ranged from about 3 Pa to 130 Pa at 593 K; 10.8 Pa of CH_3OH, CH_3OD, or CD_3OD was used for investigating the temperature dependence of the initial rate of methanol decomposition in both temperature ranges. Pressures of up to 10 Pa of CH_3OH or CH_2O were used in comparing the initial rates of decomposition of CH_3OH and CH_2O at 500 K.

Before starting a kinetic experiment, the required amount of reactant was first dosed in the manifold. The pressure of the reactant in the manifold was then recorded at the moment of admitting the reactant to the catalyst, which was held at the reaction temperature. The initial reactant pressure over the catalyst was calculated by using the following equation:

$$P(\text{man.} + \text{cat. ves.}) = r.\ P(\text{man.}) \tag{26}$$

where r = expansion factor. Assuming that at low reactant pressure (maximum reactant pressure used ≤ 130 Pa), the ideal gas law is applicable, the expansion factor, r, can be given at any reaction temperature as follows:

$$\frac{P(\text{man.})V(\text{man.})}{T(\text{man.})} = P(\text{man.} + \text{cat. ves.})\left\{\frac{V(\text{man.})}{T(\text{man.})} + \frac{V(\text{con.})}{T(\text{con.})} + \frac{V(\text{cat. ves.})}{T(\text{cat. ves.})}\right\} \tag{27}$$

where $V(\text{man.}) = 1.06\times10^{-3}$ m^3, $V(\text{cat. ves.}) = 6.0\times10^{-4}$ m^3, and V(con.) =

volume of the connections that hold the catalyst vessel to the vacuum system = 3.8×10^{-4} m^3. At room temperature, T(man.) = T(con.) = T(cat. ves.) ≈ 298 K and the expansion factor becomes:

$$r = \frac{P(\text{man.} + \text{cat. ves.})}{P(\text{man.})} = \frac{V(\text{man.})}{V(\text{man.}) + V(\text{con.}) + V(\text{cat. ves.})} = \frac{1.06\times10^{-3}\ m^3}{2.04\times10^{-3}\ m^3}$$

$$= 0.52 \ .$$

However, when T(cat. ves.) > T(man.) = T(con.) ≈ 298 K, the expansion factor can be obtained from the following equation:

$$r = \frac{P(\text{man.} + \text{cat. ves.})}{P(\text{man.})} = \frac{T(\text{cat. ves.})}{1.36\ T(\text{cat. ves.}) + 1.69\times10^{2}} \qquad (28)$$

where T(cat. ves.) = reaction temperature in degrees Kelvin. For example, when the reaction temperature is 573 K, Equation 28 yields r = 0.60. Figure 2 is an experimental verification of Equation 28 for the case T(cat. ves.) = 573 K. The slope of the least-squares line in Figure 2 is equal to the expansion factor, r. From Figure 2, r = 0.61 which is in excellent agreement with the value calculated using Equation 28. Equation 28 was found to be obeyed by several gases including CH_3OH vapor as shown in Figure 2. In the temperature range 453 K to 623 K, the variation of r with T(cat. ves.) is small ($0.58 < r < 0.62$), so a mean value r=0.60 was used in calculating the initial reactant pressure in this temperature range.

It should be pointed out that both methanol and formaldehyde were found to adsorb to the walls of the reaction enclosure with methanol being more strongly adsorbed than formaldehyde. For this reason, the methanol or formaldehyde vapor was not allowed to equilibrate in the

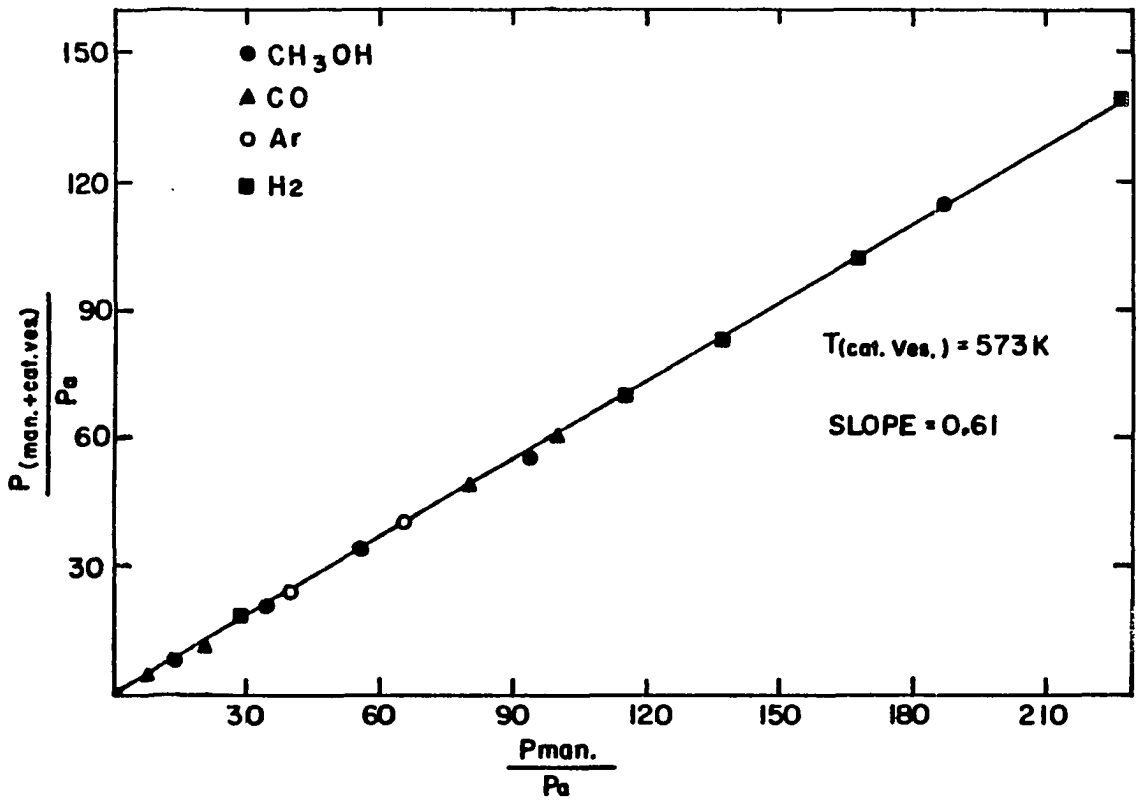

Figure 2. Plot of the relation: P(man. + cat. ves.) = rP(man.) at 573 K

manifold. This was done to avoid errors in estimating the initial reactant pressure over the catalyst that might be caused by desorption from the manifold walls after expanding the reactant vapor to the catalyst.

It was found during the course of this study that both CH_3OD and CD_3OD exchange rapidly their hydroxyl hydrogen with that of the hydroxyl group on the glass walls of the reaction enclosure as was indicated by the recorded mass spectra. In the case of CH_3OD, the recorded mass spectrum was identical to that of CH_3OH and no peak at $\frac{m}{e} = 33$ (CH_3OD) was detected. To eliminate this problem, the reaction enclosure together with the catalyst were treated with D_2O. Several cycles of dosing and pumping out of D_2O vapor were carried out until the peak of $\frac{m}{e} = 17$ (OH) became very negligible as compared to that of $\frac{m}{e} = 20$ (D_2O). The reaction enclosure was then baked out at about 650 K for about 12 hours.

Prior to each kinetic experiment, the catalyst was treated with about 67 Pa of O_2 at the reaction temperature for all the experiments carried out at $T \leq 513$ K. However, in the case of the kinetic experiments carried out at $T \geq 563$, the catalyst temperature was first lowered to about 523 K before admitting oxygen. This was done in order to have a common oxygen treatment for the low temperature and the high temperature kinetic experiments. In both cases, after admitting O_2, the catalyst temperature was raised to 623 K at a rate of 0.2 K s^{-1}. At 623 K, the oxygen was pumped out and heating was continued up to 673 K. Outgassing at this temperature lasted for 1.8×10^3 sec. The catalyst

temperature was then lowered to the reaction temperature. It should be mentioned that the termination of a kinetic experiment involved the evacuation of the gas phase over the catalyst before admitting oxygen. Mass spectrometric analysis of the gas phase over the catalyst at the end of the oxygen treatment revealed the presence of O_2, CO, CO_2, and H_2 as the major gas phase species.

In the absence of oxygen, the outgassing of the catalyst (after the termination of a CH_3OH kinetic run), while increasing the temperature up to 673 K, resulted in the formation of a zinc film on the cold parts of the catalyst vessel. This was noticeable for runs that involved about 100 Pa of methanol vapor. However, the oxygen treatment, as described above, was found to eliminate the catalyst reduction and resulted in fairly good experimental reproducibility. The ultrahigh vacuum valve, which separates the cold trap from the reaction enclosure, was valved off during the oxygen treatment. This was done in order to protect the electron multiplier of the mass spectrometer from oxygen exposure.

The variable leak value, shown in Figure 1, was left at the same setting during the course of this study. The setting was adjusted by using argon gas at a pressure of about 65 Pa. Over a period of about 1.8×10^3 sec., the argon pressure in the manifold remained almost constant and the residual gas pressure in the mass spectrometer chamber was below 5×10^{-3} Pa. While higher leak rates might improve the mass spectrometer sensitivity, the mass spectrometer assembly must be maintained under a vacuum of 5×10^{-3} Pa or better. Such a vacuum is necessary to prevent slow discharge of the radio frequency section and arcing

of the electron multiplier. The mass spectrometer was operated at a filament emission current of 1 mA and an electron energy of 70 eV.

Since the initial rates of product formation were measured during 120 sec. of reaction or less, the loss of a product due to leakage through the leak valve is negligible. In this case, the vacuum system used in this study was essentially a static reactor.

The decomposition of CH_3OH and/or CH_2O was followed by monitoring peaks at $\frac{m}{e} = 2$ (H_2), $\frac{m}{e} = 28$ (CO), and $\frac{m}{e} = 44$ (CO_2). The contribution of CO_2 to the $\frac{m}{e} = 28$ fragment was taken into consideration and was subtracted from the total signal of the $\frac{m}{e} = 28$ peak. The mass spectrum of pure CO_2 revealed that

$$\frac{h(\frac{m}{e} = 28)}{h(\frac{m}{e} = 44)} = 0.1,$$

where h = peak height. Consequently, in a mixture of CO and CO_2, the contribution of CO_2 to the $\frac{m}{e} = 28$ peak will be $(0.1)[h(\frac{m}{e} = 44)]$.

The initial rate of total hydrogen production during the decomposition of CH_3OD was determined by monitoring peaks at $\frac{m}{e} = 2$ (H_2), $\frac{m}{e} = 3$ (HD), and $\frac{m}{e} = 4$ (D_2). The sensitivity factors required for converting the mass spectrometer signal into Pa s^{-1} or *mol* s^{-1} were obtained by the direct calibration of the mass spectrometer against the capacitance manometer for H_2, D_2, CO, or CO_2. The sensitivity factor for HD was obtained by dosing a 1:1 mixture of H_2 and D_2 in the manifold followed by leaking to the mass spectrometer. The following reaction:

$$H_{2(g)} + D_{2(g)} = 2HD_{(g)} \qquad (29)$$

was found to be promoted by the walls of the reaction enclosure at room temperature. Probably the reaction took place via adsorption on a metal surface. The ionization gauge wires, although the gauge was off, might have catalyzed this reaction. However, rapid equilibration of H_2 and D_2 was observed when an electric discharge coil (Tesla coil) was brought close to the glass part of the manifold. The HD sensitivity factor was calculated as follows:

Equilibration at room temperature (~298 K) gives the following relation:

$$\frac{[P(HD)]^2}{P(H_2)\cdot P(D_2)} = K_{298} \tag{30}$$

Urey and Rittenberg [55] calculated a value of 3.27 for K_{298}, while Jones and Sherman [56] reported a value of 3.28 for K_{298}. A value of 3.28 was assumed for K_{298} in calculating the sensitivity factor of HD. Interestingly, it was found that the HD sensitivity factor obtained from knowledge of the equilibrium constant is equal to the arithmetic mean of the D_2 and H_2 sensitivity factors. It should be pointed out that only the total hydrogen production was of interest during the decomposition of CH_3OD. Whether the H_2-D_2 equilibration was attained or not is immaterial.

The initial rates used for evaluating the apparent activation energies were obtained by carrying out the reaction under consideration for 120 sec. The initial rate of product formation was then assumed to be the average amount of a product produced in 120 sec. The same procedure was also adopted in calculating the initial rates of CH_3OH

and CH_2O decomposition at 500 K. However, the initial rates of H_2, CO, and CO_2 production at 593 K were obtained by carrying out the kinetic experiment of CH_3OH decomposition for 60 sec.

To express the initial rates of H_2, CO, or CO_2 production in a form suitable for reasonable literature comparison, the following procedure was used for reporting the initial rates:

Initial rate of production of gas phase species "i" = R_i

$$R_i = \frac{P_i}{wARt}\left\{\frac{V(man.) + V(con.)}{T(man.)} + \frac{V(cat.\ ves.)}{T_r}\right\} \qquad (31)$$

Knowing that R = 8.32 m^3 Pa mol^{-1} K^{-1}, V(man.) = 1.06×10^{-3} m^3, V(con.) = 3.8×10^{-4} m^3, V(cat. ves.) = 6.0×10^{-4} m^3, A = catalyst specific surface area = 3.0×10^{3} m^2 Kg^{-1}, w = weight of catalyst used = 1.0×10^{-3} Kg, and T(man.) = ambient temperature ≈ 298 K, Equation 31 reduces to:

$$R_i = (4.01\times10^{-2})(4.83\times10^{-6} + \frac{6.0\times10^{-4}}{T_r})(\frac{P_i}{t})\ \text{mol}\ m^{-2}\ s^{-1} \qquad (32)$$

where P_i = pressure of gas phase species "i" in Pa ($P_i << 10^2$ Pa), t = reaction time in sec. ($t \leq 120$ sec.), and T_r = reaction temperature in degrees Kelvin.

Materials

All of the gases used in the kinetic and isotopic studies were research grade gases. D_2 (99.5%), $C^{12}O^{16}$ (99.97%), $C^{12}O_2^{16}$ (99.998%), Ar (99.9995%), and O_2^{16} (99.995%) were purchased from the Linde division of Union Carbide. H_2 (99.999%) was purchased from Matheson Gas Products. $C^{13}O^{18}$ (90% C^{13}, 95% O^{18}) was purchased from Prochem

Isotopes. All of these gases were purchased in pyrex glass bulbs with breakable seals. Their purities were confirmed mass spectrometrically before use.

D_2O (99.7%) was purchased from Merck & Co., Inc. in a capped glass bottle. Chromotropic acid (analytical reagent grade) was purchased from Aldrich Chemical Co. as a hydrated sodium salt (4,5-dihydroxynaphthalene-2,7-disulfonic acid, disodium salt dihydrate). Paraformaldehyde (purified trioxymethylene) was purchased from Fisher Scientific Co. The formaldehyde was prepared by the thermal depolymerization of paraformaldehyde at about 350 K in an apparatus similar to that used by Spence and Wild [54]. An edible white mineral oil was used as a heat-transferring medium in the preparation of the formaldehyde. The formaldehyde vapor, after leaving the depolymerization flask, was condensed at 195 K. It was then frozen at 77 K in order to pump out any CO and/or H_2 that might have resulted during the depolymerization step of paraformaldehyde. After this treatment, the formaldehyde was stored at 195 K in the liquid phase. This liquid was used as a source of gas monomeric formaldehyde. Mass spectrometric analysis of the prepared monomer provided cracking patterns that agreed well with literature data [57]. Three major peaks were observed at $\frac{m}{e} = 30$ (CH_2O), $\frac{m}{e} = 29$ (CHO), and $\frac{m}{e} = 28$ (CO). The major peak was that of $\frac{m}{e} = 29$. No peaks were observed beyond $\frac{m}{e} = 32$. This observation implies the absence of the potential impurities methyl formate and trioxane.

The CH_3OH used in the kinetic study was of spectral quality and

was purchased from Burdick & Jackson Laboratories, Inc. The CH_3OH sample used in this study was purified by bulb-to-bulb vacuum distillation before use. The sample was loaded onto the vacuum system in a pyrex bulb with breakable seal. CH_3OD (>99.5%) and CD_3OD (99.5%) were purchased from the Alfa division of Ventron Corporation. CH_3OD was delivered in a capped bottle, while CD_3OD was delivered in an ampule. The two deuterated methanols were transferred from their original containers into predeuterated glass vials. The handling was carried out in a dry box under argon atmosphere. The deuteration of the vials was carried out by rinsing them with D_2O several times. The vials were capped with rubber caps in order to allow the use of a micro syringe as means of transferring the deuterated methanols from the vials to the vacuum system.

After being loaded in the vacuum system, the three methanols gave mass spectra in agreement with those reported by Lester et al. [58]. The only exception was the abundance of the $\frac{m}{e} = 28$ fragment. The three methanols gave a higher abundance (about 4 times) compared to that of reference [58]. Possible contamination with N_2 was considered and was ruled out on the basis of the similarity between the mass spectra of CH_3OH before and after several thaw-and-freeze cycles. A possible explanation for the high abundance of the $\frac{m}{e} = 28$ fragment (CO), is a catalytic decomposition of methanol on the hot filament of the ionizer assembly inside the mass spectrometer chamber.

The zinc oxide sample, used as a catalyst in this study, was purchased from the New Jersey Zinc Company. The sample was specified

by the manufacturer as ZnO SP 500 ultra grade (99.99%) and was manufactured by burning zinc metal in oxygen. The manufacturer's certificate of analysis of the ZnO sample (freshly ignited at 823 K to 873 K for 30 min.) indicated that sulfur is the major impurity (total sulfur as SO_3 = 0.002%). The elements Fe, Cu, Mn, Pb, As, Cd, Al, Ca, Na, Si, and Mg were reported as trace impurities (<100 PPM). A check on the supplied certificate of analysis was carried out by high dispersion emission spectrographic analysis and the energy dispersive x-ray fluorescence spectroscopic techniques. The results were in agreement with those reported by the manufacturer.

The BET surface area of the ZnO sample was found to be 3.0×10^3 m^2 Kg^{-1}. The amount of ZnO catalyst used throughout this study was 1.0×10^{-3} Kg. All the kinetic and isotopic results were obtained on the same batch of the catalyst. Before being placed in the catalyst vessel, the ZnO catalyst sample was heat-treated at 823 K for 90 min. After this thermal treatment, the catalyst sample was never subjected to temperatures beyond 673 K.

The helium gas, used for the detection of formaldehyde in the flow reactor, was a high-purity helium and was supplied by the U.S. Department of the Interior, Bureau of Mines, Amarillo, Texas.

RESULTS AND DISCUSSION

Temperature Dependence of CH_3OH Decomposition

The early stages of the work to be described here involved a preliminary study aimed at the establishment of the temperature dependence of CH_3OH decomposition over ZnO. The study has indicated that a slow evolution of H_2 gas commences at 423 K, while a fast CH_3OH decomposition takes place at 633 K. At the latter temperature, the formation of H_2 was accompanied by evolution of CO, CO_2, and formation of a Zn film on the cold part of the catalyst vessel. On the other hand, no measurable gas phase thermal decomposition of CH_3OH was detected up to 633 K. This observation is in accordance with the work of Fletcher [59], who reported measurable CH_3OH thermal decomposition rates at $T \geq 900$ K. This implies that decomposition of methanol, as reported in the present study, at $T \leq 633$ K over ZnO is solely a catalytic decomposition.

To identify the temperature at which CO and/or CO_2 is being produced via the catalytic decomposition of CH_3OH, some nonisothermal decomposition experiments were carried out. Formation of both CO and CO_2 commenced at $T \geq 550$ K. Repeated isothermal decomposition experiments confirmed this result. It was also observed that CO and CO_2 were produced concurrently.

Another interesting result obtained from the preliminary study is the observation that about 15% of the methanol hydrogen is being released in the temperature range 453 K to 513 K without being accompanied by CO and/or CO_2. This observation suggests that the decomposition of

methanol is probably occurring in stages.

In an attempt to identify the first step in methanol decomposition, the decomposition of CH_3OH was compared with that of CH_3OD in the temperature range 453 K to 513 K. The decomposition of CH_3OD resulted in the formation of H_2, HD, and D_2. Furthermore, the initial rates of hydrogen evolution were the same for the two methanols. In the case of CH_3OD, the isotopic scrambling indicates that both the methyl and hydroxyl groups are responsible for hydrogen evolution. Formation of H_2, HD, and D_2 has also been reported by Goodman and his coworkers during the decomposition of CH_3OD on Ru [60]. The observation that both CH_3OH and CH_3OD have the same decomposition rates suggests that the dissociation of the hydroxyl hydrogen, during the adsorption step on the catalyst surface, is unlikely to be a rate-determining step. A similar remark has been made by McKee [61] for the decomposition of methanol on Pt. The labile nature of the hydroxyl hydrogen in the methanol molecule has been demonstrated by carrying out the hydrogen exchange reaction between D_2 and CH_3OH on Ni [62], ZnO, and other metal films [63] whereby CH_3OD was the major deuterated methanol. This was confirmed by mass spectrometric and IR measurements. Evidence and conclusions concerning the hydrogen isotope effect will be discussed later.

On the basis of the aforementioned observations, the kinetics of methanol decomposition was studied over two temperature ranges, 453 K to 513 K and 563 K to 613 K. These two temperature ranges will be referred to as the low temperature and the high temperature ranges, respectively. The first range was chosen to study the kinetics of H_2

evolution, while the second range was chosen to study the kinetics of CO and CO_2 evolution.

Detection of CH_2O

In his pioneering study on the catalytic decomposition of CH_3OH on ZnO, Dohse [41] pointed out that the decomposition proceeds via a scheme of two first-order consecutive reactions. The first step is the dehydrogenation of CH_3OH into H_2 and CH_2O, and the second step is the decomposition of CH_2O into CO and H_2. The presence of CH_2O as an intermediate during the decomposition of CH_3OH is not well-documented. Some researchers who tackled the kinetics of CH_3OH decomposition on ZnO adopted Dohse's scheme [42-45, 64, 65], while others made no mention of CH_2O [46, 66, 67].

In the present study, formation of CH_2O via the catalytic decomposition of CH_3OH on ZnO was confirmed for both a flow reactor and a static one. In the case of the flow reactor, a chemical method was used to test for CH_2O. The effluent gas, after leaving the catalyst bed, was passed through a flask containing distilled water. Addition of chromotropic acid to the test solution resulted in the formation of a purple color, which is indicative of the presence of CH_2O. Formation of CH_2O was confirmed at 523 K and 573 K. Chromotropic acid has been suggested as an analytical reagent for microdeterminations of formaldehyde [68]. On the other hand, formation of CH_2O in the ultrahigh vacuum system (static reactor) was confirmed by means of a mass spectrometer. This was done by observing the height ratio of two CH_3OH peaks, namely,

$h(\frac{m}{e} = 29)/h(\frac{m}{e} = 31)$. The mass spectrum of CH_3OH has its intense peak at $\frac{m}{e} = 31$ while CH_2O has its intense peak at $\frac{m}{e} = 29$. Consequently, the mass spectrum of a mixture of CH_3OH and CH_2O should give the result $[h(\frac{m}{e} = 29)/h(\frac{m}{e} = 31)] > 1$. It was found in this study that both CH_3OH and CH_2O give rise to an intense peak at $\frac{m}{e} = 28$. The fact that CO also gives rise to a peak at $\frac{m}{e} = 28$, which is used to monitor CO, demanded the condensation of both CH_3OH and CH_2O before reaching the mass spectrometer. This trapping made the detection of CH_2O more difficult during the course of a CH_3OH decomposition experiment. However, when the condensed vapor was released from the trap which separates the leak valve from the mass spectrometer, the recorded mass spectrum revealed an intense peak at $\frac{m}{e} = 29$ with the ratio $[h(\frac{m}{e} = 29)/h(\frac{m}{e} = 31)] > 1$. This observation indicated the presence of CH_2O as a reaction product and was further substantiated by recording a mass spectrum for a mixture of CH_3OH and CH_2O leaked directly to the mass spectrometer.

Formation of CH_2O via CH_3OH decomposition has been reported during CH_3OH thermal decomposition [59], catalytic decomposition of CH_3OH on ZnO [43, 69], on Ru [60], on W [70], and on Au [71]. CH_2O can also be obtained via the partial oxidation of CH_3OH on Cu [72], on Ag, and on MoO_3-Fe_2O_3 [28]. The last three catalysts are the traditional industrial catalysts used for the manufacture of CH_2O via the partial oxidation of CH_3OH [28].

Catalyst Reduction and Evolution of CO_2

As mentioned earlier, exposure of ZnO to CH_3OH at 633 K resulted in the formation of a zinc film on the cold parts of the catalyst vessel.

Formation of CO_2 was always observed whenever CH_3OH was brought in contact with ZnO at T ≥ 550 K. However, an overnight pumping on a ZnO sample at 673 K did not result in the formation of a zinc film. This observation rules out the possibility of a surface sublimation or a thermal decomposition of ZnO. A surface reduction might take place by H_2 and/or CO during a methanol decomposition experiment. To clarify this matter, a series of experiments was carried out. This included interactions of ZnO with $C^{13}O^{18}$, O_2^{16}, H_2, $C^{12}O^{16}$, CH_3OH and the effect of oxygen treatment on the catalyst activity and CO_2 production.

Interaction of $C^{13}O^{18}$ with ZnO

In a series of runs, 7 Pa of $C^{13}O^{18}$ was admitted to ZnO at different temperatures. The results at 573 K and 623 K are shown in Figure 3. The mass spectrum of $C^{13}O^{18}$, before admitting to the catalyst, revealed the major peak at $\frac{m}{e} = 31$. Small peaks at $\frac{m}{e} = 30$, 29, and 28 were also observed. These small peaks are probably due to the presence of CO isotopic impurities, i.e., $C^{12}O^{18}$, $C^{13}O^{16}$, and $C^{12}O^{16}$, respectively. The mass spectrum of the gas phase over the catalyst revealed that peaks of $\frac{m}{e} = 31$ and $\frac{m}{e} = 30$ were decreasing with time, while peaks of $\frac{m}{e} = 29$ and $\frac{m}{e} = 28$ were increasing. This behavior can be explained if we assume the following oxygen exchange reactions:

$$C^{13}O^{18}_{(g)} + ZnO^{16}_{(s)} = ZnO^{18}_{(s)} + C^{13}O^{16}_{(g)} \qquad (33)$$

$$C^{12}O^{18}_{(g)} + ZnO^{16}_{(s)} = ZnO^{18}_{(s)} + C^{12}O^{16}_{(g)} \qquad (34)$$

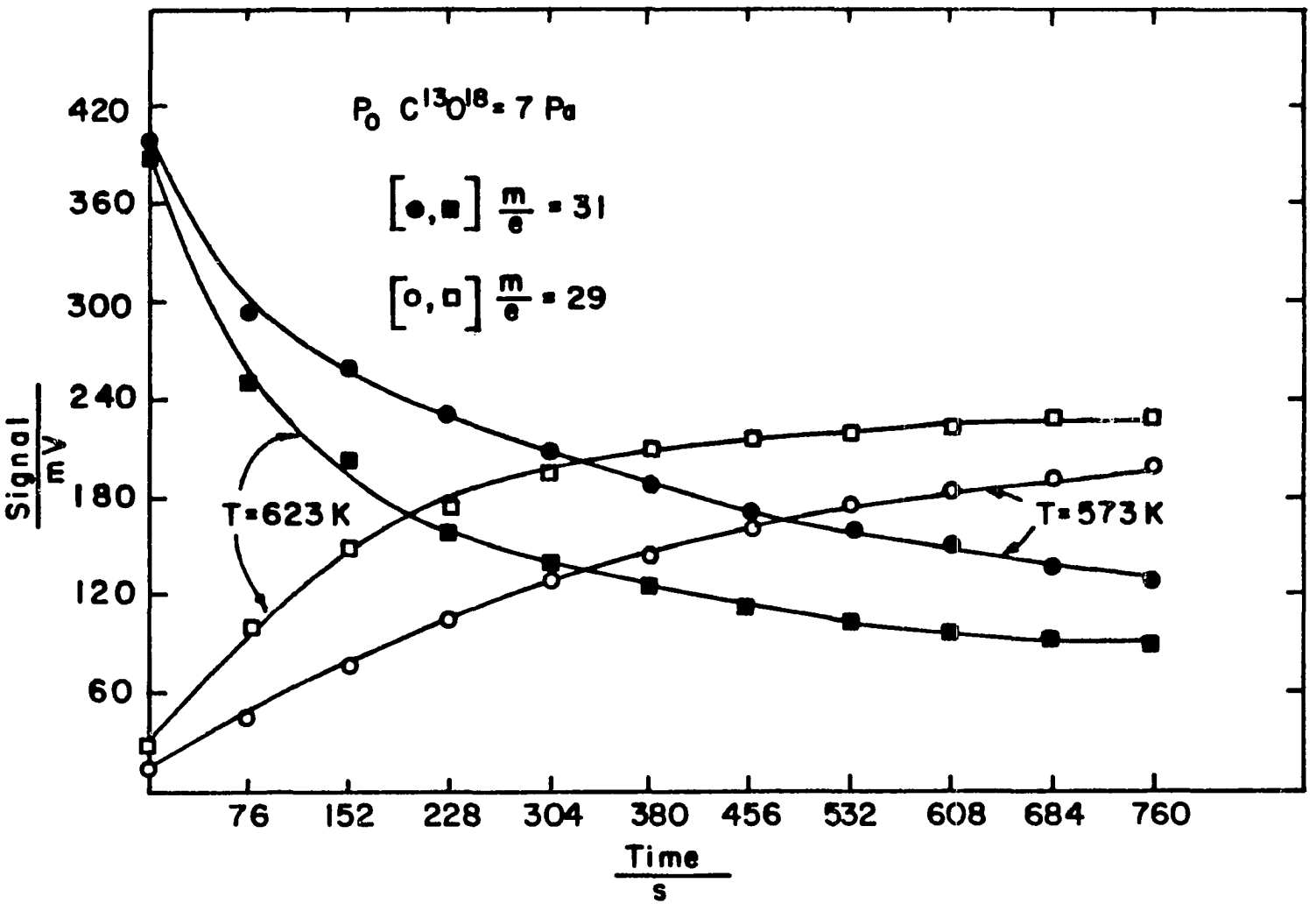

Figure 3. Oxygen exchange between $C^{13}O^{18}$ and ZnO^{16}

$$C^{13}O^{16}_{(g)} + ZnO^{16}_{(s)} = ZnO^{16}_{(s)} + C^{13}O^{16}_{(g)} \quad (35)$$

$$C^{12}O^{16}_{(g)} + ZnO^{16}_{(s)} = ZnO^{16}_{(s)} + C^{12}O^{16}_{(g)} \quad (36)$$

The last three reactions are believed due to isotopic impurities of CO. Of course, the last two reactions result in no chemical change. This scheme suggests that only $C^{13}O^{18}$ and $C^{12}O^{18}$ will be depleted from the gas phase, while $C^{13}O^{16}$ and $C^{12}O^{16}$ will increase with time. Indeed this was the actual behavior of the peaks as indicated by the mass spectrometer. Since $C^{12}O^{18}$ is an impurity in $C^{13}O^{18}$, which has 90% C^{13} and 95% O^{18}, only the changes in height of the $\frac{m}{e} = 31$ and $\frac{m}{e} = 29$ are shown in Figure 3. The fact that no peak was detected at $\frac{m}{e} = 47$ ($C^{13}O^{18}O^{16}$) during the interaction of $C^{13}O^{18}$ with ZnO is an indication that CO_2 was not being produced in these experiments. The oxygen exchange reaction between ZnO and $C^{13}O^{18}$ was used as a means of enriching the ZnO surface with O^{18} for further studies. Figure 3 also shows that the exchange reaction is enhanced by raising the temperature. The oxygen exchange reaction between ZnO and CO has been reported by Carnisio et al. [73].

Interaction of O_2^{16} with O^{18}-enriched ZnO

Another experiment, which supplements the previous oxygen exchange reactions, consisted of treating the O^{18}-enriched ZnO with O_2^{16} gas (at T = 623 K and 66 Pa O_2) after pumping out the $C^{13}O^{18}$ gas. After two hours of O_2^{16} interaction with zinc oxide, a mass spectrum was recorded which revealed the existence of the following gas phase species:

O_2^{16} ($\frac{m}{e}$ = 32), $O^{16}O^{18}$($\frac{m}{e}$ = 34), $C^{13}O^{16}$ ($\frac{m}{e}$ = 29), $C^{12}O^{16}$ ($\frac{m}{e}$ = 28), $C^{12}O^{18}$($\frac{m}{e}$ = 30), $C^{12}C_2^{16}$($\frac{m}{e}$ = 44), $C^{13}O_2^{16}$($\frac{m}{e}$ = 45), and $C^{12}O^{18}O^{16}$ ($\frac{m}{e}$ = 46). No peaks were observed for $C^{12}O_2^{18}$, $C^{13}O^{16}O^{18}$, $C^{13}O^{18}$, and $C^{13}O_2^{18}$. The absence of the last three species implies that no $C^{13}O^{18}$ was left in a molecular form on the catalyst surface after evacuation at 623 K prior to the admission of O_2^{16} gas. On the other hand, formation of the other C-containing species, detected after the oxygen treatment, might be attributed to the reaction of oxygen with a carbon deposit on the catalyst surface. This deposit may be due to a dissociative chemisorption of $C^{13}O^{18}$ and $C^{12}O^{16}$ during the exposure of ZnO to $C^{13}O^{18}$ and CH_3OH prior to the oxygen treatment. This result also demonstrates the value of the oxygen treatment after each methanol decomposition experiment for removing possible carbon residues, and it was used consistently throughout this study.

Interaction of H_2 with O^{18}-enriched ZnO

The O^{18}-enriched ZnO was exposed to 6.3 Pa of H_2 gas at 623 K for a period of 1×10^3 sec. At the end of the experiment, the decrease in $P(H_2)$ amounted to 8% of the initial pressure. This decrease in H_2 pressure can be explained in two ways. First, $H_{2(g)}$ might be consumed via the reduction reaction

$$H_{2(g)} + ZnO_{(s)} = H_2O_{(g)} + Zn_{(g)} \quad (37)$$

$$Zn_{(g)} = Zn_{(s)} \text{ (condensation on cold parts of system)} \quad (38)$$

$$H_2O_{(g)} + ZnO_{(s)} = HO\text{-}Zn - O\text{-}H \quad (39)$$

The second alternative is that $H_{2(g)}$ is being consumed via an adsorption process, i.e.,

$$H_{2(g)} + ZnO_{(s)} = H - Zn - OH \qquad (40)$$

The absence of a Zn deposit and of a peak at $\frac{m}{e} = 20$ (H_2O^{18}) rules out the occurrence of the reduction reaction.

Adsorption of H_2 on ZnO and its desorption have been repeatedly investigated by many researchers. The identity and the number of surface species have been the subject of an extended polemic in the literature [74-76]. In early works [77, 78], two types were postulated, A and B. Type A was said to be a low temperature chemisorption which occurs up to 423 K, and Type B is a high temperature one. Eischens et al. [74], who were the first to report on the IR of H_2 adsorption on ZnO, indicated that at about 300 K there may be as many as four different types of hydrogen surface species. The same number of surface species was observed by Narvaez and Taylor [79] in the range 273 K to 673 K. Scholten and Van Montfoort [80] reported three types at room temperature: (a) reversible and active in IR, (b) reversible and inactive in IR, and (c) irreversible adsorption. On the other hand, Dent and Kokes [76, 81], Chang and Kokes [82], Chang et al. [83], and Dixon et al. [84] reported the existence of the following types: (a) type I reversible, occurring rapidly at room temperature, active in IR; (b) type II irreversible, occurring at room temperature, inactive in IR; (c) type III reversible, occurring at 78 K, active in IR; and (d) type IV, a high temperature chemisorption.

One of the complicating factors in determining the number of the

hydrogen surface species is the fact that the so-called "high temperature" chemisorption cannot be excluded at room temperature. In a recent temperature-programmed desorption study, Baranski and Galuszka [85] claimed the existence of six or seven types of hydrogen species on ZnO. Using the notation of Dent and Kokes [76], the reversible type occurring at room temperature (type I) is attributed to a dissociative chemisorption of H_2 on ZnO pair sites giving bands at 1710 and 3500 cm^{-1}, due to ZnH and ZnOH species respectively as was established by the work of Eischens et al. [74]. According to Kokes and Dent [86], the hydrogen that gives rise to these bands is limited to 5 to 10% of the surface. Type I hydrogen was found to exchange readily with D_2 gas [86, 87]. Recently Griffin and Yates [88] found that type I desorbs in two stages characterized by maxima in the TPD (temperature programmed desorption) spectra at 240 K and 300 K. A recent IR study [89] resulted in the assignment of broad bands near 3400 and 1475 cm^{-1} to dissociated H atoms bridged between neighboring oxygen and zinc ions, respectively. This is believed to be type II hydrogen species. Type III species is believed to be molecularly adsorbed hydrogen, which produces a band at 4019 cm^{-1} [83].

With regard to the possible reduction of ZnO by H_2, Kubokawa [90] concluded that hydrogen desorption is reversible up to 673 K. The same conclusion was also arrived at by Garner [91]. On the other hand, Hart and Sebba [92] found that a reduction took place on ZnO, ZnO doped with Li_2O, and ZnO doped with Ga_2O_3 at all H_2 pressures in the range 523 K to 593 K. The reduction was evidenced by Zn metal formation, darkening

of the adsorbent, and failure of the pressure versus time curve to flatten out to a constant value.

In the present study, reduction of ZnO by H_2 did not occur under the experimental conditions used, and the catalyst pretreatment with H_2 (as will be discussed later) did not affect the catalyst activity towards methanol decomposition.

Interaction of $C^{12}O^{16}$ with O_2-treated ZnO

Several experiments of $C^{12}O^{16}$ interaction with O^{18}-enriched ZnO were carried out with the objective of detecting $C^{12}O_2^{16}$ and $C^{12}O^{16}O^{18}$ (if any). The ZnO surface was first enriched by O^{18} by carrying out the oxygen exchange reaction between $C^{13}O^{18}$ and ZnO. Prior to admitting $C^{12}O^{16}$, the O^{18}-enriched ZnO was cleaned with O_2^{16} under conditions similar to those used for cleaning the catalyst after a CH_3OH decomposition experiment. A typical result is shown in Figure 4, which reveals that no carbon dioxide was produced. In this figure, the signal corresponding to $\frac{m}{e} = 44$ represents the residual amount of $C^{12}O_2^{16}$ in the system. The constancy of the $\frac{m}{e} = 44$ peak throughout the experiment rules out the occurrence of the following reactions:

$$C^{12}O^{16}_{(g)} + O^{16}_{(a)} = C^{12}O^{16}_{2(g)} \tag{41}$$

$$2C^{12}O^{16}_{(g)} = C^{12}_{(s)} + C^{12}O^{16}_{2(g)} \tag{42}$$

$$C^{12}O^{16}_{(g)} + ZnO^{16}_{(s)} = Zn_{(g)} + C^{12}O^{16}_{2(g)} \tag{43}$$

The absence of a peak at $\frac{m}{e} = 46$ ($C^{12}O^{16}O^{18}$) implies that a surface

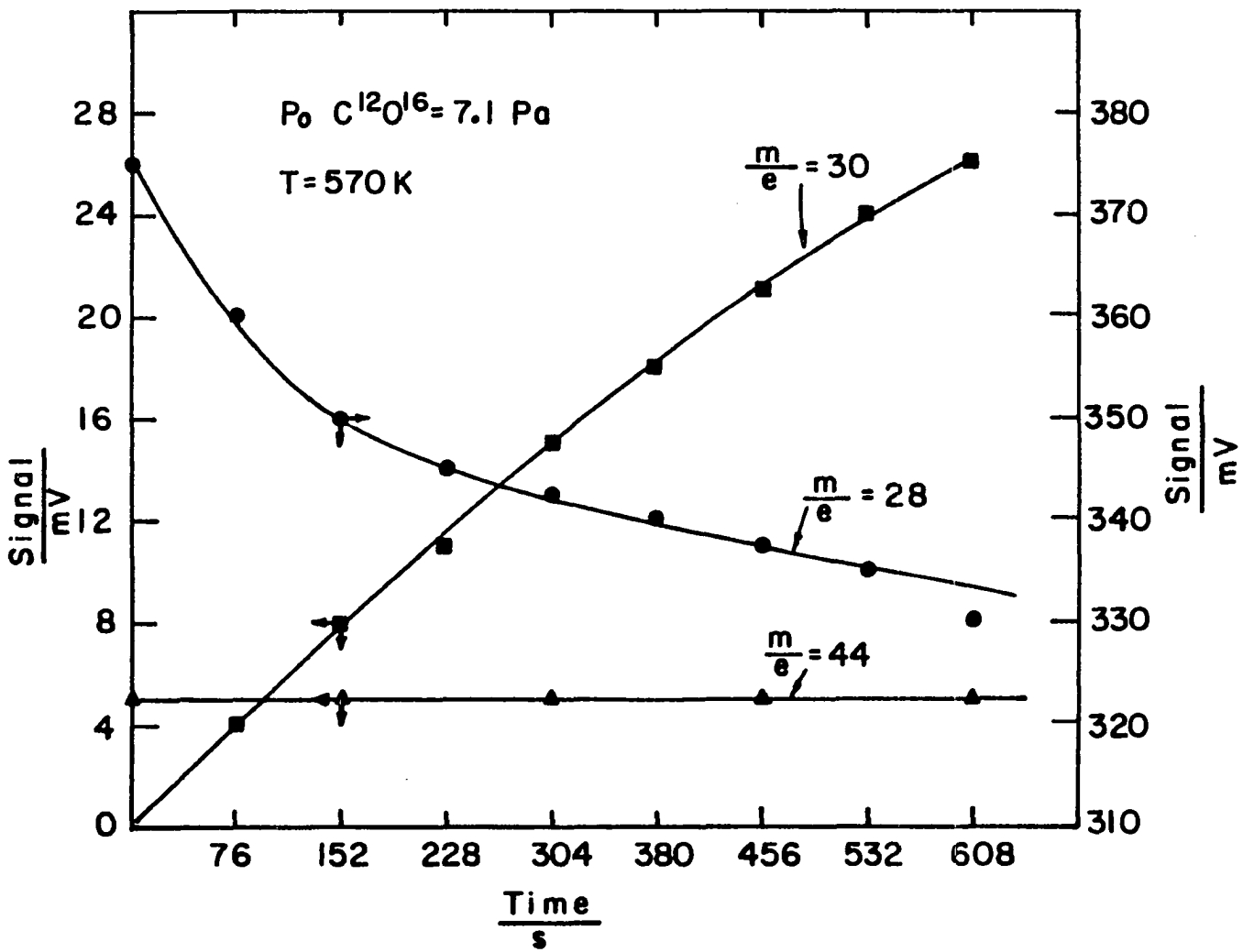

Figure 4. Oxygen exchange between $C^{12}O^{16}$ and ZnO^{18}. Signal at $\frac{m}{e} = 44$ represents residual CO_2

reduction (similar to reaction 43) involving $C^{12}O^{16}$ and ZnO^{18} did not occur.

However, Figure 4 indicates that $C^{12}O^{16}$ does interact with ZnO via the following oxygen exchange reaction:

$$C^{12}O^{16}_{(g)} + ZnO^{18}_{(s)} = ZnO^{16}_{(s)} + C^{12}O^{18}_{(g)} \qquad (44)$$

This exchange reaction explains the decrease in the height of $\frac{m}{e} = 28$ peak and the increase in the height of $\frac{m}{e} = 30$ peak, as shown in Figure 4. Figure 4 also shows that about two-thirds of the consumed $C^{12}O^{16}$ reappear in the gas phase as $C^{12}O^{18}$. The remainder is probably lost via adsorption processes on the catalyst surface.

A noteworthy observation is that even after several O_2^{16} treatments at 623 K, the ZnO is still retaining O^{18}. This might imply that $C^{13}O^{18}$ is probably more efficient than O_2^{18} in enriching ZnO with O^{18}.

The adsorption of CO on ZnO has been the subject of numerous investigations. Garner [91] and Kubokawa [93] have pointed out that two types of chemisorption exist. The first type is a nonactivated, reversible adsorption occurring at room temperature. The second type is a high temperature activated chemisorption, which partially desorbs as CO_2. Measurements of the interaction of CO with ZnO powders by infrared spectroscopy have shown that the CO stretching frequency increases upon adsorption [94-98] contrary to its general behavior for organometallic compounds. A carbonate-like structure has been detected by IR measurements on ZnO [97-99].

Using UPS (ultraviolet photoelectron spectroscopy) and work function

measurements on (0001), (000$\bar{1}$), (10$\bar{1}$0), and (11$\bar{2}$0) low-index surfaces of ZnO, Gay et al. [100] concluded that the low temperature adsorption occurs on zinc sites. Hotan et al. [101] have also studied the CO adsorption on the nonpolar (10$\bar{1}$0) ZnO surface by means of electrical conductivity, TDS (temperature desorption spectroscopy), AES (Auger electron spectroscopy), EELS (electron energy loss spectroscopy), and LEED (low energy electron diffraction) techniques. They concluded that CO is irreversibly adsorbed even at room temperature. In conclusion, it seems that the low temperature CO adsorption on ZnO occurs on zinc sites via the carbon end of the CO molecule with negligible π-back donation from the metal to the π^* orbital of the CO molecule [100]. The high temperature adsorption is believed to occur on the oxide ions [91], which might account for the appearance of carbonate structures and the desorption of CO as CO_2.

In the present study, no CO_2 was detected during the interaction of CO with ZnO under conditions similar to those used in the kinetic study of CH_3OH decomposition on ZnO. Besides the oxygen exchange between CO and ZnO, the present study indicates that some dissociative adsorption is occurring. This leads to the formation of a carbon layer, which is removable as CO and/or CO_2 upon treating the catalyst with O_2 gas at about 623 K.

Decomposition of CH_3OH over O^{18}-enriched ZnO

Since the interaction of both $C^{13}O^{18}$ and $C^{12}O^{16}$ with ZnO did not result in the formation of any CO_2 under conditions similar to those

encountered in CH_3OH decomposition, where CO_2 is observed, CO_2 must come via the decomposition of a surface species which results from the interaction of CH_3OH with ZnO. Formate ion, HCOO (ads.), is a species likely to exist on the ZnO surface with the extra oxygen coming from ZnO. Formate resulting from the dissociation of HCOOH on ZnO [102] or from the coadsorption of H_2 and CO_2 on ZnO [103] yields CO and/or CO_2 upon decomposition, suggesting that CO_2 observed in CH_3OH decomposition may result from a formate intermediate.

Several infrared spectroscopic studies on the adsorption of CH_3OH on metal oxides confirmed the formation of a formate-like structure on an oxide surface. Greenler [104] identified three surface species from the adsorption of CH_3OH on Al_2O_3: (a) weakly-bound layer of liquid CH_3OH removable by evacuation at 308 K; (b) surface methoxide species at 308 K to 703 K; and (c) a formate-like structure at 443 K to >673 K. The identifications were confirmed with isotopic band shifts using CH_3OD, CD_3OH, and $C^{13}H_3OH$. Similar observations were also reported by Kagel [105] for the adsorption of C_1 to C_4 normal alcohols on γ-Al_2O_3, by Unland [106] for the decomposition of CH_3OH on alkali metal x-type zeolites, and by Thornton and Harrison [107] during CH_3OH decomposition on SnO_2. However, the room temperature adsorption of CH_3OH on ZnO resulted only in the formation of hydroxyl and methoxide species and no formate species were detected in the work of Nagao and Morimoto [108]. On the other hand, Herd et al. [66] and Ueno et al. [46] reported that they detected and studied the decomposition of both the methoxide and the formate species during the oxidation of CH_3OH [66] and its decomposition on ZnO [46].

To demonstrate that the formation of CO_2 during CH_3OH decomposition on ZnO requires the participation of an oxygen species from the ZnO lattice, an experiment was carried out to enrich ZnO with O^{18} via the oxygen exchange reaction

$$C^{13}O^{18}_{(g)} + ZnO^{16}_{(s)} = C^{13}O^{16}_{(g)} + ZnO^{18}_{(s)}$$

The above supposition, i.e., participation of ZnO to produce CO_2 through CH_3OH decomposition, is plausible if, during the course of CH_3OH decomposition over the O^{18}-enriched ZnO, the gas phase species $C^{12}O^{16}O^{18}$ ($\frac{m}{e} = 46$), and $C^{12}O^{18}$ ($\frac{m}{e} = 30$), together with the expected $C^{12}O_2^{16}$ ($\frac{m}{e} = 44$), and $C^{12}O^{16}$ ($\frac{m}{e} = 28$) are obtained. To accomplish this, a series of CH_3OH decomposition experiments was carried out over the O^{18}-enriched ZnO at 573 K with $P(CH_3OH)$ = 10.8 Pa. Each run lasted about 1.2×10^3 sec. and resulted in about 50% carbon conversion into carbon monoxide and carbon dioxide. A typical result is shown in Figure 5, which indicates that besides the usual oxides CO_2 ($\frac{m}{e} = 44$) and CO ($\frac{m}{e} = 28$), new carbon oxides appeared. These new carbon oxides are $C^{12}O^{16}O^{18}$ ($\frac{m}{e} = 46$) and $C^{12}O^{18}$ ($\frac{m}{e} = 30$). These observations confirm the supposition that the formation of CO_2 requires oxygen participation from the ZnO lattice, probably via a formate species.

Another interesting observation evident in Figure 5 is the leveling off of CO_2 despite the continuous evolution of CO. The same behavior was also exhibited by the decomposition of CD_3OD on ZnO^{16} at 588 K as shown in Figure 6. In both cases, the maximum carbon conversion into CO_2 amounted to about 20%. The amount of CO_2 produced in each case was

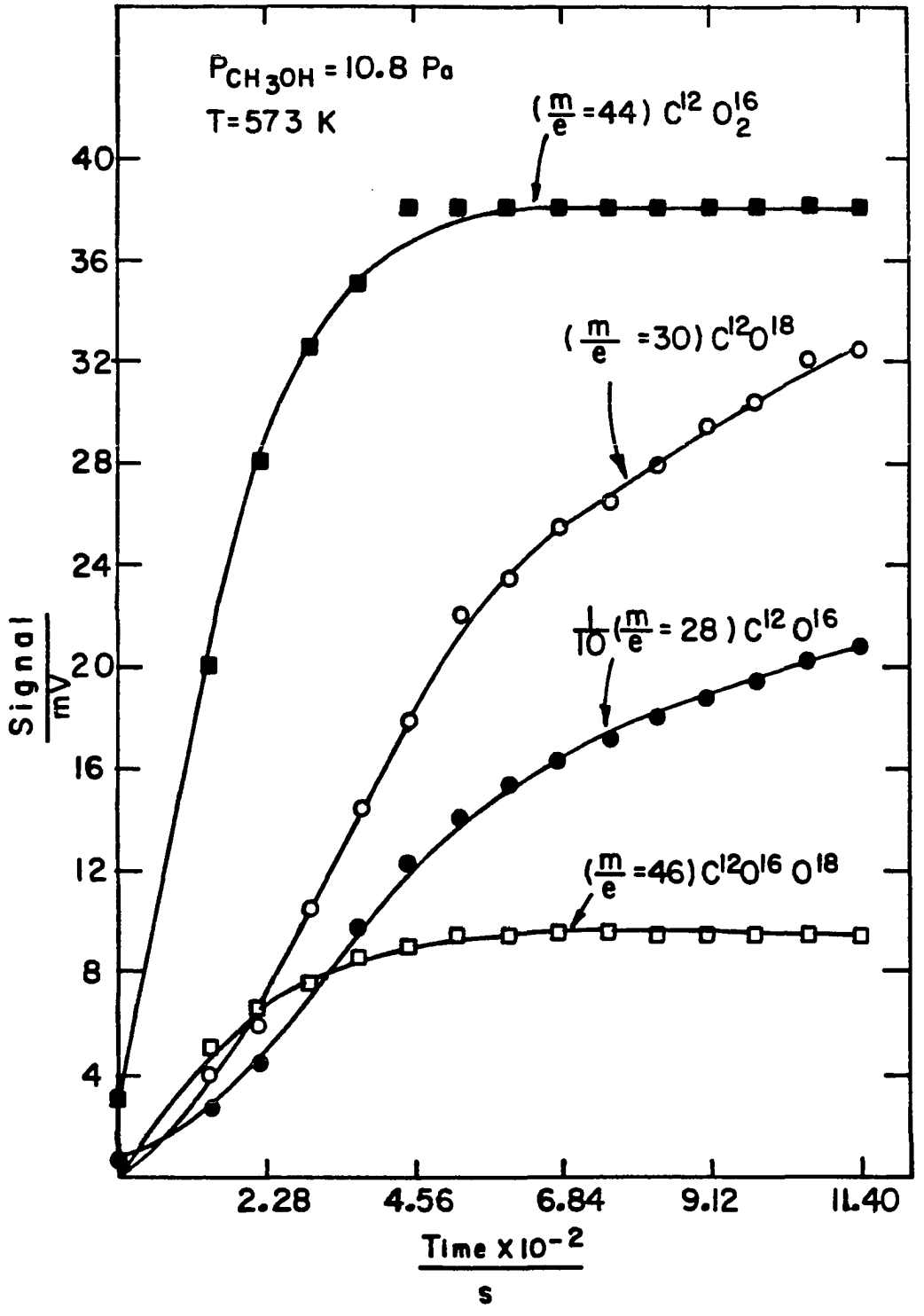

Figure 5. Formation of carbon oxides during CH_3OH decomposition on O^{18}-enriched ZnO

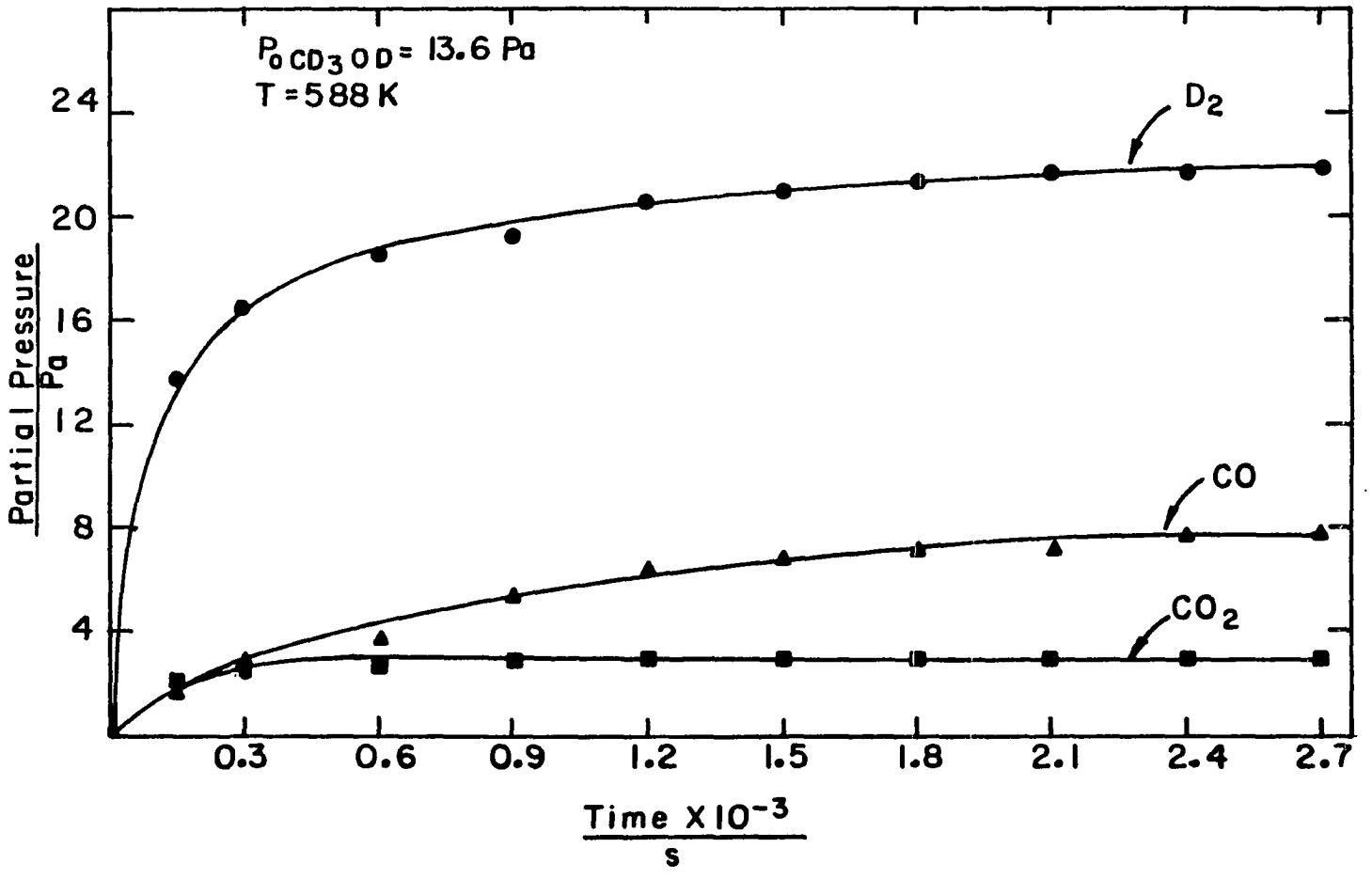

Figure 6. Decomposition of CD_3OD over ZnO

estimated to be 1.9×10^{-6} mol. Assuming that the surface atom density of the oxide ions is 5×10^{14} atom cm^{-2}, and knowing the total surface area of the catalyst to be 3 m^2, the fraction of the surface oxygen removed as CO_2 was estimated to be 0.08.

Figures 5 and 6 also suggest that the formation of CO_2 is a side reaction which levels off during the course of methanol decomposition on ZnO. The leveling off could be due to a charge accumulation, Zn^{2+}, on the catalyst surface due to consumption of the oxide ions via a surface reduction reaction. This charge accumulation inhibits further depletion of the oxide ions from the surface, and consequently the CO_2 production levels off. A similar phenomenon was encountered by Hotan et al. [101]. They found that the increase in the ZnO surface conductivity, after admission of CO onto ZnO, attains a constant value within about 3×10^2 sec. This was explained on the basis of the formation of a negatively-charged species, similar to a CO_2 ion-molecule, accompanied by the formation of an oxygen vacancy. The slow diffusion of the vacancy at $T < 500$ K into the bulk inhibits further surface reduction.

In the present study, the total initial rate of carbon oxide production, $R(CO) + R(CO_2)$, was taken as a measure of the total decomposition of the C-containing precursor.

Evolution of CO_2, during the course of CH_3OH decomposition on ZnO and its derivatives, has been reported by Tsuchiya and Shiba [67], Uchida and Ogino [69], Cheng and Kung [109], and Ueno et al. [46]. The only reported explanation for CO_2 formation is that of Ueno et al. [46]. They propose that CO_2 is formed from the reaction of a gas phase

CH_3OH molecule with a surface formate species. In the absence of gas phase CH_3OH, the formate species decomposes solely into CO.

To test the relevance of gas phase CH_3OH, a decomposition experiment was interrupted twice by pumping out the gas phase over the catalyst as shown in Figure 7. The partial pressure of CO_2, produced during CH_3OH decomposition, responded to pumping, i.e., decreased during the pumping out of the gas phase (60 sec. each). The behavior of CO_2 pressure after the first pumping and its leveling off after the second pumping cycle indicate that CO_2 formation is more likely to be occurring via a surface reaction. The time at which the CO_2 pressure levels off (about 450 sec.) and the total amount produced in this experiment, as estimated from Figure 7 including amount pumped out, are essentially the same as those obtained from Figures 5 and 6. This result rules out the supposition that participation of gas phase CH_3OH is necessary for CO_2 evolution. With regard to the work of Üeno et al. [46], the amount of CO_2 was always larger than that of CO with no leveling in CO_2 production at an early stage of the CH_3OH decomposition.

Effect of oxygen treatment on ZnO activity and CO_2 production

In an attempt to trace any connection between the oxygen treatment and the catalyst activity towards CO_2 production, a series of CD_3OD decomposition experiments was carried out at 588 K and $P(CD_3OD)$ = 10.8 Pa as indicated in Figure 8. The method of cleaning the catalyst surface after each decomposition experiment involved the admission of about 67 Pa of O_2 gas onto the catalyst at 573 K. The catalyst temperature was

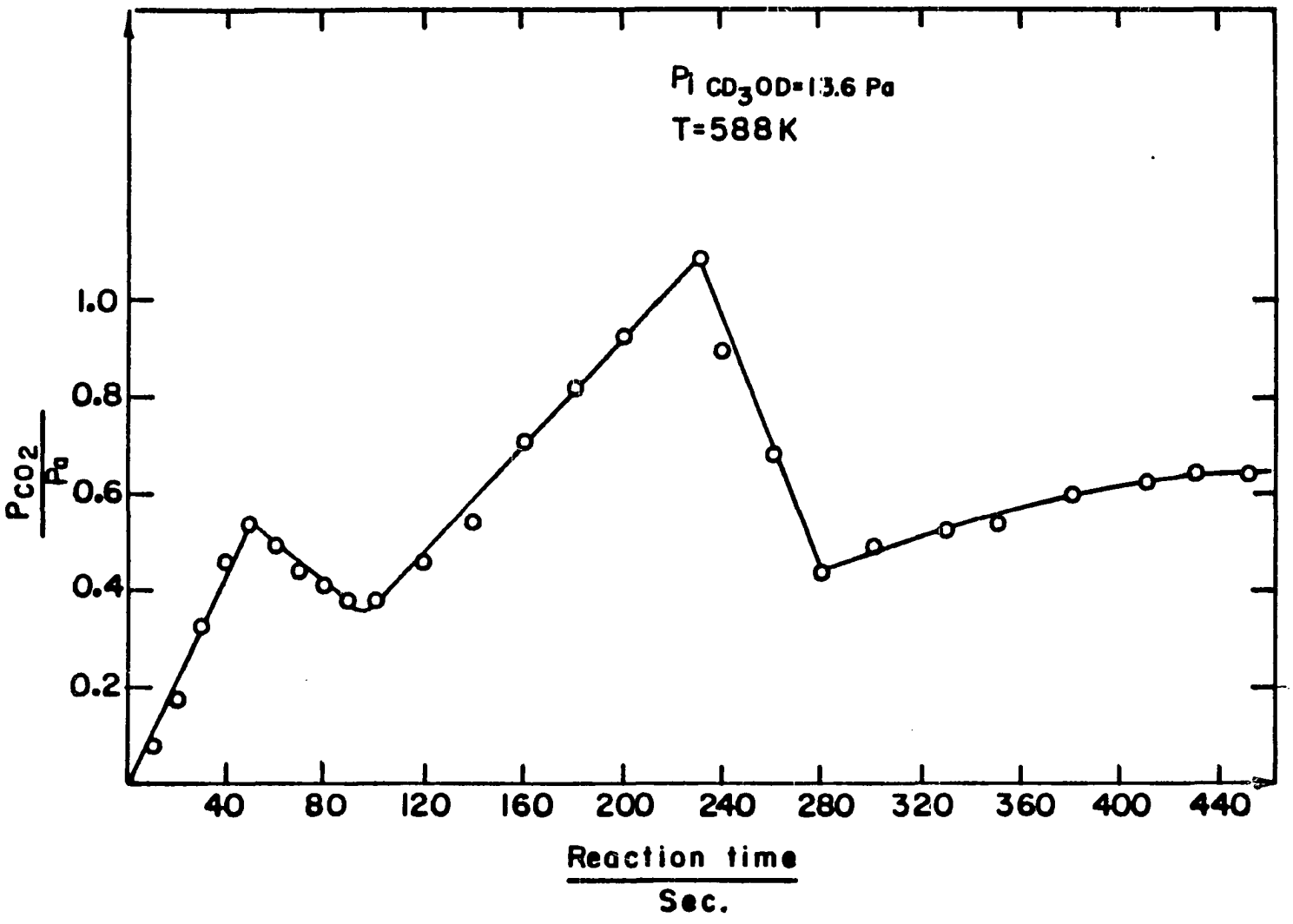

Figure 7. Effect of two 60-sec. pumping cycles on the production of CO_2 during CD_3OD decomposition over ZnO

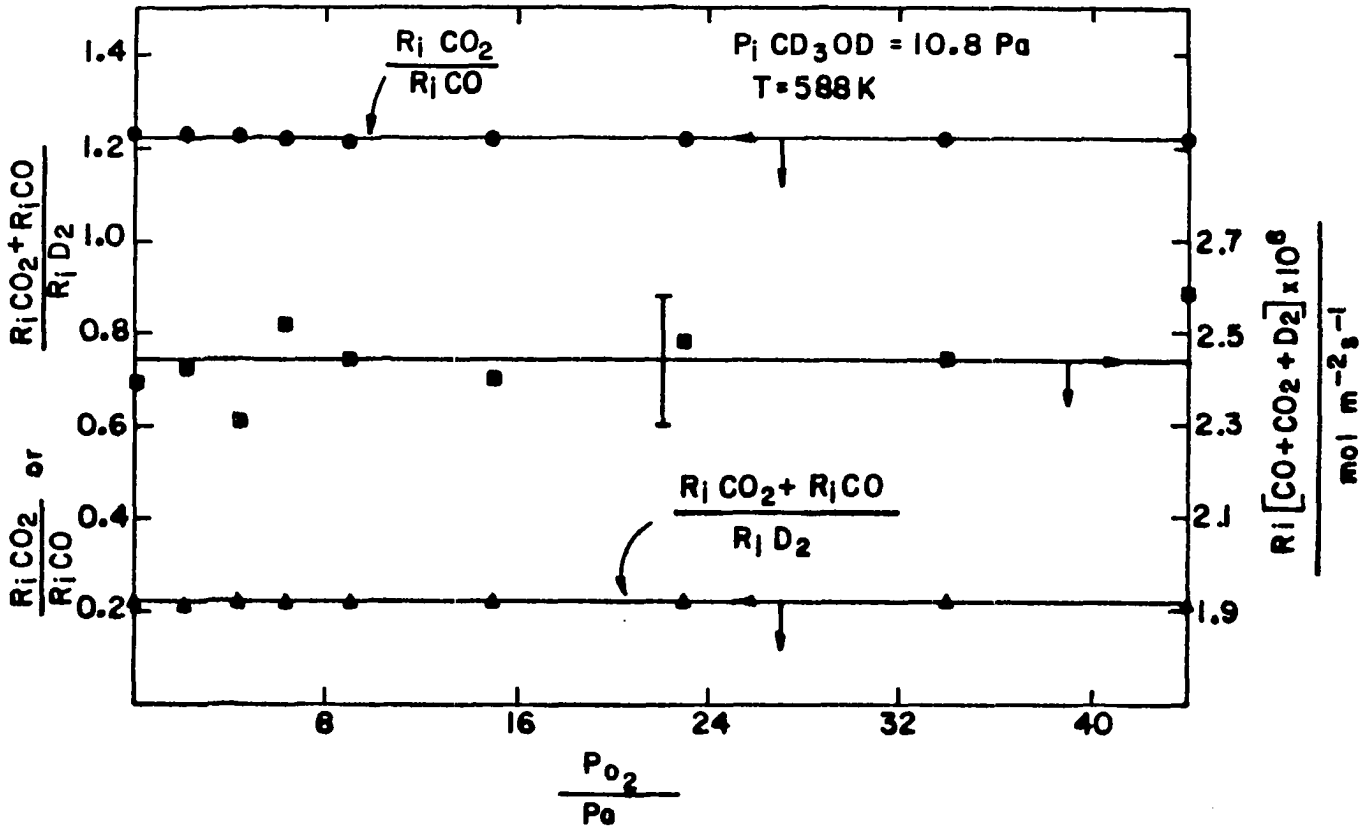

Figure 8. Effect of oxygen pretreatment on the CO_2/CO ratio, $(CO_2 + CO)/D_2$ ratio, and the catalyst activity [$=R_i (CO + CO_2 + D_2)$ mol m^{-2} s^{-1}] for CD_3OD decomposition over ZnO

then raised to 623 K at a rate of 0.2 K sec^{-1}. At 623 K, the oxygen was pumped out and heating was continued up to 673 K. Outgassing at this temperature lasted for 1.8×10^3 sec. The catalyst temperature was then lowered to 588 K. Before starting a run, the required amount of O_2 gas was admitted to the catalyst at the reaction temperature, 588 K. Contact of O_2 with ZnO at this temperature lasted 6×10^2 sec.; after that, the O_2 gas was pumped out and pumping continued for another 6×10^2 sec. After 120 sec. of CD_3OD decomposition on the oxygen-pretreated ZnO, the ratios CO_2/CO, $(CO_2 + CO)/D_2$, and the catalyst activity (expressed as total initial rate of $D_2 + CO + CO_2$ in mol m^{-2} s^{-1}) were determined. The results are shown in Figure 8. This figure suggests that the extra oxygen pretreatment has no effect on the course of CD_3OD decomposition. If CO_2 is produced via reaction of CO, which results from methanol decomposition, with some residual oxygen left behind on the catalyst surface during the oxygen treatment, one should anticipate an increase in the ratio CO_2/CO as the pressure of O_2 is increased. This was not the case since the ratio remained constant as shown in Figure 8.

On the basis of the results shown in Figures 3, 4, 5, 6, 7, and 8, it seems that a likely mechanism for CO_2 evolution, during methanol decomposition on ZnO, involves a surface reduction via the formation of a formate species, which further decomposes into CO_2 and/or CO.

Kinetic Results

H isotope effect and apparent activation energies

The fact that no CO and/or CO_2 were produced initially up to $T \geq 550$ K, and the detection of CH_2O below and above $T = 550$ K has led to the

conclusion that decomposition of CH_3OH catalyzed by ZnO proceeds in two steps as follows:

$$CH_3OH_{(g)} = CH_2O_{(g)} + H_{2(g)} \qquad \text{(Step 1)} \qquad (45)$$

$$CH_2O_{(g)} = CO_{(g)} + H_{2(g)} \qquad \text{(Step 2)} \qquad (46)$$

The kinetics of the first step was studied at 453 K to 513 K, while the kinetics of both steps was studied at 563 K to 613 K.

In an attempt to investigate the hydrogen isotope effect on the kinetics of methanol decomposition, the decomposition of CH_3OH, CH_3OD, and CD_3OD was studied in both temperature ranges. The results corresponding to the first step of decomposition are shown in Figure 9 and those of the second step are shown in Figure 10.

As shown in Figure 9, the initial rates of decomposition of both CH_3OH and CH_3OD are the same and the apparent energy of activation for both methanols is $E = 89.0$ kJ mol^{-1}. However, CD_3OD decomposes at a slower rate with an apparent energy of activation $E' = 95.7$ kJ mol^{-1}. These observations suggest that the cleavage of the oxygen-hydrogen bond in the methanol molecule is unlikely to be a rate-determining step. This also implies that the adsorption of methanol on the catalyst surface is not a rate-determining step. Since CD_3OD decomposes at a slower rate, as compared to CH_3OD, it seems that cleavage of a carbon-hydrogen bond is a rate-determining step.

In the case of CH_3OD, the low temperature decomposition, step 1, resulted in the formation of H_2, HD, and D_2. This is evidence against

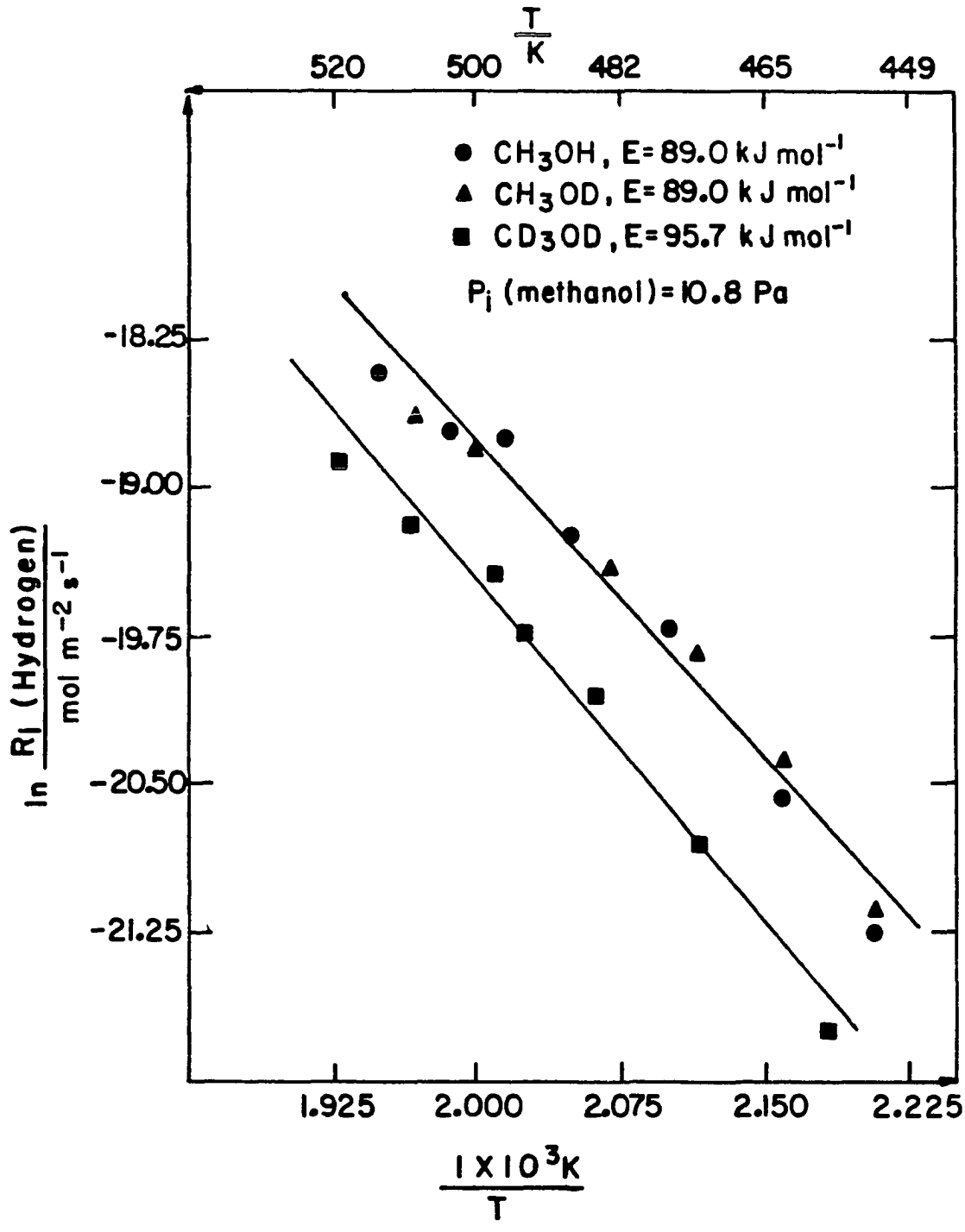

Figure 9. Hydrogen isotope effect and apparent energies of activation for the decomposition of CH_3OH, CH_3OD, and CD_3OD over ZnO. Ordinate corresponds to the dehydrogenation step into formaldehyde and hydrogen

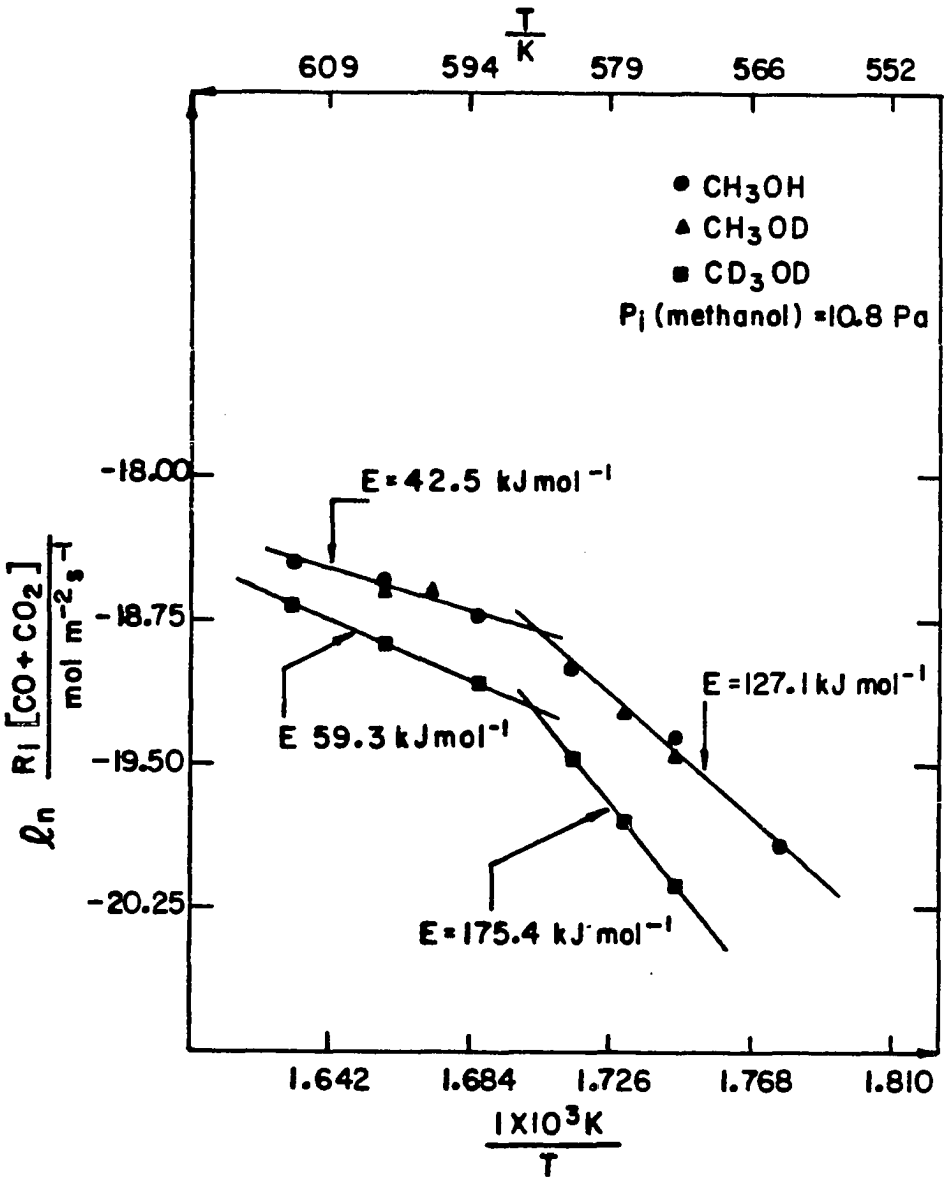

Figure 10. Temperature dependence of the initial rates of total carbon oxides production. Ordinate corresponds to the second step of methanol decomposition

the model proposing that the low temperature hydrogen comes solely from hydroxyl hydrogen. Participation of the methoxy group is required, probably via the step

$$CH_3O_* + D_* \rightarrow CH_2O_{(g)} + HD_{(g)} + 2* \quad (* = \text{surface site}). \quad (47)$$

The hydrogen isotopic scrambling can result via the steps:

$$HD_{(g)} + D_* \rightarrow H_* + D_{2(g)} \quad (48)$$

$$H_* + CH_3O_* \rightarrow CH_2O_{(g)} + H_{2(g)} \quad (49)$$

It should be mentioned that ZnO is known to promote the isotopic mixing between H_2 and D_2 [84, 110]. Support for the nonparticipation of the methyl hydrogen in a direct isotopic exchange with HD and/or D_2 is deduced from the infrared studies on the adsorption of methanol on ZnO and other metals. The work of Yasumori et al. [62] indicated that admission of D_2 gas onto a ZnO surface covered with CH_3O_* and H_* surface species resulted in the replacement of the H_* species by D_* and no isotopic band shifts occurred for the methoxy hydrogen. Anderson and Kemball [63] have also shown that CH_3OD is the only deuterated methanol obtained from the hydrogen exchange reaction between D_2 and CH_3OH on ZnO and some other evaporated metal films.

In the high temperature range, where evolution of CO and CO_2 is observable, the initial rate of step 2 is assumed to be the sum of the initial rates of CO and CO_2, as indicated in Figure 10. The results shown in this figure suggest that both CH_3OH and CH_3OD give the same initial rates of carbon oxide production, while CD_3OD decomposes at a

slower rate. This implies that the formaldehyde hydrogen is totally originating from the methyl hydrogen in the parent methanol molecule. On this basis, both CH_3OH and CH_3OD should give the same formaldehyde, i.e., CH_2O. The fact that CD_3OD decomposes into carbon oxides at a rate slower than that of CH_3OH or CH_3OD suggests that the rate-determining step of the formaldehyde decomposition might involve the cleavage of a hydrogen-carbon bond.

Figure 10, which refers to the temperature effect on the initial rate of formation of CO and CO_2, shows a bend at about 590 K. The fact that the ordinate of Figure 10 does not correspond to a specific rate constant implies that the slope at any temperature gives only the apparent activation energy of the reaction. This quantity might include contributions from heats of adsorption, heats of desorption, and a true activation energy corresponding to the slowest elementary step in the reaction mechanism. The importance of any of these contributions can only be evaluated after deriving a rate law from a proposed mechanism.

A similar break in the Arrhenius plot of ln R(CO) versus $\frac{1}{T}$ was reported by Dohse [41], and by Uchida and Ogino [69] at about 600 K. The same break in the Arrhenius plot was also reported at about 600 K in cases where the initial rate of increase in the total pressure was taken as a measure of methanol decomposition on catalysts containing ZnO [41, 44, 45, 65, 111, 112]. Dohse [41] attributed the break in the Arrhenius plot to the occurrence of the consecutive steps

$$CH_3OH \rightarrow CH_2O + H_2 \rightarrow CO + 2H_2$$

Wicke and Brotz [111] interpreted the lowering of the apparent activation energy as a transition from the chemical to the strong-pore diffusion regime within the catalyst. Fuderer-Luetic and Sviben [45] attributed the variation in the activation energy, revealed on undoped and doped ZnO, to either a change in semiconductivity of the catalysts or a change in the controlling step of the overall methanol decomposition reaction. Wencke and Heise [112], who studied the methanol decomposition on ZnO-Cr_2O_3 mixed oxides, attributed the break to the diffusion of CH_2O formed into the catalyst bed. On the other hand, Morrelli et al. [65], who studied the methanol decomposition on ZnO catalysts compacted under different pressures, concluded that the variation in the activation energy with increasing reaction temperature is caused by a change either in the catalyst properties or in the reaction mechanism. They also remarked that diffusion effects may occur, too, contributing to the lowering of the activation energy when the particle size is high enough. A comparison between the values of the apparent energies of activation found in this work and those reported in the literature is shown in Table 1.

From Table 1, it seems that only the values reported by Dohse [41] are in good agreement with those of the present study. Dohse's work involved decomposition of CH_3OH films on ZnO, a condition close to the low pressure of CH_3OH used in this study as compared to the high pressures used by other researchers. It should be pointed out that a fine powder sample of ZnO was used in the present study with an average particle diameter = 4×10^2 nm.

Table 1. Values of the apparent energies of activation corresponding to the scheme $CH_3OH \xrightarrow{E_1} CH_2O + H_2 \xrightarrow{E_2} CO + 2H_2$

Catalyst	E_1/kJ mol^{-1}	E_2/kJ mol^{-1}	Reference
None	284.5	186.2[a]	59, 113
ZnO	94.1	146.4	41
ZnO	102.5	184.1	44
ZnO	115.1	255.4	45
ZnO/Cr_2O_3	180	125.1	42
ZnO	172-322[b]	--	64
ZnO	89.0	127.1[c]	this work

[a]Value obtained from homogeneous decomposition of CH_2O.

[b]Range corresponds to four catalysts compacted under different pressures.

[c]Value corresponds to the range 563 K to 590 K in Figure 10.

Comparison between decomposition and uptake of CH_3OH and CH_2O

To supplement the proposed stepwise decomposition scheme of methanol, the catalytic decomposition of CH_2O on ZnO was compared with that of CH_3OH on the same batch of the catalyst at 500 K. The results are shown in Figure 11. From this figure, it is obvious that the initial rate of CH_3OH decomposition is almost ten times that of CH_2O. For example, at $P(CH_3OH) = P(CH_2O) = 5$ Pa, the ratio

$$\frac{R(H_2,f)}{R(H_2,m)} = \frac{1.4\times10^{-3}\ \text{Pa s}^{-1}}{0.66\times10^{-2}\ \text{Pa s}^{-1}} = 0.2$$

where $R(H_2,f)$ = initial rate of CH_2O decomposition and $R(H_2,m)$ = initial rate of CH_3OH decomposition. This result fits well with the observation

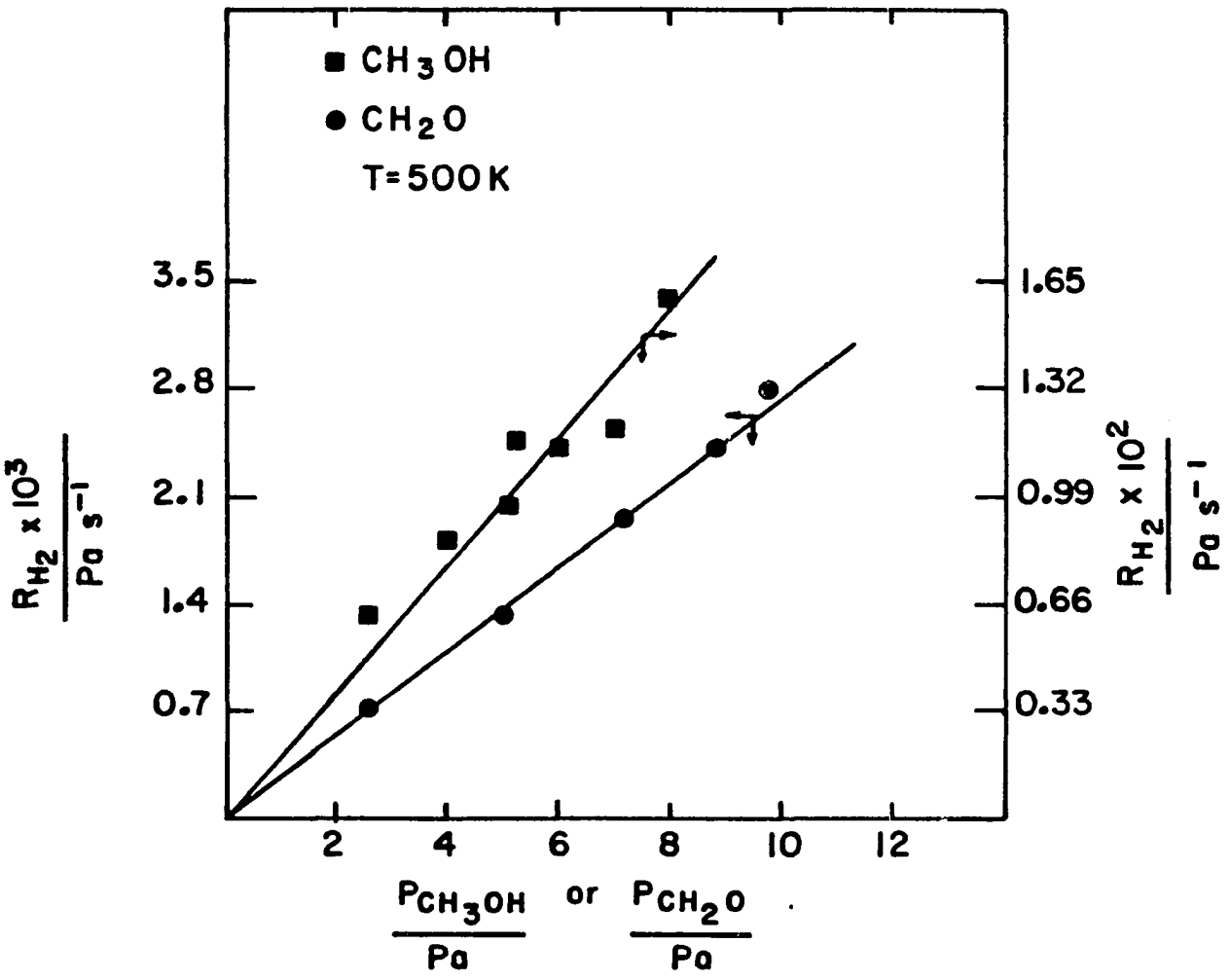

Figure 11. Comparison between the initial rates of decomposition of CH_3OH and CH_2O over ZnO. Rate in Pa s^{-1} x 2.42×10^{-7} = Rate in mol m^{-2} s^{-1}

that, during CH_3OH decomposition in the low temperature range, no carbon oxides were detected up to 550 K during the time in which about 15% of the total methanol hydrogen was being produced.

An estimate of the initial uptake of both CH_2O and CH_3OH by ZnO at 500 K is shown in Figure 12. In this figure, the abscissa, P(calc.), represents the initial pressure of CH_2O or CH_3OH over the catalyst at the moment vapor was admitted from the manifold to the catalyst vessel. P(calc.) was determined from knowledge of the expansion factor assuming no adsorption by the catalyst. The ordinate of Figure 12 represents the initial uptake of ZnO = $F \cdot \Delta P$ mol m^{-2}, where $F = 2.42 \times 10^{-7}$ mol m^{-2} Pa^{-1} at 500 K, and $\Delta P = [P(calc.) - P_o]$ Pa; P_o was determined by extrapolating the total pressure over the catalyst to zero time reaction. It should be emphasized that Figure 12 does not represent an actual isotherm. However, the figure does imply that CH_3OH adsorption is relatively faster than that of CH_2O. For example, at $P(calc.) = P(CH_3OH) = P(CH_2O) = 13$ Pa, one finds from the least-squares lines in Figure 12 that

$$\frac{(A,f)}{(A,m)} = \frac{1.08 \text{ mol } m^{-2}}{1.56 \text{ mol } m^{-2}} = 0.65$$

where (A,f) = uptake of CH_2O and (A,m) represents the corresponding value for CH_3OH. The difference in the uptake might be attributed to a difference in the ratio $P(calc.)/P_s$, where P_s = saturation vapor pressure of CH_3OH or CH_2O. Since the boiling point of CH_2O = 252 K and that of CH_3OH = 338 K, the ratio $P(calc.)/P_s$ is much higher for CH_3OH than for

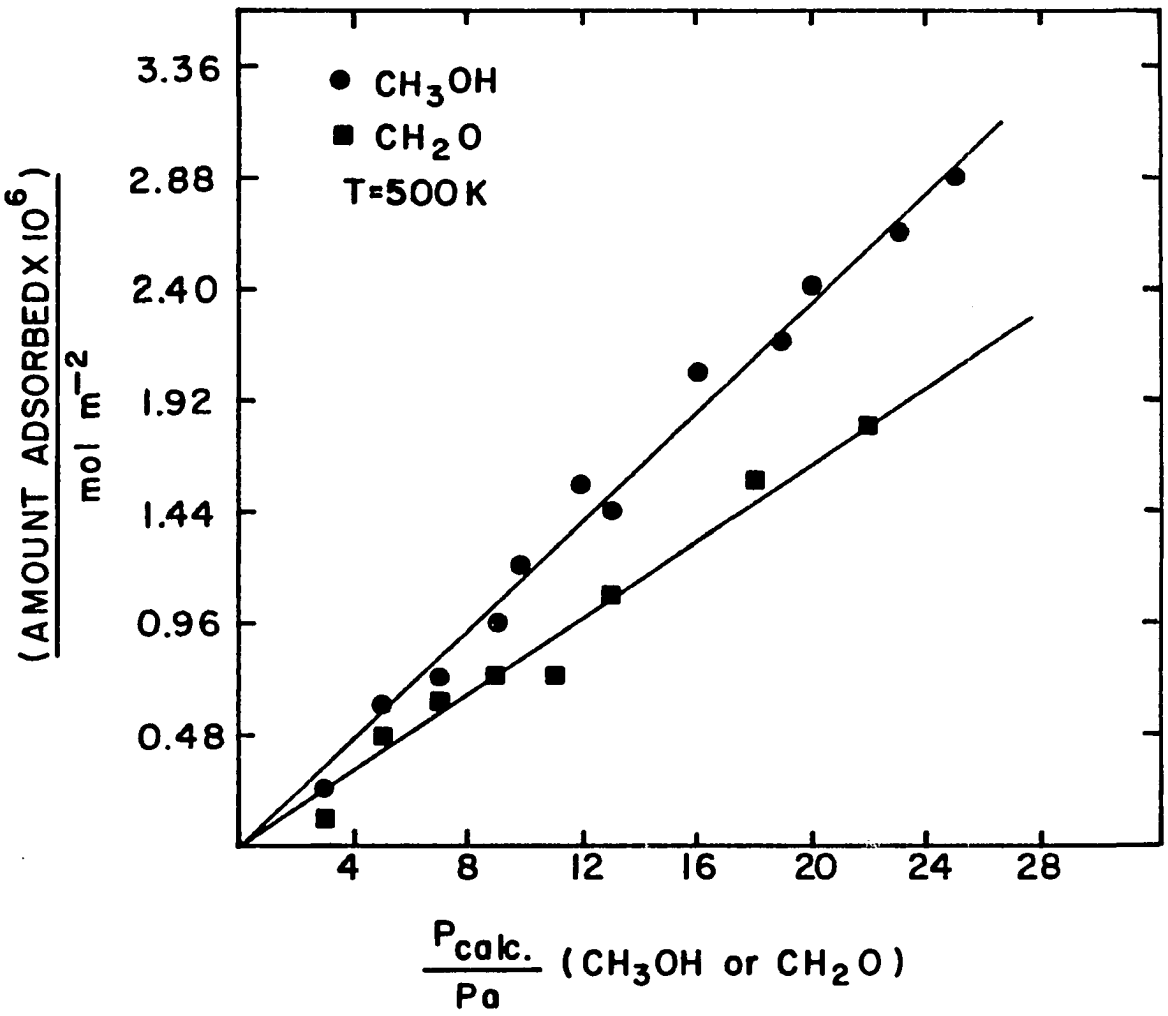

Figure 12. Comparison between CH_2O and CH_3OH initial uptake by ZnO

CH_2O at a particular adsorption temperature. Consequently, the van der Waals attraction of the adsorbent is greater for CH_3OH than for CH_2O. Van der Waals interaction energy tends to "track" condensation energy.

The decomposition of CH_2O on ZnO at 500 K was found to produce H_2 and CO in a 1:1 ratio and no CO_2 was detected. The significance of this result with regard to the problem of CO_2 concurrent evolution with CO at T > 550 K, during CH_3OH decomposition, is to rule out the possibility of any surface reduction that might be caused by the generated CO. Although no spectroscopic studies have been reported on the adsorption of CH_2O by ZnO, formation of formate species has been reported by Unland [106] after absorbing CH_2O on alkali metal x-type zeolites. Even if a formate species is being generated during CH_2O decomposition on ZnO at 500 K, evolution of CO_2 at this temperature, via formate decomposition, might not be significant due to the stability of formate species. Ueno et al. [46] reported that the formate species decomposes more slowly than methoxy species during CH_3OH decomposition on ZnO. The formate species has been reported to withstand temperatures as high as 700 K [104-106].

Effect of $P(CH_3OH)$, $P(H_2)$, $P(CO)$, and $P(CO_2)$ on CH_3OH decomposition

Since most of the previous studies on the kinetics of the catalytic decomposition of CH_3OH on ZnO have been carried out over a narrow range of temperature and pressure [41-46, 64, 65], a major goal of this work was to study the decomposition kinetics over a wide range of temperature and pressure. Contrary to what most researchers adopted, the initial

rates were obtained directly from the variation in the partial pressure of a particular product as a function of time. In most cases, the initial rates were determined from the amount of the corresponding product produced during the first 120 sec. of reaction.

The low temperature CH_3OH decomposition, where no carbon oxides were formed, was studied by monitoring the H_2 evolution at 500 K with the initial CH_3OH pressure ranging from 2 to 31 Pa. The dependence of the initial rate of hydrogen production, $R(H_2)$, on the initial CH_3OH pressure, $P(CH_3OH)$, was found to follow the expression

$$[P(CH_3OH)/R(H_2)]^{\frac{1}{2}} = a + b\ P(CH_3OH) \qquad (50)$$

The fit of the low temperature data to Equation 50 is shown in Figure 13, where the line in the figure represents the least-squares fit. The values of the constants a and b were deduced from the intercept and the slope of the least-squares line, respectively. These values are: intercept = a = 12.4 $s^{\frac{1}{2}}$ and slope = b = 1.7 $s^{\frac{1}{2}}\ Pa^{-1}$. A comparison between the calculated $R(H_2)$ values, predicted by Equation 50, and the experimental initial rates is presented in Figure 14 in a log $R(H_2)$ versus log $P(CH_3OH)$ graph. The agreement between the calculated initial rates and the experimentally found rates is excellent.

The high temperature CH_3OH decomposition, where H_2 and carbon oxides are being produced, was studied at 593 K with the initial CH_3OH pressure ranging from 3 to 130 Pa. The initial rates were determined from the amount of product produced in 60 sec. The initial rate of evolution of carbon oxides, R_c, was obtained by summing the initial rates of CO

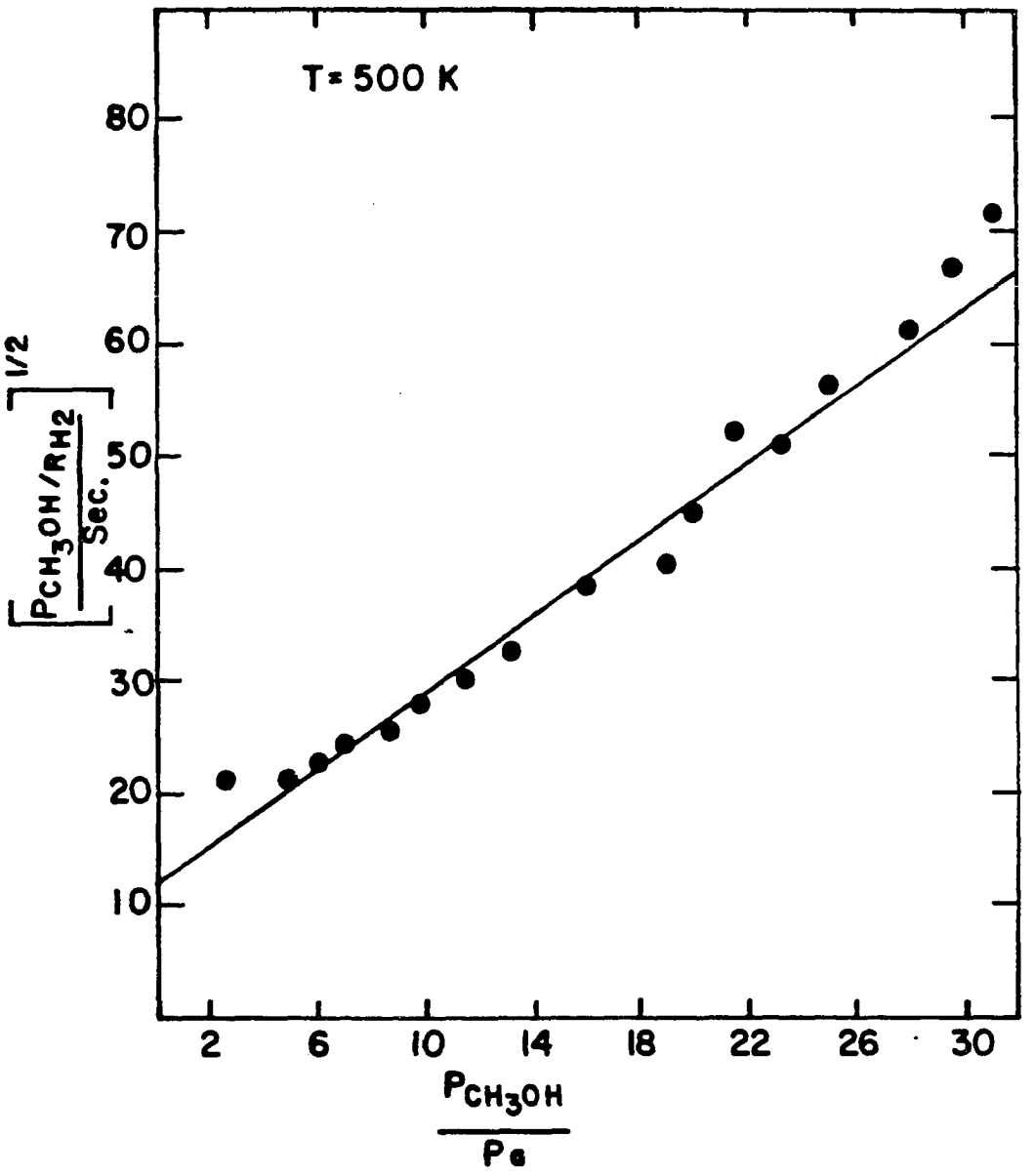

Figure 13. Fit of the low temperature CH_3OH decomposition data to the equation:

$$[P(CH_3OH)/R(H_2)]^{\frac{1}{2}} = a + b\ P(CH_3OH)$$

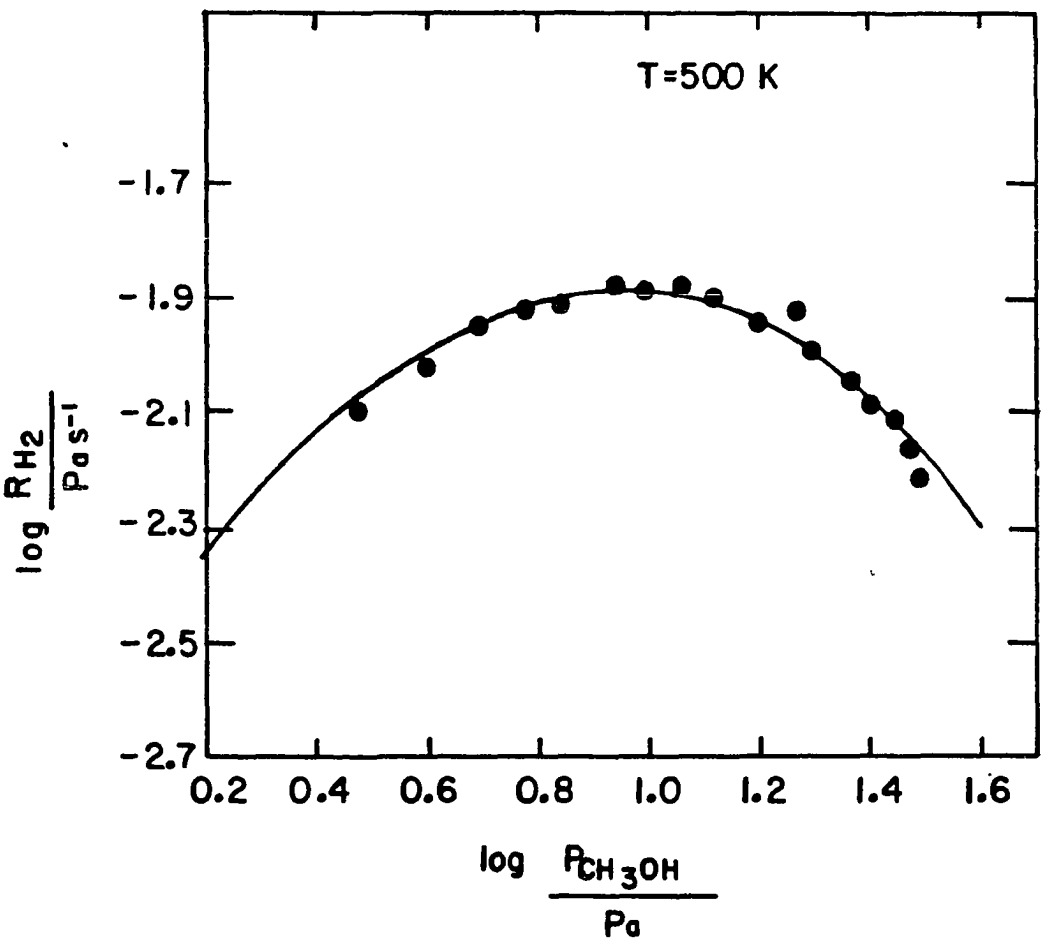

Figure 14. Comparison between calculated and experimental $R(H_2)$ values. Closed circles represent experimental values. Rate in Pa s^{-1} x 2.42×10^{-7} = Rate in mol m^{-2} s^{-1}

and CO_2 production. On the other hand, the initial rate of hydrogen production, $R(H_2)$, corresponding to the first step of CH_3OH decomposition was obtained by subtracting R_c from the initial rate of total hydrogen production. The dependence of R_c and $R(H_2)$ on $P(CH_3OH)$ was found to satisfy the following equations:

$$[P(CH_3OH)/R(H_2)]^{\frac{1}{2}} = a' + b' P(CH_3OH) \quad (51)$$

$$[P(CH_3OH/R_c]^{\frac{1}{2}} = a'' + b'' (P(CH_3OH) \quad (52)$$

The plots of these two equations for the decomposition of CH_3OH at 593 K are shown in Figure 15. The lines in the figure represent the fit of the data to the least-squares method. The values of the constants a', a'', b', and b'' were determined from the intercept and slope of the corresponding least-squares line. The values obtained are: $a' = 6.44\ s^{\frac{1}{2}}$, $b' = 0.128\ s^{\frac{1}{2}}\ Pa^{-1}$, $a'' = 10.5\ s^{\frac{1}{2}}$, and $b'' = 0.55\ s^{\frac{1}{2}}\ Pa^{-1}$. A comparison between the calculated initial rates of H_2 production $R(H_2)$, predicted by Equation 51, and experimental rates is shown in Figure 16 in log $R(H_2)$ versus log $P(CH_3OH)$ form. Using Equation 52, a similar comparison is also presented in Figure 17 for log R_c versus log $P(CH_3OH)$. In this case, Equation 52 overestimates the calculated R_c values at $P(CH_3OH) \leq 5$ Pa. For example, at $P(CH_3OH) = 5$ Pa, the calculated value of R_c is 2.85×10^{-2} Pa s^{-1}, while the experimental value of R_c is 1.86×10^{-2} Pa s^{-1}. Hence, the ratio $R_c(calc.)/R_c(expt.) = 1.5$. This discrepancy reflects the lesser weight given the low pressure region in setting parameters in Equation 52, since about 75% of the data points

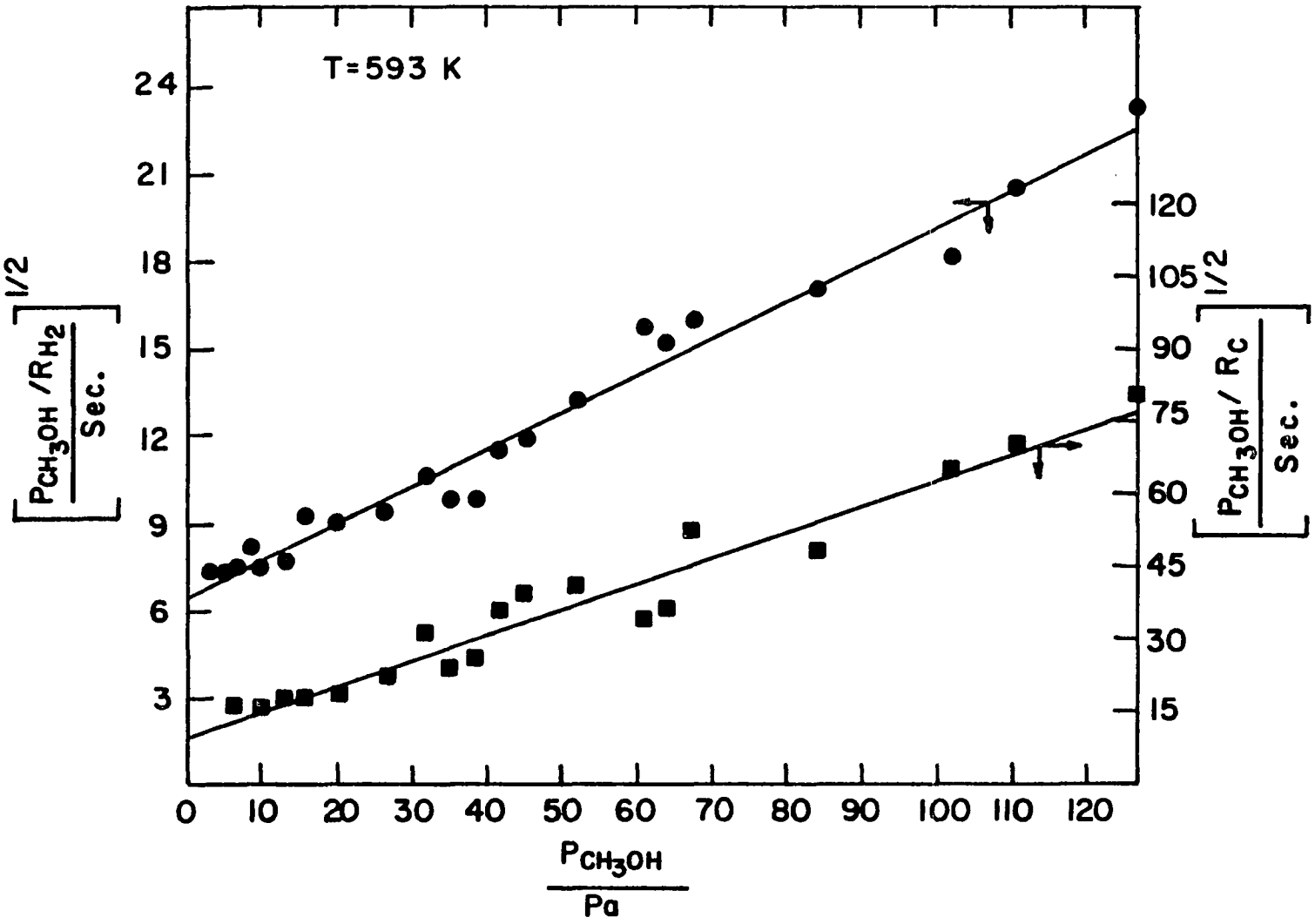

Figure 15. Variation of $[P(CH_3OH)/R(H_2)^{\frac{1}{2}}$ and $[P(CH_3OH)/R_c]^{\frac{1}{2}}$ with $P(CH_3OH)$. Rate in Pa s^{-1} x 2.34×10^{-7} = Rate in mol m^{-2} sec^{-1}

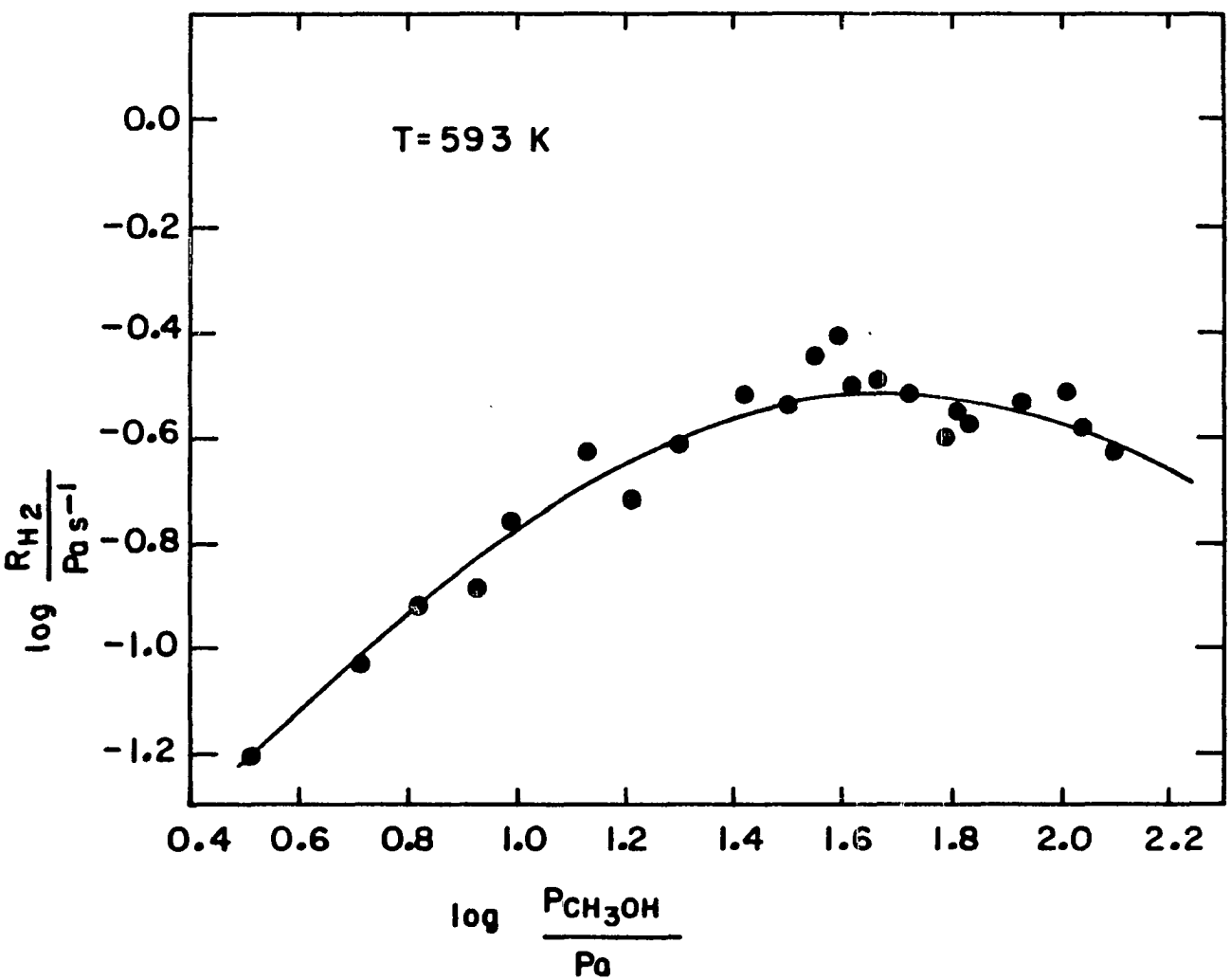

Figure 16. Comparison between calculated and experimental $R(H_2)$ values. Closed circles represent experimental values. Rate in Pa s^{-1} x 2.34×10^{-7} = Rate in mol m^{-2} s^{-1}

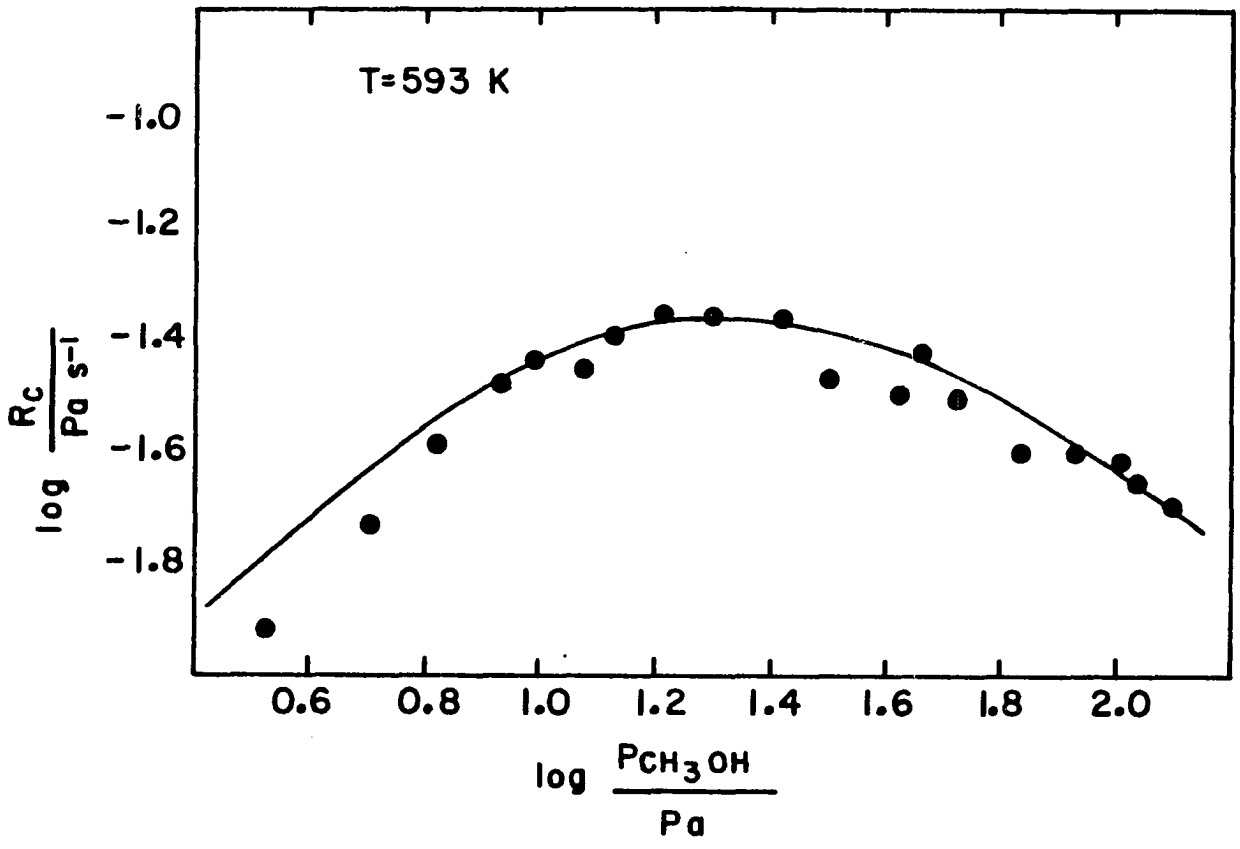

Figure 17. Comparison between calculated and experimental R_c values. Closed circles represent experimental values. Rate in Pa s^{-1} x 2.34×10^{-7} = Rate in mol m^{-2} s^{-1}

in Figure 17 have their log $P(CH_3OH)$ values > 1. However, it is found that at $P(CH_3OH)$ < 5 Pa, the R_c values are given by the equation

$$R_c = 3.61 \times 10^{-3} \, P(CH_3OH) \text{ Pa s}^{-1} \quad (53)$$

Equation 53 reflects a first-order dependence and might be considered as the low pressure limiting case of Equation 52. For these reasons, the calculated R_c values shown in Figure 17 at $P(CH_3OH)$ < 10 Pa were computed as the average of R_c values predicted by Equation 52 and those obtained from the first-order dependence given by Equation 53. This correction becomes insignificant as $P(CH_3OH)$ approaches the value 10 Pa from below. For example, at $P(CH_3OH)$ = 10 Pa, Equation 52 gives $R_c = 3.91 \times 10^{-2}$ Pa s^{-1}, and Equation 53 gives $R_c = 3.61 \times 10^{-2}$ Pa s^{-1}; the average of these two values is 3.76×10^{-2} Pa s^{-1}, which is 4% less than the value of R_c predicted by Equation 52. However, the calculated R_c values at $P(CH_3OH)$ > 10 Pa, in Figure 17, were obtained from Equation 52.

As indicated in Figure 15, the CH_3OH decomposition kinetics at 593 K was studied up to $P(CH_3OH)$ = 130 Pa. Despite the presence of a cold trap at 195 K, between the leak valve and the mass spectrometer, the CH_3OH peaks started to appear in the mass spectrum at $P(CH_3OH)$ > 130 Pa, which interfered with CO analysis. Due to this limitation, decomposition of CH_3OH at $P(CH_3OH)$ > 130 Pa was not pursued. However, the fact that the initial CH_3OH pressure was varied by two orders of magnitude assures that significant changes have been made in the concentration of the surface species, which participate in the decomposition reaction.

The effects of $P(H_2)$, P(CO), and $P(CO_2)$ on the decomposition

kinetics of CH_3OH were also examined. Due to experimental limitations, i.e., the hydrogen produced has to be monitored over a large background of H_2, the effect of $P(H_2)$ on the low temperature decomposition of CH_3OH was investigated by pretreating the catalyst with the required amount of H_2 gas at the reaction temperture for a period of $3x10^2$ sec. Pumping out of the H_2 gas was then started. After $3x10^2$ sec., the pumps were isolated and the required amount of the CH_3OH vapor was admitted to the catalyst. The effect of 0 to 21 Pa of H_2 pretreatment on the decomposition of 9.8 Pa CH_3OH at 500 K is shown in Figure 18. This figure indicates that the hydrogen pretreatment does not affect the decomposition of CH_3OH. On the other hand, the effect of $P(H_2)$ on the initial rate of formation of H_2, CO, and CO_2 at 593 K was investigated by concurrent admission of the required amount of H_2 gas and 4.6 Pa of CH_3OH. The results shown in Figure 19 suggest that the presence of H_2 gas does not affect the course of CH_3OH decomposition.

In a similar manner, the effects of P(CO), and $P(CO_2)$ on the decomposition of CH_3OH were also examined at 563 K. The results are shown in Figure 20. In this case, the partial pressures of H_2 and $P(CO+CO_2)$ were determined after $5.2x10^2$ sec. (about 26% carbon conversion). This was done to avoid errors associated with the determination of the initial rate of formation of carbon oxides, which might result due to the presence of CO or CO_2, in a relatively large quantity, before the commencement of the CH_3OH decomposition. Figure 20 indicates that neither CO nor CO_2 affects the CH_3OH decomposition.

The results presented in Figures 19 and 20 lead to the conclusion

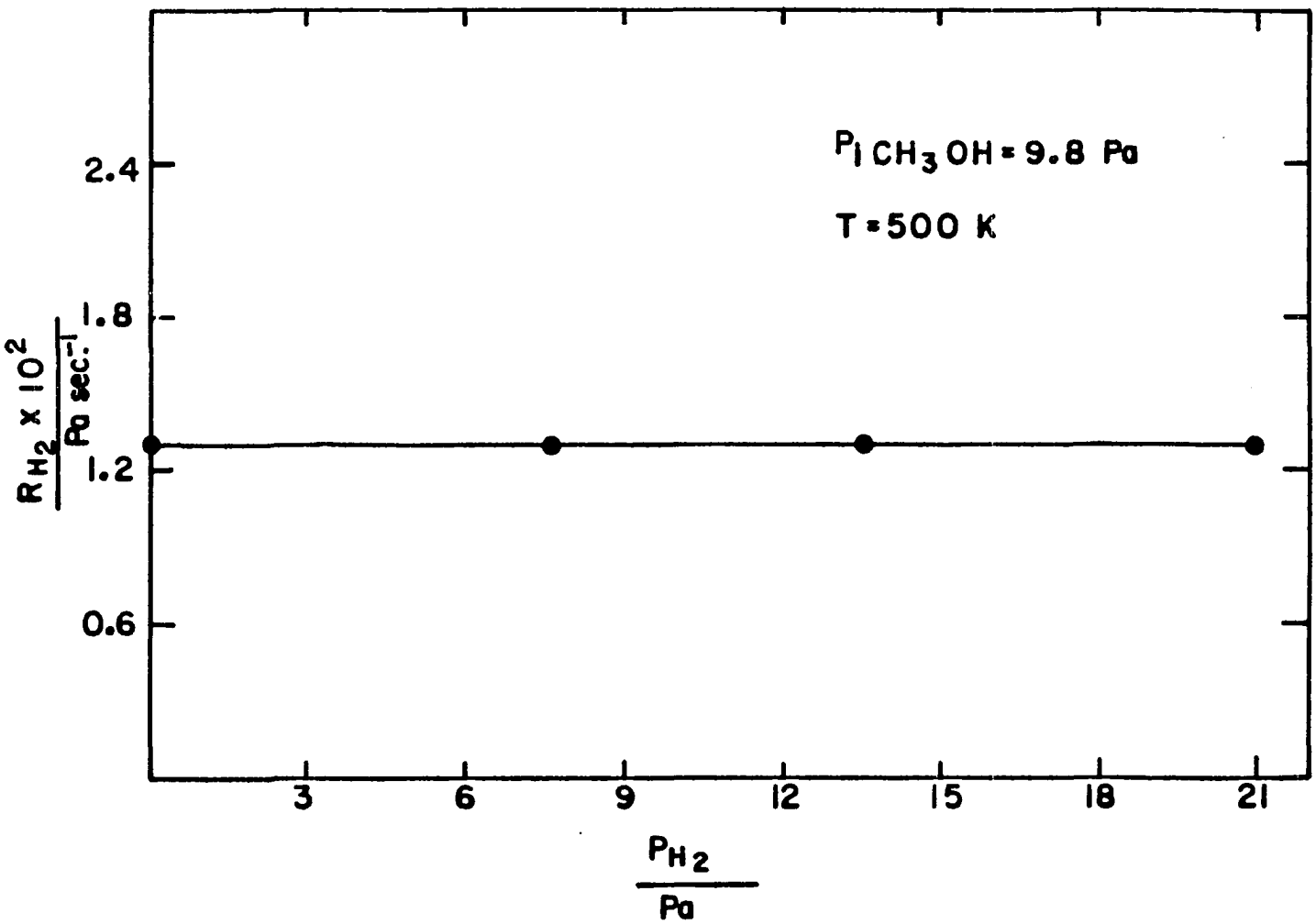

Figure 18. Effect of hydrogen pretreatment on the initial rate of CH_3OH decomposition on ZnO. Rate in Pa s^{-1} x 2.42×10^{-7} = Rate in mol m^{-2} s^{-1}

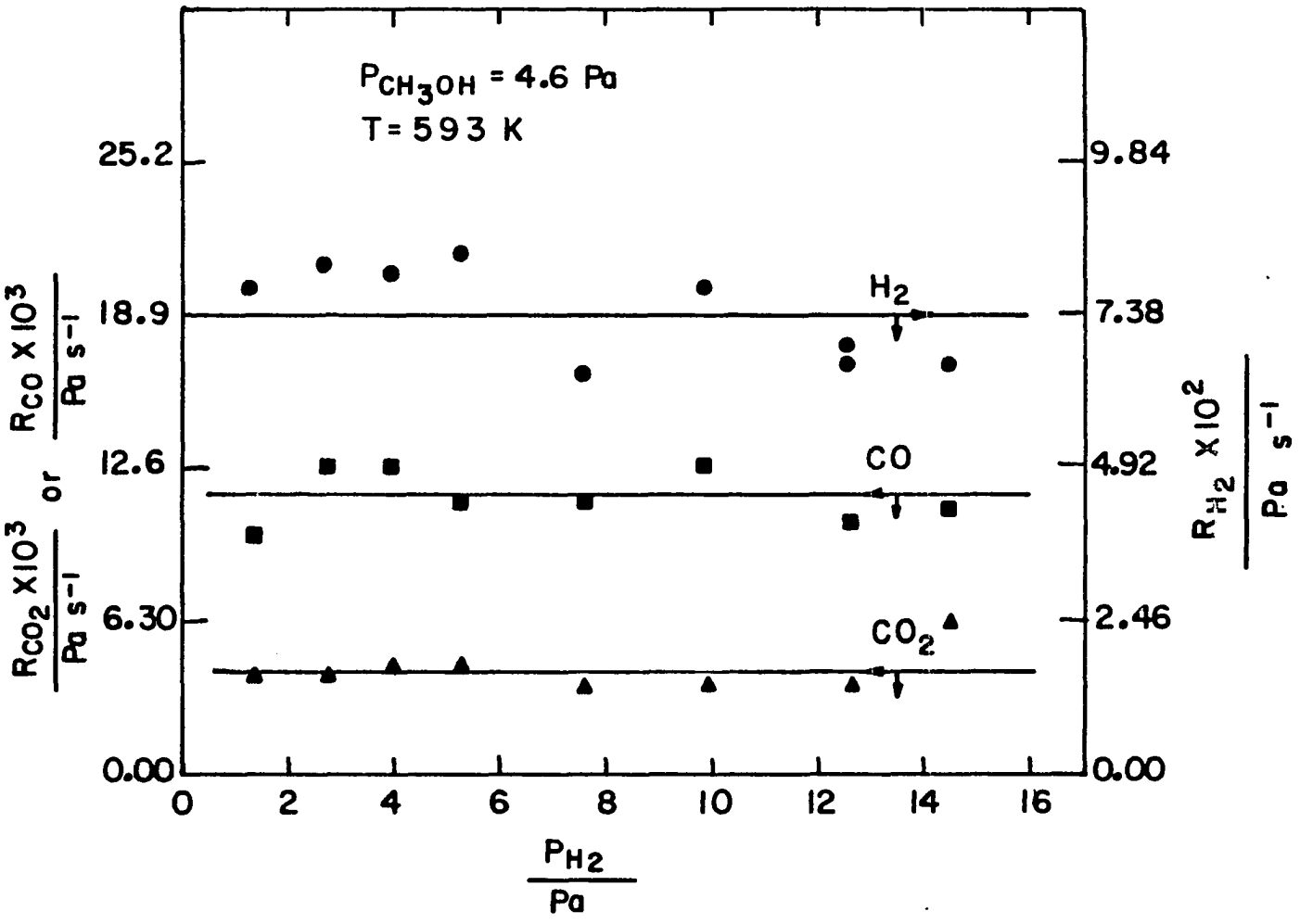

Figure 19. Effect of $P(H_2)$ on the initial rates of production of CO, CO_2, and H_2 during CH_3OH decomposition on ZnO. Rate in Pa s^{-1} x 2.34×10^{-7} = Rate in mol m^{-2} s^{-1}

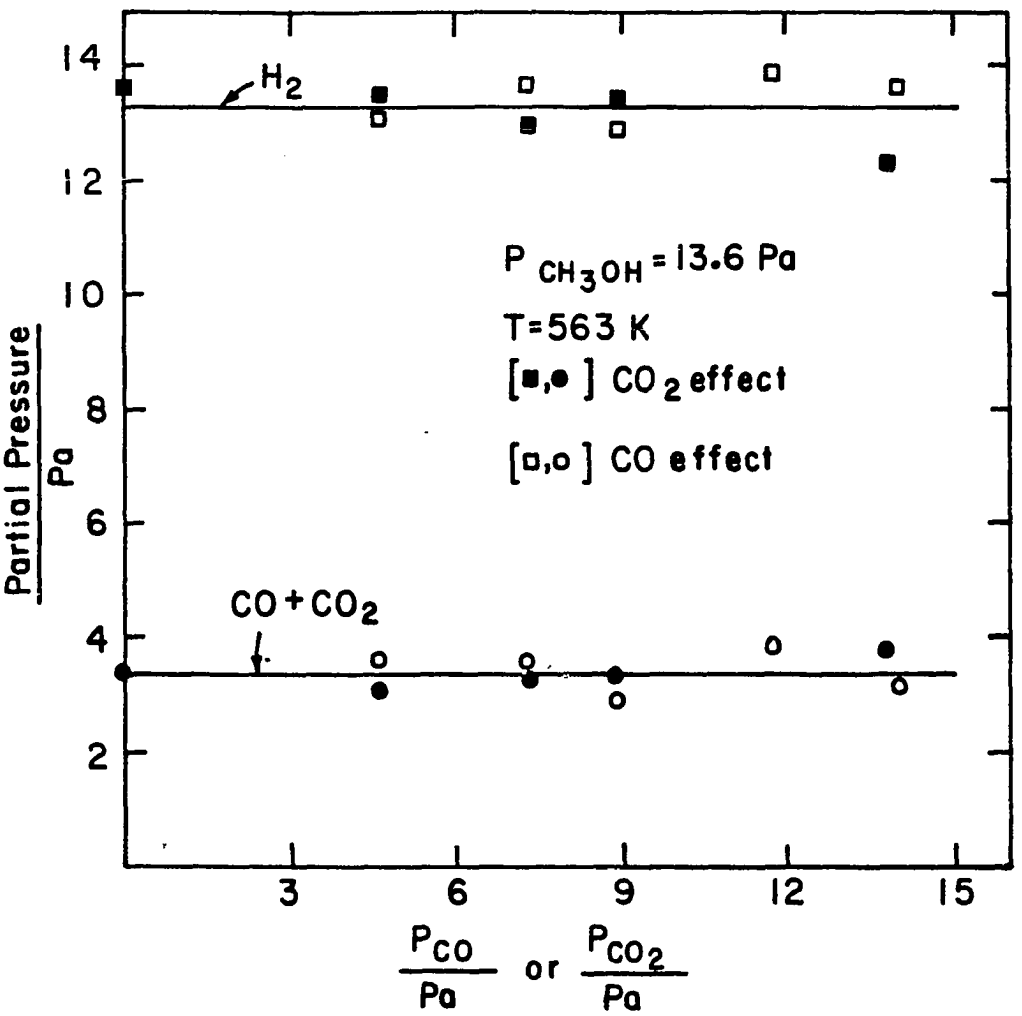

Figure 20. Effect of P(CO) and P(CO_2) on the production of H_2 and ($CO + CO_2$) during CH_3OH decomposition over ZnO. Partial pressures were determined after 5.2×10^2 sec. of reaction

that the initial rate of CH_3OH decomposition over ZnO is zero-order in $P(H_2)$, $P(CO)$, and $P(CO_2)$ over the pressure range indicated in these two figures. If H_2, CO, and CO_2 adsorb strongly on sites used for CH_3OH decomposition, the initial rate of CH_3OH decomposition on ZnO will have to decrease as the partial pressure of H_2, CO, or CO_2 is increased in the initial mixture (feed). The observation that the initial rate of CH_3OH decomposition was not retarded by the presence of any of these gases suggests that the fraction of ZnO surface occupied by any of these gases is negligible.

The apparent activation energy of CH_3OH decomposition on ZnO in the temperature range 453 K to 513 K was found to be 89.0 kJ mol^{-1} (see Figure 9). On the other hand, Baranski and Galuszka [85] reported a value of about 22 kJ mol^{-1} for the activation energy of H_2 desorption on a powder sample of ZnO at $T \leq 550$ K. Comparison of these two activation energies leads to the conclusion that hydrogen desorption is unlikely to be a rate-determining step during the ZnO-catalyzed decomposition of CH_3OH. Hotan *et al.* [101] have indicated that CO_2 completely desorbs from the $(10\bar{1}0)$ ZnO surface at $T < 500$ K. The desorption rate of CO_2 was found to peak at about 300 K, with the activation energy of desorption being 90 ± 10 kJ mol^{-1}. They also found that CO desorbs as CO_2 in about the same temperature range and with almost the same activation energy of desorption as that of CO_2. Runge and Gopel [114] have also reported TDS data on the desorption of CO_2 from a powder sample of ZnO. Most of CO_2 was found to desorb at 380 K.

In Figure 10, at $T \leq 588$ K, the apparent activation energy of total

carbon monoxide production ($CO + CO_2$) from CH_3OH is 127.1 kJ mol^{-1}. Comparison of this value with those reported in the aforementioned TDS studies of Hotan et al. [101], indicates that desorption of CO and/or CO_2 is not a rate-determining step during CH_3OH decomposition over ZnO.

A zero-order dependence was also reported by Dandy [43] for the effects of H_2, CO, CO_2, CH_2O, H_2O, and CH_4 on the high pressure decomposition of CH_3OH [$P(CH_3OH) > 1.3 \times 10^3$ Pa] on ZnO, Li_2O-doped ZnO, and Al_2O_3-doped ZnO.

Mechanistic Considerations

In this section, a mechanism will be developed to describe the kinetics of methanol decomposition on ZnO, and a rate law will be derived. The consistency of the mechanism with the literature information on methanol adsorption on ZnO and its implications with regard to the findings of this work will be discussed.

Consider the following sequence of reactions:

$$CH_3OH_{(g)} + * \overset{K_1}{\rightleftarrows} CH_3OH_* \quad \text{(step 1)} \tag{54}$$

$$CH_3OH_* + * \overset{K_2}{\rightleftarrows} CH_3O_* + H_* \quad \text{(step 2)} \tag{55}$$

$$CH_3O_* + H_* \overset{k_3}{\rightarrow} CH_2O_* + H_{2(g)} + * \quad \text{(step 3)} \tag{56}$$

$$CH_2O_* \underset{k_{-4}}{\overset{k_4}{\rightleftarrows}} CH_2O_{(g)} + * \quad \text{(step 4)} \tag{57}$$

$$CH_2O_* + * \underset{k_{-5}}{\overset{k_5}{\rightleftarrows}} CHO_* + H_* \quad \text{(step 5)} \tag{58}$$

$$CHO_* + H_* \overset{k_6}{\rightarrow} H_{2(g)} + CO_{(g)} + 2* \quad \text{(step 6)} \tag{59}$$

where the star, *, represents an unoccupied surface site on ZnO. It is obvious that formation of CO_2 is ignored in this scheme. However, to account for the initial formation of CO_2, step 6 in the mechanism should be modified. This can be done by assuming that the same species indicated in step 6 can undergo two different reactions. One reaction involves surface reduction and leads to the formation of CO_2. The other reaction is simply a bimolecular surface reaction giving CO and H_2 as indicated by step 6 in the mechanism. The occurrence of these two reactions can be depicted as follows:

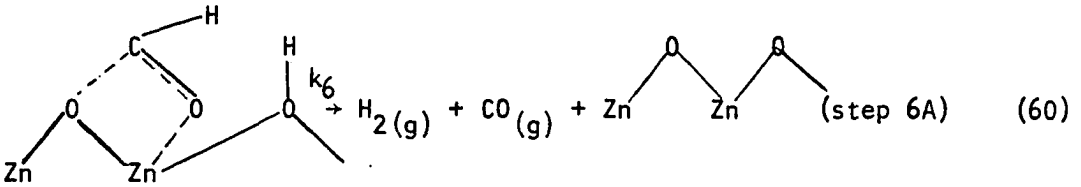

(step 6A) (60)

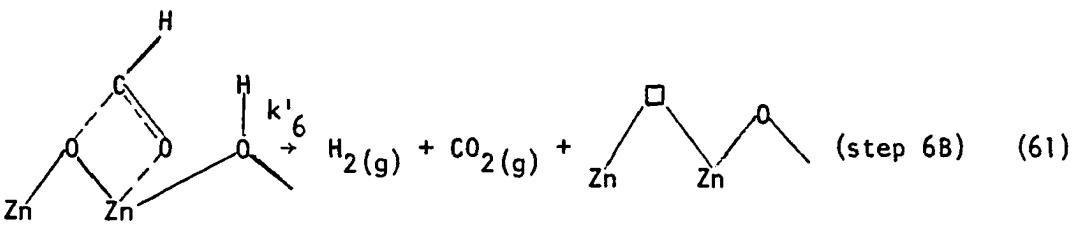

(step 6B) (61)

Since the catalyst surface was always treated with O_2 gas prior to a CH_3OH decomposition experiment, step 6B is favored at the initial stages of CH_3OH decomposition and becomes less important at later stages, probably due to unavailability of oxygen and/or inhibition by charge accumulation.

On the basis of the occurrence of steps 6A and 6B, as indicated above, the total initial rate of production of carbon oxides, R_c, will

be given as follows:

$$R_c = R(CO) + R(CO_2)$$
$$= (k_6 + k_6')[CHO_*][H_*]$$
$$= k_c[CHO_*][H_*] \qquad (62)$$

Later in this discussion the occurrence of steps 6A and 6B will be referred to as step 6 with an apparent rate constant = k_c.

In the low temperature range, i.e., when no carbon oxides are being produced, methanol decomposes into H_2 and CH_2O and the rate-determining step is postulated to be step 3. In the high temperature region, where further decomposition occurs, i.e., both methanol and formaldehyde decompose concurrently, the total CH_3OH decomposition is governed by step 6. At low temperatures, where $k_c \simeq 0$, the initial rate of H_2 production is given by the following equation:

$$\frac{dP(H_2)}{dt} = k_3[CH_3O_*][H_*] = R(H_2) \qquad (63)$$

In this case the site-balance equation is given as follows:

$$1 = [*] + [CH_3OH_*] + [CH_3O_*] + [H_*] + [CH_2O_*] + [O_*] \qquad (64)$$

where $[O_*]$ represents the fractional coverage of oxygen surface species (if any) irreversibly held on the catalyst surface after each oxygen treatment. The fractional coverage of each surface species is related to the unoccupied fraction, [*], as follows:

$$[CH_3OH_*] = K_1P_m[*] \qquad (65)$$

$$[CH_2O_*] = K_f P_f [*] \tag{66}$$

where $P_m = P(CH_3OH)$, $P_f = P(CH_2O)$, and $K_f = k_{-4}/k_4$. Neglecting readsorption of H_2 as H_*, one can equate $[CH_3O_*]$ to $[H_*]$, such that

$$[CH_3O_*] = [H_*] = (K_2K_1P_m)^{\frac{1}{2}}[*] \tag{67}$$

Substituting Equations 65, 66, and 67 into Equation 64, the site-balance equation becomes

$$1 = [*] + K_1P_m [*] + 2(K_2K_1P_m)^{\frac{1}{2}} [*] + K_fP_f[*] + [O_*] \tag{68}$$

The fact that the oxygen pretreatment did not affect the course of CH_3OH decomposition suggests that the term $[O_*]$ can be neglected. In this case, Equation 68 reduces to

$$1 = [*] + K_1P_m[*] + 2(K_2K_1P_m)^{\frac{1}{2}}[*] + K_fP_f[*] \tag{69}$$

solving for $[*]$, the result is

$$[*] = [1 + K_1P_m + 2(K_2K_1P_m)^{\frac{1}{2}} + K_fP_f]^{-1} \tag{70}$$

Using this result and Equation 67, then substituting into Equation 63 gives the result:

$$R(H_2) = \frac{k_3K_2K_1P_m}{[1 + K_1P_m + 2(K_2K_1P_m)^{\frac{1}{2}} + K_fP_f]^2} \tag{71}$$

Since the uptake of CH_2O by ZnO was found to be small compared to that of CH_3OH, one can neglect the term K_fP_f in the denominator of Equation 71. This is more likely to be the case when one considers initial rates

at low conversion. Furthermore, if it is assumed that $1 + K_1P_m >> 2(K_2K_1P_m)^{\frac{1}{2}}$, Equation 71 reduces into the following form:

$$R(H_2) = \frac{k_3K_2K_1P_m}{[1 + K_1P_m]^2} \tag{72}$$

Equation 72 can be transformed into the following form:

$$[\frac{P_m}{R(H_2)}]^{\frac{1}{2}} = (k_3K_2K_1)^{-\frac{1}{2}} + (k_3K_2K_1)^{-\frac{1}{2}}K_1P_m \tag{73}$$

this form is equivalent to the empirical form found experimentally (Equation 50) which has the form

$$[\frac{P_m}{R(H_2)}]^{\frac{1}{2}} = a + b\ P_m$$

Comparison of this equation with Equation 73 gives:

$$a = (k_3K_2K_1)^{-\frac{1}{2}} \tag{74}$$

$$b = K_1(k_3K_2K_1)^{-\frac{1}{2}} \tag{75}$$

$$\frac{b}{a} = K_1 \tag{76}$$

Values of K_1 and k_3K_2 at 500 K and 593 K will be given later.

In the high temperature range, where evolution of carbon oxides is noticeable, the initial rates of formation of hydrogen and carbon oxides are given as follows:

$$\frac{dP(CO)}{dt} + \frac{dP(CO_2)}{dt} = R(CO) + R(CO_2) = R_c \tag{77}$$

$$\frac{dP(H_2,tot.)}{dt} - [\frac{dP(CO)}{dt} + \frac{dP(CO_2)}{dt}] = \frac{dP(H_2)}{dt} \tag{78}$$

Considering initial rates, Equation 78 becomes

$$R(H_2,\text{tot.}) - R_c = R(H_2) \tag{79}$$

where $R(H_2)$ represents the initial rate of H_2 production accompanying the formation of CH_2O (step 3 in the mechanism), $R(H_2,\text{tot.})$ represents the initial rate of total H_2 produced via CH_3OH and CH_2O decomposition, and R_c designates the initial rate of production of carbon oxides.

At temperatures where further decomposition of CH_2O occurs, i.e., reaction 59 takes place (step 6 in the mechanism), the dependence of R_c on the initial methanol pressure, P_m, can be derived from the given mechanism as follows: Assuming that the only appreciable surface species are CH_3OH_* and CH_2O_*, then at high temperatures, the site-balance equation will be given as follows:

$$1 = [*] + [CH_3OH_*] + [CH_2O_*] \tag{80}$$

At high temperatures, formaldehyde formed in step 3 either goes off as gas or decomposes according to steps 5 and 6 in the mechanism. At steady state, the fractional coverage of CH_2O_* satisfies the equation:

$$[CH_2O_*]_{s.s.} = \frac{\{k_3K_2K_1P_m[*] + k_{-4}P_f\}[*]}{k_4 + k_cK_5[*]} \tag{81}$$

or neglecting P_f, Equation 81 reduces to

$$[CH_2O_*]_{s.s.} = \frac{k_3K_2K_1P_m[*]^2}{k_4 + k_cK_5[*]} \tag{82}$$

From Equation 65, $[CH_3OH_*]$ is given as follows:

$$[CH_3OH_*] = K_1P_m[*]$$

Substitution of Equations 82 and 81 into Equation 80 yields:

$$1 = [*] + K_1 P_m [*] + \frac{k_3 K_2 K_1 P_m [*]^2}{k_4 + k_c K_5 [*]} \tag{83}$$

Equation 83 can be transformed into the form

$$[*]^2 \{k_c K_5 + K_1 K_5 k_c P_m + k_3 K_2 K_1 P_m\} + [*]\{k_4 + K_1 k_4 P_m - k_c K_5\} - k_4 = 0 \tag{84}$$

which has the solution

$$[*] = \frac{-(k_4 + K_1 k_4 P_m - k_c K_5) + \{(k_4 + K_1 k_4 P_m - k_c K_5)^2 + 4k_4 (k_c K_5 + K_1 K_5 k_c P_m + k_3 K_1 K_2 P_m)\}^{\frac{1}{2}}}{2(k_c K_5 + K_1 K_5 k_c P_m + k_3 K_1 K_2 P_m)} \tag{85}$$

Consider the special case $k_c = 0$ (low temperature CH_3OH decomposition), for which Equation 85 reduces to

$$[*] = \frac{k_4 (1 + K_1 P_m)}{2k_3 K_1 K_2 P_m} \left\{\left[1 + \frac{4k_4 k_3 K_1 K_2 P_m}{k_4^2 (1 + K_1 P_m)^2}\right]^{\frac{1}{2}} - 1\right\} \tag{86}$$

If $\frac{4k_3 K_1 K_2 P_m}{k_4 (1 + K_1 P_m)^2} << 1$ and the approximation $(1+x)^{\frac{1}{2}} - 1 \approx \frac{x}{2}$ is applied, Equation 86 will reduce into the form

$$[*] = \frac{1}{1 + K_1 P_m} \tag{87}$$

which was arrived at in deriving Equation 72 for the low temperature decomposition of CH_3OH. Equation 87 can be obtained by examining the quadratic equation:

$$ax^2 + bx - c = 0 \tag{88}$$

the special case $ax^2 << bx - c$ gives $x = \frac{c}{b}$. Applying the same argument to Equation 86, where $c = k_4$ and $b = k_4(1 + K_1 P_m)$ gives the result shown in

Equation 87. However, for the general case where $k_c > 0$, use of the condition $ax^2 << bx-c$ reduces Equation 85 into the following:

$$[*] = \left[\frac{k_4}{k_4(1 + K_1P_m) - k_cK_5}\right] = \frac{1}{(1 + K_1P_m - k_cK_5/k_4)} \quad (89)$$

Equation 62 can be rewritten in the form

$$\begin{aligned} R_c &= k_c[CHO_*][H_*] \\ &= k_cK_5[CH_2O_*][*] \text{ ; (step 5 is assumed at equilibrium)} \\ &= \frac{k_cK_5k_3K_2K_1P_m[*]^3}{k_4 + k_cK_5[*]} \text{ ; (Equation 82 is used)} \\ &= \frac{k_cK_5k_3K_2K_1P_m}{(1 + K_1P_m - k_cK_5/k_4)^2 \cdot k_4(1 + K_1P_m)} \text{ ; (Equation 89 is used)} \\ &= \frac{\{(k_cK_5k_3K_2K_1)/(1 - k_cK_5/k_4)^2\}\ P_m}{[1 + K_1P_m/(1 - k_cK_5/k_4)]^2 \cdot k_4(1 + K_1P_m)} \end{aligned} \quad (90)$$

Similarly the initial rate of production of H_2 according to step 3 in the mechanism is given as follows:

$$\begin{aligned} R(H_2) &= k_3[CH_3O_*][H_*] = k_3K_2[CH_3OH_*][*] = k_3K_2K_1P_m[*]^2 \\ &= \frac{\{k_3K_1K_2/(1-k_cK_5/k_4)^2\}P_m}{[1 + K_1P_m/(1 - k_cK_5/k_4)]^2} \end{aligned} \quad (91)$$

Equations 91 and 90 predict that the ratio $R(H_2)/R_c$ should satisfy the equation:

$$\frac{R(H_2)}{R_c} = \frac{k_4}{k_cK_5}(1 + K_1P_m) \quad (92)$$

which predicts a linear relationship between $R(H_2)/R_c$ and P_m at a constant temperature. The slope of the line given by Equation 92 is (k_4K_1/k_cK_5) and the intercept is (k_4/k_cK_5).

Figure 21 shows a plot of Equation 92. The line in the figure represents the least-squares fit. Values of R_c and $R(H_2)$ were calculated from the slope and intercept of the corresponding line in Figure 15. The following information was obtained from Figure 21:

(1) Slope = 7.11×10^{-2} Pa^{-1} = (k_4K_1/k_cK_5).

(2) Intercept = 4.54 = (k_4/k_cK_5).

(3) $\frac{\text{Slope}}{\text{Intercept}} = K_1 = 1.57\times10^{-2}$ Pa^{-1}.

(4) $\frac{K_1}{1 - k_cK_5/k_4} = \frac{1.57\times10^{-2}}{1 - 0.22} = 2.01\times10^{-2}$ Pa^{-1} .

Equation 91 gives the initial rate of H_2 production via step 3 in the mechanism with concurrent evolution of carbon oxides. This equation can be rearranged in the form

$$\left[\frac{P_m}{R(H_2)}\right]^{\frac{1}{2}} = \frac{(1 - k_cK_5/k_4)}{(k_3K_2K_1)^{\frac{1}{2}}}\left[1 + \frac{K_1P_m}{(1 - k_cK_5/k_4)}\right] . \qquad (93)$$

Equation 93 gives a relationship between $R(H_2)$ and P_m similar to the experimental result shown in Figure 15 for $R(H_2)$ data. The ratio $\frac{K_1}{(1 - k_cK_5/k_4)}$ in Equation 93 can be obtained from the $R(H_2)$ data shown in Figure 15 as follows:

(1) From Figure 15: $\frac{\text{slope}}{\text{intercept}} = \frac{0.128}{6.44} = 1.99\times10^{-2}$ Pa^{-1}.

(2) From Equation 93: $\frac{\text{slope}}{\text{intercept}} = \frac{K_1}{(1 - k_cK_5/k_4)} = 1.99\times10^{-2}$ Pa^{-1}.

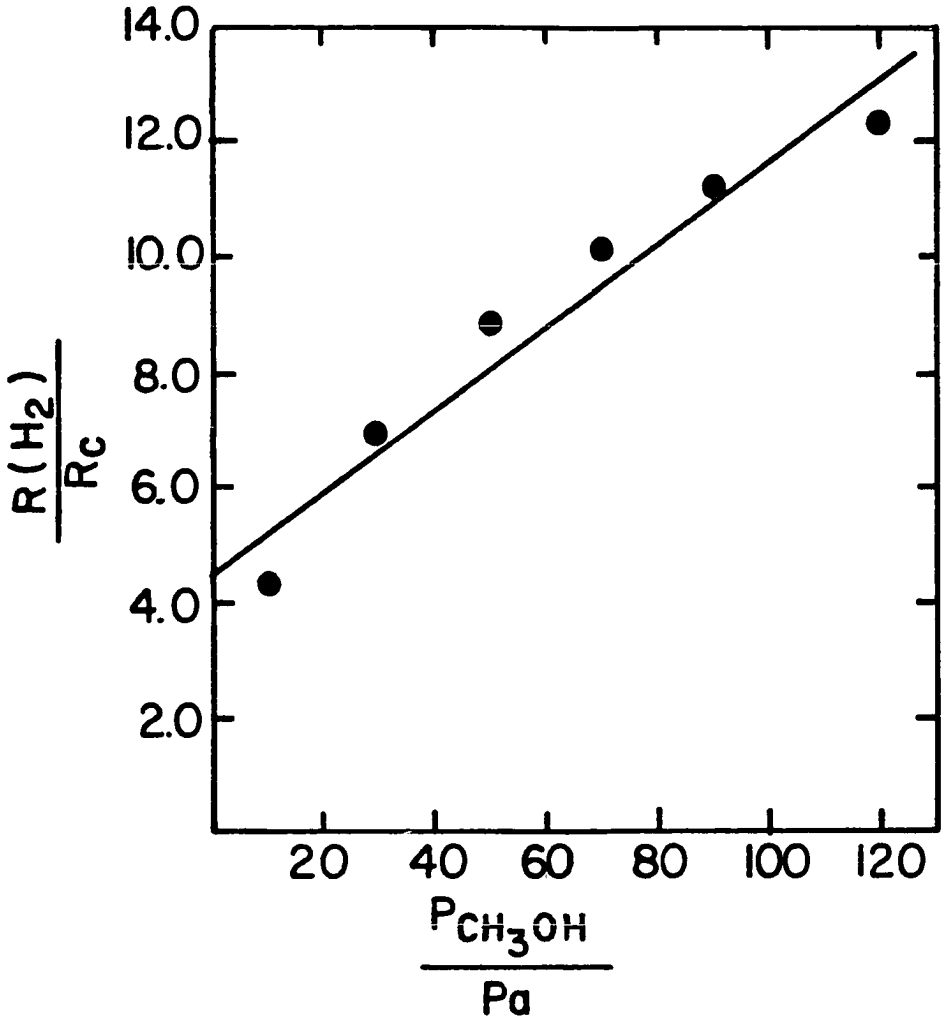

Figure 21. Plot of the equation:

$$\frac{R(H_2)}{R_c} = \frac{k_4}{k_c K_5} (1 + K_1 P_m) \text{ at } 593 \text{ K}$$

Notice the excellent agreement between the two values of $\frac{K_1}{(1 - k_c K_5/k_4)}$. The value 1.99×10^{-2} Pa^{-1} is obtained from $R(H_2)$ data, while the value 2.01×10^{-2} Pa^{-1} is obtained from $R(H_2)$ and R_c data shown in Figure 15.

With regard to the relationship between R_c and P_m, Equation 90 does not give exactly the empirical relationship depicted in Figure 15. The denominator of Equation 90 needs further discussion. To do this, some numerical information must be provided for the constants appearing in Equation 90. This information is given in Table 2.

Table 2. Values of the constants appearing in Equation 90 at 593 K

Constant	Value	Units	Source
$k_c K_5/k_4$	2.20×10^{-1}	dimensionless	Eq. 92 & Fig. 21
K_1	1.57×10^{-2}	Pa^{-1}	Eq. 92 & Fig. 21
$K_1/(1 - k_c K_5/k_4)$	2.00×10^{-2}	Pa^{-1}	Eq. 92 & Fig. 21 or Eq. 93 & Fig. 15
$k_3 K_2$	9.46×10^{-1}	$Pa\ s^{-1}$	Eqs. 92, 93 & Figs. 15, 21

Substituting the numerical values shown in Table 2 into Equation 90 yields the following expression for R_c at 593 K:

$$R_c = \frac{5.37 \times 10^{-3}\ P_m}{(1 + 2.00 \times 10^{-2}\ P_m)^2 \cdot (1 + 1.57 \times 10^{-2}\ P_m)}\ Pa\ s^{-1} \qquad (94)$$

The denominator of Equation 94 can be approximated as a polynomial of the form $(1+\alpha x)^n$. The given mechanism predicts that the value of n should be 3. On the other hand, the R_c data shown in Figure 15 indicate

a good fit for the case where n = 2 in the denominator of Equation 94. Table 3 shows a comparison between the empirical R_c values (obtained from least-squares line in Figure 15) and those obtained by Equation 94. The case (R_c, n=2) corresponds to an equation similar to Equation 94 with the term ($1 + 1.57 \times 10^{-2} P_m$) being dropped out from the denominator. The case (R_c, n=3) corresponds to Equation 94 with the full expression of the denominator being retained.

Table 3. Comparison between empirical and calculated R_c values at 593 K

$\frac{P_m}{Pa}$	$\frac{10^2 \cdot (R_c, n=2)}{Pa\ s^{-1}}$	$\frac{10^2 \cdot (R_c, n=3)}{Pa\ s^{-1}}$	$\frac{10^2 \cdot (R_c, emp.)}{Pa\ s^{-1}}$
10	3.72	3.22	3.91
30	6.27	4.26	4.12
50	6.68	3.74	3.46
70	6.49	3.09	2.92
90	6.13	2.54	2.50
120	5.53	1.93	2.05

It is obvious from Table 3 that the case (R_c,n=3) predicts rates closer to the empirical ones than the case (R_c,n=2). However, both cases give R_c values of the same order of magnitude and the choice between the two cases is a matter of accuracy in getting the R_c values.

Table 4 summarizes the values of the constants appearing in the expressions of $R(H_2)$ and R_c. Notice that $R(H_2)$ data were obtained at two different temperatures, 500 K and 593 K, while R_c data were obtained only at 593 K.

Table 4. Values of the constants in $R(H_2)$ and R_c expressions

Temperature/K	Constant	Value	Units	Remarks
500	K_1	1.37×10^{-1}	Pa^{-1}	low temp. $R(H_2)$ data
500	k_3K_2	4.75×10^{-2}	$Pa\ s^{-1}$	low temp. $R(H_2)$ data
593	K_1	1.57×10^{-2}	Pa^{-1}	high temp. $R(H_2)$ & R_c data
593	k_3K_2	9.46×10^{-1}	$Pa\ s^{-1}$	high temp. $R(H_2)$ & R_c data
593	$k_c\ K_5/k_4$	2.20×10^{-1}	dimensionless	high temp. $R(H_2)$ & R_c data

The break in the Arrhenius plot of ln R_c versus 1/T, shown in Figure 10, is unlikely to be caused by a build-up of a surface species such as CH_3O_*, or CHO_*. If the catalyst surface is being poisoned by the build-up of a certain intermediate, the low temperature part of the ln R_c versus 1/T graph should be flatter than the high temperature part. Since the opposite of this was observed, a more likely explanation for the break in Figure 10 is the decrease in the equilibrium constants K_1, K_2, and K_5 when the reaction temperature is increased. The temperature effect on K_1 is shown in Table 4. The effect of the product K_1K_2 on the initial rate, measured at different temperatures, is more pronounced in the numerator of a rate equation (see Equations 90 and 91).

In conclusion, the proposed mechanism resulted in the development of three rate laws. The first rate law relates the initial rate of H_2 production, $R(H_2)$, to $P(CH_3OH)$ at low temperatures and is given by

Equation 72. The second rate law relates the initial rate of H_2 production, $R(H_2)$, to $P(CH_3OH)$ at higher temperatures as given by Equation 91. The third rate law corresponds to the initial rate of production of carbon oxides, R_c, and is given by Equation 90. The low temperature and the high temperature $R(H_2)$ expressions have the same functional form as the empirical ones given by Equations 50 and 51, respectively. On the other hand, the expression for R_c is somewhat different from the empirical form given by Equation 52. The expression for R_c derived from the mechanism has the extra term $(1 + K_1 P_m)$ in its denominator.

The mechanism proposes that at low temperatures the ZnO surface sites are either bare or occupied by adsorbed methanol, i.e., CH_3OH_* species with coverages of other surface species being negligible. At higher temperatures, where further CH_2O decomposition occurs, the mechanism proposes that the significant coverage is that of the molecular species CH_3OH_* and CH_2O_*. The bonding of CH_3OH_* to the ZnO surface can be assumed to occur via a coordinative adsorption on a zinc ion through the oxygen of the CH_3OH molecule, or the CH_3OH molecule can be coordinated to an anion vacancy. Yet another possibility for molecular adsorption involves hydrogen bonding between the methanol oxygen and the hydrogen of a surface hydroxyl group. Residual hydroxyl groups on the ZnO surface can be detected even after treating the ZnO surface with 2.3×10^4 Pa of O_2 gas for two hours at 730 K [115]. It should be pointed out that most of the surface infrared studies concerning the adsorption of CH_3OH on metal oxides were carried out after pumping out the gas phase over the adsorbent; consequently, the molecularly adsorbed CH_3OH

might be completely lost during the evacuation step, or its surface coverage is diminished to a level below the detection limit of the IR measurement. In the present study, the molecularly adsorbed state is thought of as a precursor state for further dissociative adsorption as indicated in step 2 in the mechanism. However, the IR study of Dalla Lana and Deo [116] on the adsorption of 1-propanol on alumina has indicated the existence of a molecularly adsorbed species up to 443 K. A similar observation has also been reported by Knozinger and Stubner [117] for the adsorption of isobutyl alcohol on alumina.

With regard to the molecular adsorption of CH_2O, i.e., the surface species CH_2O_*, it is quite possible that the surface bond involves a zinc ion and the oxygen of CH_2O. A formate-like structure is also possible, where the carbon and the oxygen of the carbonyl group are being attached to an oxide ion and a zinc ion, respectively.

The methoxide and formate species have always been observed in all the IR studies of CH_3OH adsorption on metal oxides [46, 66, 104-108]. The thermodynamic feasibility of the formation of such species on metal surfaces has been recently given by Benziger and Madix [118].

With regard to the reversibility of steps 1 and 2 in the mechanism, few experiments were carried out to establish the reversibility of these steps by coadsorbing D_2 and CH_3OH on ZnO. No CH_3OD was detected. Probably high D_2 pressures, in the order of 1×10^4 Pa, are required to shift the equilibria of steps 1 and 2 to the left. However, the reversible adsorption of methanol on ZnO was deduced from the work of Anderson and Kamball [63]. Koga et al. [115] have established the

reversibility of a step similar to step 2 for the adsorption of isopropyl alcohol on ZnO. This was done by treating the alcohol-covered surface with about 2×10^4 Pa of H_2 gas. Presumably high pressures of D_2 gas were used in the work of Yasumori et al. [62] and that of Anderson and Kemball [63], who reported on the reversibility of CH_3OH adsorption on metals. However, pressures higher than 1.3×10^3 Pa were not attainable in the present work. Similarly the reversibility of step 5 in the mechanism was not established and no literature information is available on this subject.

The mechanism accounts for the hydrogen isotope results. Step 3 in the mechanism involves the cleavage of a C-H bond and predicts that the low temperature decomposition of methanol, steps 1-4, should follow the sequence: $R_h(CH_3OH) = R_h(CH_3OD) > R_h(CD_3OD)$, where R_h = initial rate of hydrogen production. Similarly, step 6 (or 6A and 6B) involves the cleavage of a C-H bond and predicts that $R_c(CH_2O) > R_c(CD_2O)$. These predictions are in accordance with the experimental findings of this study.

Finally, it should be pointed out that no such detailed mechanism, supplemented with ample experimental evidence, has ever been reported before on the decomposition of methanol on zinc oxide.

SUGGESTIONS FOR FUTURE RESEARCH

This research has provided strong evidence for the intermediate formation of CH_2O in the decomposition of CH_3OH. At lower temperatures (453 K - 513 K), the formaldehyde principally desorbs, while at higher temperatures (563 K - 613 K), it decomposes to CO and H_2. Consequently, the methanol synthesis might be visualized as follows:

$$CO_{(g)} + 2H_{2(g)} \overset{\text{step 1}}{\rightleftharpoons} H_{2(g)} + CH_2O_{(g)} \overset{\text{step 2}}{\rightleftharpoons} CH_3OH_{(g)}$$

Since the reverse of step 1 appears to be kinetically difficult in methanol decomposition (implying that step 1 is kinetically difficult in the synthesis), it is important to establish the kinetics of this reverse step by studying the kinetics of CH_2O decomposition over the same catalyst (ZnO).

The surface species HCO_* is one of several surface species proposed in the mechanism. This species is very likely to result from CH_2O decomposition on ZnO. Therefore, studying the adsorption of CH_2O on ZnO by any surface vibrational technique (such as IR or EELS) must be of value in this regard.

The mechanism also emphasizes the relevance of the molecularly adsorbed species CH_3OH_* and CH_2O_* as compared to the other surface species resulting from the dissociative adsorption of CH_3OH and/or CH_2O on the catalyst surface. Some information regarding the surface bond between a catalyst site and a surface species might be deduced by investigating the changes in the electric properties of ZnO due to its

exposure to CH_3OH or CH_2O. For example, the sign and magnitude of change in the surface electrical conductivity of ZnO, after exposure to CH_3OH or CH_2O, might be used to support a charge transfer model for surface bonding.

LITERATURE CITED

1. Monick, J. A. "Alcohols: Their Chemistry, Properties, and Manufacture"; Reinhold: New York, 1968; p. 464.

2. Brecheret, V.; Zagatto, A. J. A. In "Monohydric Alcohols: Manufacture, Applications, and Chemistry"; Wickson, E. J., Ed.; American Chemical Society: Washington, D.C., 1981; Chapter 3.

3. Kasem, A. "Three Clean Fuels from Coal"; Marcel Dekker, Inc.: New York, 1979; p. 76.

4. Takaoka, S. "Acetic Acid Synthesis from Methanol and Carbon Monoxide", Report #37A, Stanford Research Institute Process Economics, Mar. 1979, p. 83.

5. Chem. Mark. Rep., Feb. 11, 1980, 16.

6. Kennedy, T. F.; Shanks, D. In "Monohydric Alcohols: Manufacture, Applications, and Chemistry"; Wickson, E. J., Ed.; American Chemical Society: Washington, D.C., 1981; Chapter 2.

7. Hildebrandt, A. F. Hydrogen Energy Fundamentals Symposium-Course, Miami, Florida, Mar. 3, 1971, 51.

8. Brabbs, T. A. "Catalytic Decomposition of Methanol for Onboard Hydrogen Generation", NASA Technical Paper 1247, June 1978.

9. Kester, F. L.; Konopka, A. J.; Camara, E. "Automotive Storage of Hydrogen as a Mixture of Methanol and Water"; TEC-75/004, Nov. 1975.

10. Strelzoff, S. Chem. Eng. Progr. Symp. Ser. 1970, 66(98), 54.

11. Paul, J. K. "Methanol Technology and Applications in Motor Fuels"; Noyes Data Corporation: Park Ridge, New Jersey, 1978; Chapter 1.

12. Natta, G. In "Catalysis"; Emmett, P. H., Ed.; Reinhold: New York, 1955; Vol. 3, Chapter 8.

13. Kenard, R. J.; Nimo, N. M. Chem. Eng. Progr. Symp. Ser. 1970, 66(98), 47.

14. Royal, M. J.; Nimo, N. M. Hydroc. Proc. 1969, 48, 147.

15. Natta, G.; Pino, P.; Mazzanti, G.; Pasquon, I. Chim e Ind. (Milan), 1953, 27, 705.

16. Davies, P.; Snowdon, F. F. U.S. Patent 3,326,956, 1967.

17. Tarhan, M. O. U.S. Patent 3,689,575 (Bethlehem Steel).

18. Brockhaus, R. W. German Patent 2,201,429 (Chemische Werke Huls).

19. Poutsma, M. L.; Elek, L. F.; Ibarbia, P. A.; Risch, A. P.; Rabo, J. A. J. Catal. 1978, 52, 157.

20. Vannice, M. A.; Garten, R. L. Ind. Eng. Chem. Prod. Res. Dev. 1979, 18, 186.

21. Bradley, J. S. J. Am. Chem. Soc. 1979, 101, 7419.

22. Keim, W.; Berger, M.; Schlupp, J. J. Catal. 1980, 61, 359.

23. Dombek, B. D. In "Catalytic Activation of Carbon Monoxide"; Ford, P. C., Ed.; American Chemical Society: Washington, D.C., 1981; Chapter 14.

24. Meisel, S. L.; McCullogh, J. P.; Lechthader, C. H.; Weisz, P. B. Chem. Tech. 1976, 6, 86.

25. Slaughter, M. D. Ph.D. Dissertation, Iowa State University of Science and Technology, Ames, Iowa, 1979.

26. Newton, R. H.; Dodge, B. F. J. Am. Chem. Soc. 1933, 55, 4747.

27. Fischer, F. Oul und Kohle 1943, 39, 521.

28. Walker, J. F. "Formaldehyde", 3rd ed.; Reinhold: New York, 1964; Chapter 1.

29. Cherednichenko, V. M. Ph.D. Dissertation, Karpova Physics-Chemical Institute, Moscow, USSR, 1953.

30. Ewell, R. H. Ind. Eng. Chem. 1940, 32, 147.

31. Pasquon, I. Chim. Ind. 1960, 42, 352.

32. Uchida, H.; Ogino, Y. Bull. Chem. Soc. Jpn. 1958, 31, 45.

33. Leonov, V. E.; Karabaev, M. M.; Tsybina, E. N.; Petrishcheva, G. S. Kinet. Katal. 1973, 14, 970.

34. Saida, T.; Ozaki, A. Bull. Chem. Soc. Jpn. 1964, 37, 1817.

35. Temkin, M. Zh. Fiz. Khim. 1957, 31, 1072.

36. Shimomura, K.; Ogawa, K.; Oba, M.; Kotera, Y. J. Catal. 1978, 52, 191.

37. Herman, R. G.; Klier, K.; Simmons, G. W.; Mehta, S. J. Catal. 1979, 57, 339.

38. Herman, R. G.; Klier, K.; Simmons, G. W.; Finn, B. P.; Bulko, J. B.; Kobylinski, T. P. J. Catal. 1979, 56, 407.

39. Herman, P. "The Chemistry of Catalytic Hydrocarbon Conversions"; Academic Press: New York, 1981; Chapter 8.

40. Saussey, J.; Lavalley, J.; Lamotte, J.; Rais, T. J. Chem. Soc. Chem. Commun. 1982, 278.

41. Dohse, H. Z. Phys. Chem. 1930, 8B, 159.

42. Tamura, M. Rev. Phys. Chem. Jpn. 1942, 16, 71.

43. Dandy, J. A. J. Chem. Soc. 1963, 5956.

44. Menold, R. Chem. Ing. Tech. 1960, 32, 801.

45. Fuderer-Luetic, P.; Sviben, I. J. Catal. 1965, 4, 109.

46. Ueno, A.; Onishi, T.; Tamaru, K. Trans. Faraday Soc. 1971, 67, 3585.

47. Yates, J. T.; Goodman, D. W.; Madey, T. E. Proc. 7th Intern. Vac. Congr. & 3rd Intern. Conf. Sol. Surf., Vienna 1977, 1133.

48. Nishiyama, Y.; Wise, H. J. Catal. 1974, 32, 50.

49. Egelhoff, W. F.; Perry, D. L.; Linnett, J. W. J. Elect. Spectrosc. Rel. Phenom. 1974, 5, 339.

50. Gasser, R. P. H.; Holt, D. E. Surf. Sci. 1976, 55, 690.

51. Rubloff, G. W.; Demuth, J. E. J. Vac. Sci. Technol. 1977, 14, 419.

52. Fisher, G. B.; Madey, T. E.; Waclawski, B. J.; Yates, J. T. Proc. 7th Intern. Vac. Congr. & 3rd Intern. Conf. Sol. Surf., Vienna, 1977, 1071.

53. Mills, G. A.; Steffgen, F. W. Cat. Rev. 1973, 8, 159.

54. Spence, R.; Wild, W. J. Chem. Soc. 1935, 338.

55. Urey, H. C.; Rittenberg, D. J. Chem. Phys. 1933, 1, 137.

56. Jones, T.; Sherman, A. J. Chem. Phys. 1937, 5, 375.

57. Stenhagen, E.; Abrahamson, S.; Mclafferty, F. W. "Atlas of Mass Spectral Data"; Interscience Publishers: New York, 1969; Vol. 1, p. 4.

58. Lester, G. R.; Fontaine, A. E.; Beynon, J. H. Int. J. Mass Spect. Ion Phys. 1968, 1, 1.

59. Fletcher, C. J. M. Proc. Roy. Soc. Lond. 1934, 147, 119.

60. Goodman, D. W.; Yates, J. T.; Madey, T. E. Chem. Phys. Lett. 1978, 53, 479.

61. McKee, D. W. Trans. Faraday Soc. 1968, 64, 2200.

62. Yasumori, I.; Nakamura, T.; Miyazaki, E. Bull. Chem. Soc. Jpn. 1967, 40, 1372.

63. Anderson, J. R.; Kemball, C. Trans. Faraday Soc. 1955, 51, 966.

64. Morrelli, F.; Giorgini, M.; Tartarelli, R. J. Catal. 1972, 26, 106.

65. Morrelli, F.; Giorgini, M.; Guerrini, R.; Tartarelli, R. J. Catal. 1972, 27, 471.

66. Herd, A. C.; Onishi, T.; Tamaru, K. Bull. Chem. Soc. Jpn. 1974, 47, 575.

67. Tsuchiya, S.; Shiba, T. J. Catal. 1966, 6, 270.

68. Bricker, C. E.; Vail, W. A. Anal. Chem. 1950, 22, 720.

69. Uchida, H.; Ogino, Y. Bull. Chem. Soc. Jpn. 1956, 29, 587.

70. Gasser, R. P. H.; Jackson, G. V.; Rolling, F. E. Surf. Sci. 1975, 52, 199.

71. Roberts, M. W.; Stewart, T. I. In "Chemisorption and Catalysis"; Hepple, P., Ed.; Elsevier: London, 1970; p. 16.

72. Wachs, I. E.; Madix, R. J. J. Catal. 1978, 53, 208.

73. Carnisio, G.; Garbassi, F.; Petrini, G.; Parravano, G. J. Catal. 1978, 54, 66.

74. Eischens, R. P.; Pliskin, W. A.; Low, M. J. D. J. Catal. 1962, 1, 180.

75. Cvetanovic, R. J.; Amenomiya, Y. Adv. Catal. 1967, 17, 103.

76. Dent, A. L.; Kokes, R. J. J. Phys. Chem. 1969, 73, 3772.

77. Taylor, H. S.; Strother, C. O. J. Am. Chem. Soc. 1934, 56, 586.

78. Kesavulu, V.; Taylor, H. A. J. Phys. Chem. 1960, 64, 1124.

79. Narvaez, R.; Taylor, H. A. J. Phys. Chem. 1965, 69, 2500.

80. Scholten, J. J. F.; Van Montfoort, A. In "Proceedings of the Fifth International Congress of Catalysis"; Hightower, J. W., Ed.; North-Holland: Amsterdam, 1972; Vol. 1, p. 385.

81. Dent, A. L.; Kokes, R. J. J. Phys. Chem. 1969, 73, 3781.

82. Chang, C. C.; Kokes, R. J. J. Am. Chem. Soc. 1971, 93, 7107.

83. Chang, C. C.; Dixon, L. T.; Kokes, R. J. J. Phys. Chem. 1973, 77, 2635.

84. Dixon, L. T.; Dent, A. L.; Chang, C. C.; Kokes, R. J. J. Am. Chem. Soc. 1972, 94, 4429.

85. Baranski, A.; Galuszka, J. J. Catal. 1976, 44, 259.

86. Kokes, R. J.; Dent, A. L. Adv. Catal. Relat. Subj. 1972, 22, 1.

87. Tamaru, K.; Onishi, T.; Hagiwara, E.; Shimizu, H.; Naito, S. Trans. Faraday Soc. 1971, 67, 1519.

88. Griffin, G. L.; Yates, J. T. J. Catal. 1982, 73, 396.

89. Boccuzzi, F.; Borello, E.; Zecchina, A.; Bossi, A.; Camia, M. J. Catal. 1978, 51, 150.

90. Kubokawa, Y. Bull. Chem. Soc. Jpn. 1960, 33, 743.

91. Garner, W. E. J. Chem. Soc. 1947, 1239.

92. Hart, P. M. G.; Sebba, F. Trans. Faraday Soc. 1960, 56, 551.

93. Kubokawa, Y. Bull. Chem. Soc. Jpn. 1960, 33, 555.

94. Voroshilov, I. G.; Roev, L. M.; Kozub, G. M.; Lunev, N. K.; Pavloskii, N. A.; Rusov, M. T. Theor. Exp. Chem. (Engl. Transl.) 1975, 11, 212.

95. Boccuzzi, F.; Garrone, E.; Zecchina, A.; Bossi, A.; Camia, M. J. Catal. 1978, 51, 160.

96. Hush, N. S.; Williams, M. L. J. Mol. Spectrosc. 1974, 50, 349.

97. Taylor, J. H.; Amberg, C. H. Can. J. Chem. 1961, 39, 535.

98. Amberg, C. H.; Seanor, D. A. Proc. 3rd Intern. Cong. Catal. 1965, 450.

99. Edwards, J. F.; Schrader, G. L. Appl. Spectrosc. 1981, 35, 559.

100. Gay, R. R.; Nodine, M. H.; Henrich, V. E.; Zeiger, H. J.; Solomon, E. I. J. Am. Chem. Soc. 1980, 102, 6752.

101. Hotan, W.; Haul, R.; Gopel, W. Surf. Sci. 1979, 83, 162.

102. Noto, Y.; Fukuda, K.; Onishi, T.; Tamaru, K. Trans. Faraday Soc. 1967, 63, 3081; Bull. Chem. Soc. Jpn. 1967, 40, 2722.

103. Ueno, A.; Onishi, T.; Tamaru, K. Trans. Faraday Soc. 1970, 66, 756; Bull. Chem. Soc. Jpn. 1969, 42, 3040.

104. Greenler, R. G. J. Chem. Phys. 1962, 37, 2094.

105. Kagel, R. O. J. Phys. Chem. 1967, 71, 844.

106. Unland, M. L. J. Phys. Chem. 1978, 82, 580.

107. Thornton, E. W.; Harrison, P. G. J. Chem. Soc. Faraday Trans. I 1975, 71, 2468.

108. Nagao, M.; Morimoto, T. J. Phys. Chem. 1980, 84, 2054.

109. Cheng, W. H.; Kung, H. H. Surf. Sci. 1981, 102, L21; "Book of Abstracts", 183rd National Meeting of the American Chemical Society, Las Vegas, Nevada, March 1982; American Chemical Society: Washington, D.C., 1982; COLL 249.

110. Tamaru, K.; Onishi, T.; Hagiwara, E.; Shimizu, H.; Naito, S. Trans. Faraday Soc. 1971, 67, 1519.

111. Wicke, E.; Brotz, W. Chem. Ing. Tech. 1949, 12, 219.

112. Wencke, K.; Heise, G. Monatsber. Dent. Akad. Wiss. Berl. 1965, 7, 887.

113. Fletcher, C. J. M. Proc. Roy. Soc. Lond. 1934, 146, 357.

114. Runge, F.; Gopel, W. Z. Phys. Chem. W. 1980, 123, 173.

115. Koga, O.; Onishi, T.; Tamaru, K. J. Chem. Soc. Faraday I 1980, 76, 19.

116. Dalla Lana, I. G.; Deo, A. V. J. Phys. Chem. 1969, 73, 716.

117. Knozinger, H.; Stubner, B. J. Phys. Chem. 1978, 82, 1526.

118. Benziger, J. B.; Madix, R. J. J. Catal. 1982, 74, 67.

ACKNOWLEDGMENTS

I would like to express my sincere gratitude to Dr. Robert S. Hansen for his kind help and guidance throughout this research. His fruitful discussions and suggestions were invaluable.

My thanks are due Dr. Harry J. Svec and Mr. Gerald D. Flesch for their assistance in solving some problems regarding the mass spectrometer, Mr. Edward L. DeKalb for checking the catalyst purity, Mr. James A. Herriott for measuring the catalyst surface area, and Dr. James H. Espenson for providing a computer program suitable for analysis of two first-order consecutive reactions and for the use of his computer facility.

I also would like to express my gratitude to Yarmouk University for providing me with the full scholarship which made it possible for me to continue my graduate studies and complete this work.

My sincere gratitude and appreciation are due my parents and my family for their support and encouragement over the long years of my schooling. Special thanks are due my first teacher, my father, who fired my interest in learning.

The love, care, and encouragement of my wife, Alia, made it possible for me to accomplish this project. The love and happiness that Rami, our son, and his mother have provided made my life more than enjoyable.